UNIVERSITY OF CALIFORNIA,

IRVINE

Energy and economic assessment of distributed renewable gas and electricity generation from organic solid municipal waste in an Advanced Energy Community

THESIS

submitted in partial satisfaction of the requirements

for the degree of

MASTER OF SCIENCE

in Mechanical and Aerospace Engineering

by

Rochelle E. Silverman

Thesis Committee:

Professor Jacob Brouwer, Chair

Adjunct Professor Vincent McDonell

Assistant Professor Yoonjin Won

2019

TABLE OF CONTENTS

LIST OF FIGURES

LIST OF TABLES

NOMENCLATURE & SYMBOLS

Superscripts and Subscripts

cap	capacity
capital	capital cost
e	electricity
NG	natural gas

Abbreviations

AC	axial compressor
AD	anaerobic digestion
AEC	alkaline electrolyzer
AFLEET	Alternative Fuel Life-Cycle Environmental and Economic Transportation
ATO	anode tailgas oxidizer
BGU	biogas upgrading
CAISO	California Independent System Operator
CAPEX	capital expenditure
CB	centrifugal blower
CEC	California Energy Commission
CET	cathode exit temperature
CHP	combined heat and power
CLH	combination long-haul
CNG	compressed natural gas
CSH	combination short-haul
DER	distributed energy resource
EC	electrolysis
GGE	gasoline gallon equivalent
GREET	Greenhouse gases, Regulated Emissions, and Energy use in Transportation
GVWR	gross vehicle weight rating
HHV	higher heating value
ICE	internal combustion engine
LCOE	levelized cost of energy
Li-ion	Lithium ion
LPM	liters per minute
Max	maximum
MMBTU	million British thermal units
MPG	miles per gallon
MT	methanation
NEM	net energy metering
NREL	National Renewable Energy Laboratory
O&M	operation and maintenance
OFMSW	organic fraction of municipal solid waste
OVWTS	Oak View waste transfer station

Pb-A	Lead acid
PEMEC	proton exchange membrane electrolyzer
PI	natural gas pipeline injection
PtG	power-to-gas
PV	photovoltaic
RNG	renewable natural gas
SCE	Southern California Edison
SCG	Southern California Gas Company
SOEC	solid oxide electrolyzer
SOFC	solid oxide fuel cell
SMR	steam methane reformation
SNG	synthetic natural gas
SULH	single unit long haul
SUSH	single unit short-haul
TBW	total body water
TDV	time-dependent valuation
tpy	tons per year
TS	total solids
US	utility-side
ZNE	zero-net-energy

ACKNOWLEDGEMENTS

I would like to express my deepest gratitude to my advisor and committee chair, Prof. Brouwer, and to Dr. Robert Flores for their guidance and support throughout the process of completing this thesis. I would also like to thank my committee members, Prof. Vincent McDonell and Prof. Yoonjin Won, for their time and insightful feedback that helped frame the final presentation of these results in the broader context of current fuel and electricity markets.

I gratefully acknowledge the financial support for this work which was provided by the California Energy Commission, and the significant leadership and contributions of Rachel Salazar, the Contract Manager.

ABSTRACT OF THE THESIS

Energy and economic assessment of distributed renewable gas and electricity generation from organic solid municipal waste in an Advanced Energy Community

By

Rochelle E. Silverman

Master of Science in Mechanical and Aerospace Engineering

University of California, Irvine, 2019

Professor Jacob Brouwer, Chair

A methodology for assessing the efficiency and economic viability of renewable gas generation and energy conversion to compliment residential PV is proposed and demonstrated for a 10,000 resident example community in Huntington Beach, California. Dynamic solid oxide fuel cell (SOFC) performance on two fuels was explored to inform electricity production assumptions. These efforts included operating an SOFC on natural gas, using experimental data to verify an SOFC model, and simulating SOFC operation on clean biogas. Renewable fuel production processes included in the community zero-net-energy assessment are 1) through the processing of community-produced organic fraction of municipal solid waste (OFMSW) in an anaerobic digester and 2) using solar generation paired with power-to-gas technologies. Six pathways – ending in natural gas pipeline injection or SOFC electricity production – were evaluated for two PV capacity scenarios. The renewable fuel production potential of community-produced OFMSW was determined to be 0.24 MMBTU/y of renewable natural gas (RNG) from anaerobic digestion and up to 2.85 MMBTU/y of hydrogen from electrolysis using excess solar PV electricity. A payback period of 7 years, equal to that of a modern natural-gas power plant, requires the renewable fuel sale price to be 5.2-15 times larger than the 2017

California residential average natural gas price and the renewable electricity sale price to be 3.0-6.8 times larger than the 2017 local average residential electricity price. Results show >80% of the community electrical demand can be met through a combination of solar PV, anaerobic digestion, and SOFC operation. In this scenario, solar PV meets 52% of the community electrical load, while excess solar production produces hydrogen that is passed through a fuel cell to meet 26% of the electrical load. The remaining 3% is met using RNG produced through anaerobic digestion using only organic waste from the studied community.

INTRODUCTION

Overview

Recent California laws and policies including the California Energy Commission's 2019 Building Energy Efficiency Standards require boosts in energy efficiency [1]–[3], significant increases in renewable energy reduction [4], and a statewide decrease in greenhouse gas emissions [5]. Both energy efficiency and solar energy generation have been critical towards meeting current and future California energy and sustainability goals. Traditionally, both energy efficiency and solar generation have been supported through a combination of incentive and rebate programs [6]–[8]. Although successful, critics of such programs cite equity issues faced when attempting to implement energy efficiency and renewable energy measures in low income, urban, and/or multifamily communities [9]. In order to overcome these critiques, the concept of "the community energy project" has emerged [9].

These energy projects can include community scale design of energy efficiency retrofits, district energy systems, combined heat and power, renewable generation, and community energy storage [10]–[14], with particular focus on community solar photovoltaic (PV) [15]. As grid connected solar energy systems proliferate, challenges from handling excess solar generation must be dealt with [16]. Conventional methods for handling excess and unwanted solar output are to use the excess energy to provide ancillary services, charge energy storage, or curtailment. Considering the future need for a renewable fuel [17], another use of excess solar energy is through an electrolysis process to generate renewable hydrogen. Electrolysis of water to hydrogen using excess renewable energy, or power-to-gas (PtG) can be used to provide seasonal energy storage to balance intermittent and inflexible renewable generation [18], [19]. PtG includes any technology that converts electrical power to a gaseous fuel, usually hydrogen or methane. Hydrogen gas is the favored fuel produced by PtG technologies because it has a high energy density, is storable on large timescales, requires fewer steps to produce than methane, and produces no greenhouse gases when converted back to electricity [18].

It is easy to hypothesize that use of community solar to provide PtG would suffer from poor economies of scale, or that such a project would face “not in my back yard” – NIMBY – challenges [20]. One scenario in which both challenges could potentially be overcome is when the PtG electrolyzer is collocated with an urban waste transfer facility. The benefits of the system would be the introduction of the system into an industrial location, possible proximity to a community energy project, and the potential to develop renewable gas production using onsite organic waste. Previous studies have examined community energy projects that include optimizing waste handling and usage, including optimized recycling pathways. [14], [21]–[23]. Currently, little to no work is found on the literature on colocation of PtG technology and waste transfer operations within an urban environment.

Electricity production from two possible community scale solar PV systems and community-scale methane gas production via anaerobic digestion (AD) of residential organic solid municipal waste were modeled. Using these energy streams, six energy pathways involving combinations of electrolysis (EC), methanation (MT), solid oxide fuel cell (SOFC), and natural gas pipeline injection (PI) technologies were evaluated for energy efficiency, cost-effectiveness, and ability to meet community electricity demand. The contribution of this thesis is to provide a simple, replicable, and scalable model to help direct future energy-and sustainability-conscious construction and retrofitting in existing communities.

Additionally, a 1.5 kW SOLIDpower SOFC was installed as part of a CHP energy generation system in a simulated ZNE home setting. A MATLAB Simulink model previously developed at the NFCRC was modified to simulate the SOFC dynamic performance on natural gas fuel and clean biogas [24]. The practicality of using small-scale SOFC power production as a dynamic distributed power resource to complement intermittent solar PV power production was assessed using cost models found in the literature and SOFC performance characterization data determined experimentally. Final evaluation considerations of the practicality of renewable fuel production and use in ZNE communities include system energy consumption, energy efficiency, solar PV capacity and rooftop requirements, cost-

effectiveness, and infrastructure needs. This thesis is organized as follows: Section **Error! Reference s ource not found.** describes relevant technology characteristics and costs, Section **Error! Reference source not found.** describes the modeling methodology, Section CHAPTER 3: presents results based on the included technology and model methodology, and Section CHAPTER 4: summarizes the work in conclusion.

Goal

The goal of this work is to evaluate renewable gas generation, conversion, and to determine its ability meet ZNE criteria in mostly residential communities similar to the Oak View neighborhood in Huntington Beach, California.

Objectives

To accomplish this goal, the following objectives will be carried out

1. Conduct a thorough literature review to acquire all relevant background knowledge,
2. Evaluate potential sources of sustainably produced fuel in an example community,
3. Install and evaluate the performance of a representative SOFC system operating on natural gas in a simulated ZNE environment for model verification,
4. Develop a dynamic simulation environment for evaluating SOFC operation on natural gas and verify with experimental data,
5. Develop a dynamic model for an SOFC system operating on biogas, and
6. Use the SOFC models to determine the viability of renewable fuel use in an SOFC system to complement PV use and achieve ZNE in a community.

CHAPTER 1: BACKGROUND

1.1 Distributed Energy Conversion and Zero-Net-Energy Regulations

Several factors have increased demand for efficient electric power production, supply, and transport technology. In the United States, power generation plants produce the majority of pollutant emissions, including fine particulate matter, sulfur dioxide, and ammonia, according to 2008 data [25]. These pollutants contribute to global climate change and are known to have adverse health and environmental impacts [25]. Most American electric power generation plants are coal-driven and have electrical efficiencies of 30-40% [26]. In addition to heat losses, 6-8% of power plant-manufactured electricity is lost during transmission and distribution [26]. Data from 2012 suggests that the U.S. total energy efficiency is 38.4% [27]. Many newer technologies like fuel cells and gas turbines can achieve total efficiencies exceeding 80%, especially when integrated to form combined cycles or combined heating and power (CHP) systems [28]. Distributed energy resources (DER), i.e. those that produce electric power and/or heat near the point-of-use, that use these sustainable energy technologies are becoming increasingly popular methods to reduce energy loss during transmission and increase local grid resilience. Photovoltaic systems are the most common DER and are widely deployed throughout California. Distributed energy systems reduce transmission and distribution energy losses while providing access to waste heat for CHP systems.

Reinforcing and restructuring the aging and outdated U.S. electrical grid to connect with new smart technologies and distributed energy systems has been a major legislative focus in recent years [29]. The American Recovery and Reinvestment Act of 2009 dedicated 4.5 billion USD to modernizing the nation's electrical grid, reducing energy demand, and increasing the use of renewable energy technologies [29]. The private electric sector has provided an additional 5 billion USD to fund design and construction projects to replace old transmission lines, build smart grids, and institute policies that promote distributed generation and cogeneration for both commercial and residential buildings [30]. In

support of these efforts, the 2015 Executive Order titled *Planning for Federal Sustainability in the Next Decade* by U.S. President Barack Obama mandates that 15% of existing federal buildings conform to energy efficiency standards for High Performance and Sustainable Buildings by 2025 and that all new federal buildings be Zero-Net-Energy by 2020 [31]. Similarly, the California Energy Commission has required that all new commercial buildings (and 50% of existing commercial structures) must meet ZNE standards by 2030 and that all new construction single-family homes must also meet ZNE standards beginning in 2020 [3].

A Zero-Net-Energy Code Building is defined by the CEC as "one where the societal value of the amount of energy provided by on-site renewable energy sources is equal to the value of the energy consumed by the building . . ." [32]. The CEC gives all electric power, both produced on-site and from the grid, a monetary value equivalent. This time-dependent valuation (TDV) is based on the time of production and the typical energy demand at that time. The TDV consumption value must equal the TDV generation value over the course of a year for a building to earn a ZNE classification. The keystone element of a ZNE building is the use of a renewable distributed generation system. This can be achieved by generating electricity directly from renewable sources like wind or solar power when they are available regardless of demand or by using renewably generated electricity to produce fuel to store the energy for later use. To-date, nearly all residential distributed generation systems have been photovoltaic (PV), which have daily peak electric power production during off-peak power demand [3].

Solar PV provides clean renewable energy that has the capacity to meet significant portions of current electrical demand [33]. However, the current grid infrastructure cannot support the increased intermittent renewable power without also increasing installation of supporting distributed energy conversion and storage technologies [34]. The California Independent System Operator (CAISO) published a graph (Figure 1) plotting California's actual and projected net electrical loads, equal to the normal load minus wind and PV generation, for an example spring day in 2012-2020 [35]. This figure has

become known as the “Duck Chart” because of the chart’s shape that is similar to the outline of a duck. The figure shows a large drop in mid-day net electrical load when solar PV production is highest that increases as PV penetration increases over time. The chart also shows the significant need for ramping resources in the evening. The chart raises concerns that the current power system which utilizes many resources requiring long start-up times will not be able to match the steep afternoon ramp rate at high PV penetrations [34].

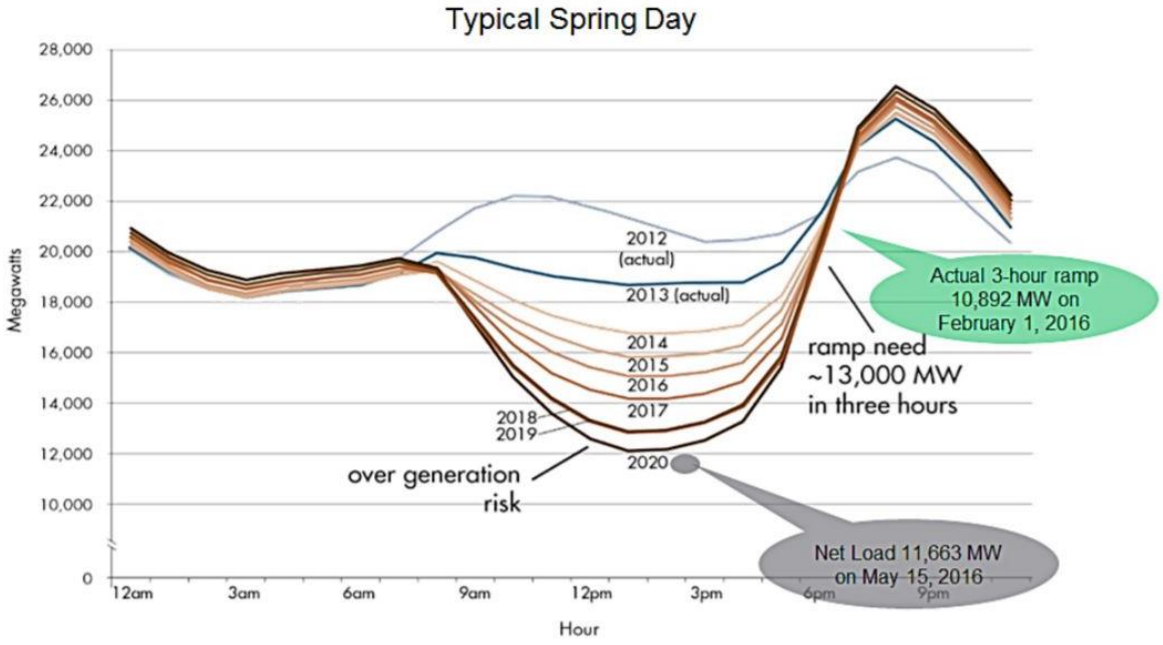

Figure 1. CAISO Duck Chart showing a large drop in mid-day net electrical load as solar PV penetration increases over time [35].

Much of the over-generation is fed back onto the utility grid network on a net energy metering (NEM) basis (electricity generation and consumption are valued equivalently at the meter) [33], [35], [36]. Under this policy the utility grid network is expected to handle all over-generation in the middle of the day and all of the generation lost as the sun goes down without compensation [34], [37].

More traditional power generation plants have very limited ability to follow dynamic loads and must be run near steady-state conditions [34]. If solar power cannot be fully utilized because other power resources are online simultaneously, more power is produced than demanded [34]. The simplest technical solution to this PV over-generation is renewable curtailment, decreasing output from wind or

PV below what it would normally produce, effectively increasing the cost of renewable energy production and reducing the environmental benefits [34].

A 2015 study by the National Renewable Energy Laboratory (NREL) concluded that under business-as-usual power system management California solar penetration as low as 20% could lead to marginal curtailment rates greater than 30% [34]. Figure 2 shows CAISO historical renewable curtailment data for each month in 2014 through October 2018. The recent trend in increased renewable curtailment is clear. Curtailment and the emergence of negative electricity prices during over-generation hours in the California energy market have generated significant interest in energy storage [34], [38]. Allowing or requiring storage along with the installation of distributed PV could increase system flexibility, reduce curtailment, and allow greater penetration of renewable power generation [34].

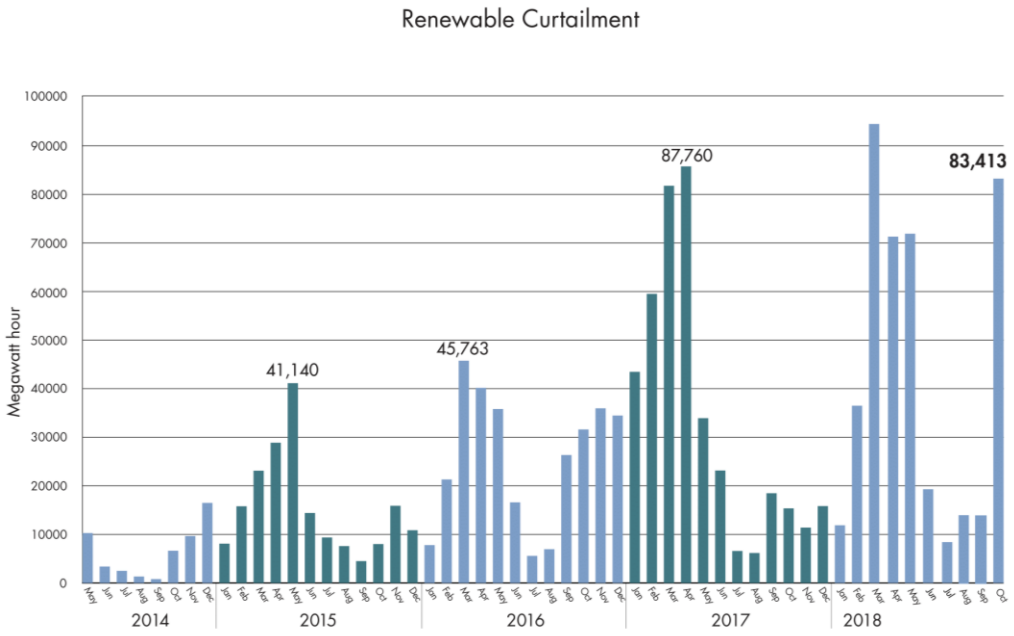

Figure 2. CAISO historical renewable curtailment chart [39].

1.2 Community Description

The Oak View community is a small subsection of the City of Huntington Beach located in Southern California. This community was selected as the design community, representative of a

disadvantaged community which may be difficult to make ZNE, due to a combination of a poor CalEnviroScreen 3.0 rating of between 76% and 80% [40], local per capita income falling well below average income levels, and over 80% of all buildings being built prior to 1980 [41]. The community is home to approximately 10,000 residents, and contains multiple commercial and industrial entities, including a waste separation and transfer station. Most of the 10,000 Oak View residents live in multi-family residences with no air conditioning, and the neighborhood has a history of substandard air quality as determined and enforced by the South Coast Air Quality Management District [42]. When considering California State goals, the local pollution levels, aging building stock, and variety of building end uses, Oak View is a prime challenging candidate for exploring community net zero energy methods and technologies.

1.3 Relevant Technologies and Cost Models

The current work examines renewable fuel production and conversion pathways, requiring a myriad of technologies and methods to be implemented. This section reviews the technical and economic characteristics of the different technologies included in this work.

During the cost analysis, cost of energy through renewable fuel pathways is compared to average residential and commercial costs in Southern California. In 2017, the average residential and commercial cost of natural gas was $12.04 and $8.45 per MMBTU, respectively [43]. The average price of residential and commercial electricity in 2017 from Southern California Edison, the local provider in Huntington Beach, was $0.1660 and $0.1441 per kWh, respectively [44].

1.3.1 Cost Summary

Table 1 presents the capital and annual operating and maintenance cost models determined for each relevant technology discussed in Section 1.3. For technologies with an expected lifetime less than 30 years, the expected lifetime of a power or fuel generation plant, replacement costs are included in

the O&M costs shown in Table 1. Replacement costs were calculated as monthly payments over the lifetime of the previous component or component cell stack with an 8% annual credit on payments.

Table 1. Summary of capital and O&M costs for all relevant technologies.

System Component	Capital Cost		Annual O&M Cost	
Residential Solar PV	$\$2{,}530 * P_{kWe}$	[45]	$\$21 * P_{kWe}$	[46]
Commercial Solar PV	$\$1{,}395 * P_{kWe}$	[45]	$\$21 * P_{kWe}$	[46]
Lithium Ion Battery	$\$0.853 * E_{kWh}$	[47]	$\$0.0922 * E_{kWh}$	[a]
MSW Anaerobic Digestion	$\$2{,}508{,}900(MSW_{CAP})^{0.5}$	[37]	$\$162{,}775(MSW_{CAP})^{0.6}$	[37]
Biogas Upgrading for Pipeline	$\$1{,}370{,}000(flow_{RNG})^{0.56}$	[37]	$\$101{,}625(flow_{RNG})^{0.81}$	[37]
Alkaline Electrolysis	$\$1{,}200 * P_{kWe}$	[18], [19], [48]	$\$57.4 * P_{kWe}$	[49], [50]
Catalytic Fixed-bed Methanation	$\$0.007(CAP_{kW})^{0.6823}$	[b]	$0.0835 * Capital_{MT}$	[51]
SOFC	$\$5{,}000 * P_{kWe}$	[52], [53]	$\$959 * P_{kWe}$	[52]
Renewable Natural Gas Injection	$\$615{,}750(flow_{RNG})^{0.42}$	[37]	$\$28{,}425(flow_{RNG})^{0.35}$	[37]

$\boldsymbol{P_{kWe}}$ is electric power in kW.
$\boldsymbol{E_{kWh}}$ is battery energy storage in kWh.
$\boldsymbol{MSW_{CAP}}$ is the digester capacity in thousands of tons/y of MSW input.
$\boldsymbol{flow_{RNG}}$ is the output flowrate of renewable natural gas in MMBTU/h.
$\boldsymbol{P_{kWe}}$ is the electrical power capacity of the electrolyzer in kW.
$\boldsymbol{MT_{Capital}}$ is the capital cost of the methanation system.
$\boldsymbol{P_{Capital}}$ is the capital cost of the RNG pipeline.
[a] Includes only replacement cost as batteries require little-to-no O&M expenses.
[b] Equation was obtained from best-fit line of values found in the literature.

Any real system would require dynamic operation of equipment as intermittent renewable resources are available and used. In this case, dynamic operation should be considered for the efficiency and cost analysis. Alternatively, natural gas and grid electricity could be used to supplement sustainable fuel and electricity as needed to operate technologies at steady-state. This study does not account for possible increased operation and maintenance costs of dynamic equipment operation.

1.3.2 Solar PV

The first commercial silicon PV cells debuted in 1956 by Western Electric, but high costs prevented their widespread use [54]. Since the beginning of the twenty first century, commercial solar PV power generation technologies have steadily matured and decreased in price causing the number of PV installations to drastically and steadily increase in California [33]. Five recent developments, alongside decades of world-wide government financial incentives [55] have contributed to the recent growth of PV in the state: (1) the United States government permitting lower cost solar panels produced in China to be imported, (2) the emergence of third-party-owned residential solar systems, (3) the

completion and success of large scale PV power plants, and (4) ongoing manufacturing consolidation [33]. California was the first U.S. state to install over 1 GW of PV for utility power generation in 2012 [33] with the Energy Information Administration and the CEC reporting that nearly 12.5 GW of installed solar panels generated 24.3 GWh of electric power in 2017 [56], [57]. Residential solar PV has a capital cost of $2,530/kW, and commercial solar PV has a capital cost of $1,395/kW [45]. Both have operational lifetimes of 30 years and annual operation and maintenance (O&M) costs of $21/kW [46]. Capital as well as operating and maintenance (O&M) costs – accounting for replacement costs where applicable – are summarized in Table 5 for all referenced technologies.

1.3.3 Batteries

Batteries are typically used to provide energy storage for relatively short timescales - from seconds to hours. They can be used to control frequency and voltage, shift demand, provide ramp rate compensation, smooth fluctuations in solar renewable power generation, and prevent curtailment [58], [59]. Lead-acid (Pb-A) batteries are the most mature and widely used battery technology [58]. Lithium-ion (Li-ion) batteries were first commercialized in 1990 and have been gaining popularity in recent decades because of their high cycle life, high energy density, and high efficiency [58]. These two main battery technologies are compared in Table 2.

The lifetime of batteries varies depending upon their thermal environment and charge and discharge control strategies [59]. A life prediction model developed by the National Renewable Energy Laboratory suggests that grid-connected batteries subject to a relatively constant average ambient temperature of 30^{o}C, a depth of discharge of 74%, and daily charge cycling can last 7.3 years before degrading to 70% of its rated current flow [59]. This model concluded that integrated battery-PV systems attempting to minimize energy exchange with the grid can have expected lifetimes of 7 to 10 years [59]. Battery replacement cost in this study assumes a capacity factor of 0.3 and a 7-year lifetime.

Table 2. Popular battery technology characteristics.

Battery Type	Pb-A		Li-ion	
Cycle life (cycles @ % state of charge variation)	50-200 @ 80%; 1000s for shallow cycles	[58]	3000 @ 80%	[60]
Energy density (Wh/L)	50-80	[61], [62]	200-550	[58], [63]
Power density (W/L)	300-400	[61], [62]	4500	[58]
Self-discharge per day	<0.5%	[60]	0.1-0.3%	[58], [60]
Cycle efficiency	63-90%	[58]	80-98%	[58]
Commercial cost ($/kWh)	1.06-1.15	[47]	0.853	[47]
Maturity level	Mature	[58]	Commercial	[58]

1.3.4 Anaerobic Digestion and Biogas Upgrading

Three commercial technologies convert biomass to electricity and biogas fuel: combustion, gasification, and anaerobic digestion [64]. Combustion uses the heat produced from burning biomass to create steam to turn a steam turbine, producing electricity. Gasification reacts biomass with limited oxygen and/or steam to produce syngas, a gaseous fuel rich in hydrogen and carbon monoxide. Anaerobic digestion is a series of biological processes in which microorganisms break down biodegradable material in the absence of oxygen to produce biogas, a methane-rich gaseous fuel. AD uses organic wastes, including livestock manure, municipal wastewater solids, food waste, the organic fraction of municipal solid waste, along with fats, oils, and grease that would otherwise be landfilled, incinerated, or used directly as agricultural fertilizer, as feedstock to maintain the digestion reactions [65]. As hydrogen has also been shown to be an effective fuel source, research has been conducted to demonstrate additional AD methods that produce hydrogen-rich biogas [66]–[69]. These processes, however, are currently only in the laboratory stages [35]. AD is the only one of these technologies that is nearly carbon neutral and does not emit criteria pollutants from combustion [70].

Anaerobic digestion systems can be configured in several different ways and can be categorized into mesophilic versus thermophilic, wet versus dry, continuous versus batch feeding, and single-stage versus multi-stage systems. Mesophilic or thermophilic categorization describes the digester operating temperature. Mesophilic digesters operate in an ideal temperature range of 30-40°C , while

thermophilic digesters operate in an ideal temperature range of 50-60°C [71]. Mesophilic digestion is better established and more widely used because mesophilic species are more tolerant to changes in environmental conditions than thermophiles. This has given Mesophilic digestion the reputation of being much more stable while also, on average, having lower maintenance costs [71]. Thermophilic systems feature significantly shorter digestion periods than mesophilic systems to produce comparable amounts of biogas [65]. Typical thermophilic retention times are 10-16 days, and typical mesophilic retention times are 30-60 days [65].

Wet versus dry digestion describes the total solids (TS) content of digestate. Wet systems are suitable for liquid feedstocks with TS concentration below 16%, and dry systems are suitable for dry feedstocks with a TS content greater than 22% [72]. Liquid feedstocks such as manure slurry or waste water sludge can be pumped from one system stage to the next. Operating a wet digestion system requires less input energy, because pumping is significantly more efficient than are the specialized technologies for loading moving solid feedstock required by dry digestion systems [73]. Wet systems typically have higher methane yields while dry digestion systems have higher contaminant tolerances and require less maintenance [73].

Continuous or batch feeding characterizes the manner in which feedstock is added to the digester. In continuous digestion systems, feedstock is continually fed into the digester and digestate is continually taken out of the digester [74]. In discontinuous digestion, feedstock is digested in batches [74]. Batch feeding systems are less expensive than continuous feeding systems; however, each batch turnover must undergo the maintenance-heavy aerobic starting phase. For industrial-scale digestion systems, continuous feed is generally advantageous [71].

The number of reactors used during the digestion process is described as stages. Single-stage systems use only one reactor, while multi-stage systems typically use two reactors. Multi-stage systems work by separating the hydrolysis and acidification processes from the acetogenesis and

methanogenesis processes. This is done because each process has different ideal operating conditions [72]. Multi-stage systems usually have slightly higher methane yields and better stability than single-stage systems, but are also more expensive to build and maintain [72].

Biogas yields of AD are strongly dependent upon feedstock composition, which is highly variable with location, population density, season, sector of the source material, and use of pre-treatment options [75]. Municipal solid waste (MSW) typically has greater than 25% total solids and is therefore categorized as a feedstock best suited for dry AD [64], [76]. The first MSW digester plants operated as continuous-feed wet digester systems [64]. Since 2007, however, most MSW AD plants have been batch-fed dry systems [64]. Relevant literature recommends that MSW be mixed with chipped wood to produce a feedstock containing about 44% total solids to be digested over 30 days after a 3-4 day aerobic pre-treatment that slowly raises the feedstock from ambient temperature to 37 ^{o}C [64], [76]. Each digestion batch should consist of half new feedstock material and half digestate from the previous batch [64].

Biogas is typically composed of 50-70 vol% methane, 30-50 vol% carbon dioxide, and a few percent by volume of trace volatile organic compounds [64], [75]–[77]. Common contaminants include sulfur, halogens, organic silicon, and aromatic compounds and must be removed before the biogas can be used to produce electricity [64], [76], [78]. Biogas is typically upgraded to renewable natural gas (RNG) through a multi-step process that includes carbon dioxide removal, gas drying, minor contaminant removal, and compression in upgrading systems with energy efficiencies of 85-98% [79]. At small scales biogas upgrading is prohibitively expensive [37]. Government-funded feed-in tariffs, which guarantee a set purchase price of renewable gas or electricity by the utility, have been used in California to offset high costs encourage the development of small-scale bioenergy projects [80], [81]. However, these programs are currently suspended [80], [81].

Upgraded biogas can be used locally by the producer, compressed and sold as compressed natural gas (CNG) vehicle fuel, or injected into the natural gas pipeline distribution network. CNG production is less expensive than RNG production from biogas, however, local CNG demand must be strong to make its production economically feasible. Anaerobic digestion and, especially, biogas upgrading demonstrates strong economies of scale [37], [78], [82]. The economic feasibility of anaerobic digestion as waste treatment depends upon a large number of location-specific variables such as local energy and waste markets, population density, and climate [83]. Estimates in existing literature are highly varied and often site-specific [83]–[85]. Parker, et al. defined functions approximating anaerobic digestion system capital and O&M costs specific to California markets that are referenced in Table 1. The assumed lifetime of an AD facility is 30 years.

Another consideration when siting an anaerobic digester is potential resistance from local residents and stakeholders. Public interviews of Oak View residents and stakeholders revealed that the siting of an anaerobic digester at the local waste transfer station is undesirable. As a result, RNG production from community waste requires transfer to an existing AD system. Further interviews with the waste transfer station operators indicated that transfer of organic waste to an AD system located in Perris, CA is planned. The process of transferring organic waste from the Oak View community to the Perris, CA digester system is included in this work.

Using the 2017 Alternative Fuel Life-Cycle Environmental and Economic Transportation (AFLEET) Tool, a module of the GREET 2016 software, produced by U.S. Department of Energy's Argonne National Laboratory, the expected emissions for trucking OFMSW processed at the Oak View waste transfer station to the AD located in Perris, CA, were calculated [86]. Figure 3 shows the Google Maps suggested driving route between these locations. The shortest driving distance between the facilities is 66.6 miles (133.2 miles roundtrip) [87].

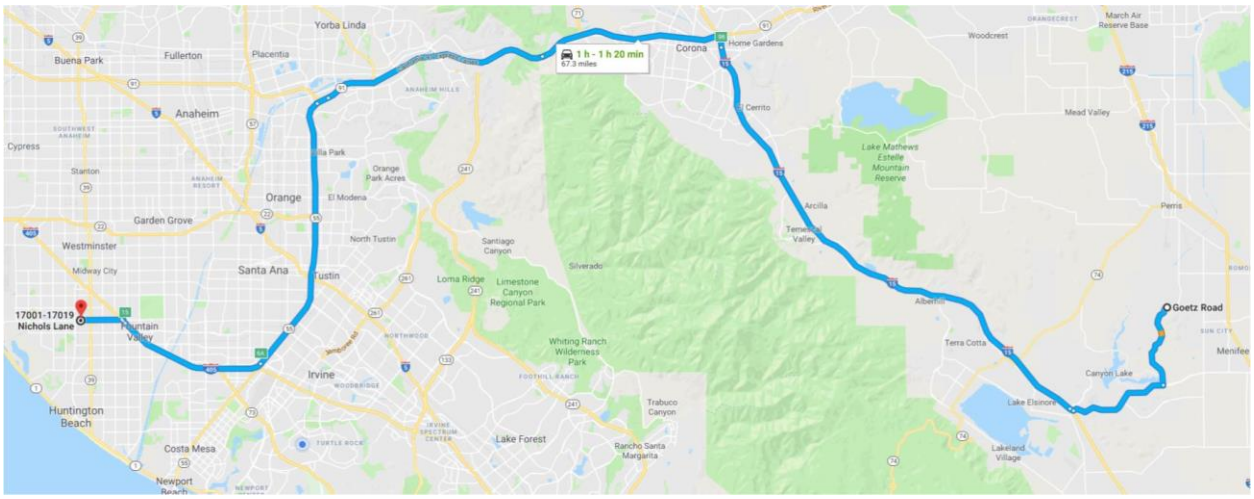

Figure 3. Google Maps suggested driving routes between Oak View (17001 – 17019 Nichols Lane) to the anaerobic digester (Goetz Road) [87].

1.3.5 Power-to-Gas

The need for seasonal and yearly energy storage to balance intermittent and inflexible electricity supply has motivated the development of power-to-gas technologies [18]. PtG includes any technology that converts electrical power to a gaseous fuel, usually hydrogen or methane. It has become an established compliment to increasing shares of wind and solar power in the energy sector [19]. Hydrogen gas is the favored fuel produced by PtG technologies because it has a high energy density, is storable on large timescales, requires fewer steps than methane production, and produces no greenhouse gases when converted back to electricity [18]. The foundation of all PtG systems is water electrolysis, which involves passing an electric current through an electrolyzer to decompose water into oxygen and hydrogen (reaction (1)). In an oxygen-ion (O^{2-}) conducting electrolytic cell, liquid water is reduced at the negatively charged cathode (reaction (2)), and oxygen ions are oxidized at the positively charged anode (reaction (3)).

$$H_2O\ (l) \rightarrow H_2(g) + \frac{1}{2}O_2(g) \quad (1)$$

$$H_2O + 2e^- \rightarrow H_2 + O^{2-} \quad (2)$$

$$O^{2-} \rightarrow \frac{1}{2}O_2 + 2e^- \quad (3)$$

Efficiencies of existing electrolyzer technologies and steam methane reformation are compared in Table 3. Electrolyzer efficiencies are calculated by dividing the energy of hydrogen fuel produced using its higher heating value (HHV) by the electrical and heat energy input to the process. The overwhelming majority of hydrogen gas production today uses steam methane reformation (SMR), which reacts natural gas and steam with approximately is 85% efficiency [88]–[90].

Table 3. Efficiencies of hydrogen fuel production processes in order from highest to lowest.

H_2 Production Process	Efficiency	
High-Temperature Solid Oxide Electrolysis (using waste heat)	85-90%	[88], [89]
Steam Methane Reformation	85%	[89], [91]
Low-Temperature PEM Electrolysis	67-82%	[92]
Alkaline Electrolysis	62-82%	[92]
High-Temperature Solid Oxide Electrolysis (producing own heat)	60-70%	[88], [89]

Table 5 compares characteristics of the three major electrolysis technologies: alkaline electrolysis (AEC), proton exchange membrane electrolysis (PEMEC), and high-temperature solid oxide electrolysis (SOEC). Alkaline electrolysis is the most mature electrolysis technology and has been commercially available for decades [19]. AEC systems are typically well-suited to PtG applications where the power supply is often intermittent and fluctuating. AEC systems at ambient temperatures start in 30-60 minutes and can be operated between 20% and 150% of their design capacity [19]. The cost of an AEC is estimated at \$1,200/kW_e for a 1 MW_e system [18], [19], [48].

PEMECs are also a fairly mature technology with the first commercial system produced in 1978 [19]. PEMECs have the quickest start times of the three systems and produce high purity hydrogen gas [19]. They can operate at 5% of their design capacity and couple extremely well with dynamic power sources [19]. The capital cost of a 1 MW_e PEMEC systems is estimated at \$2,170/ kW_e, twice the cost of AEC systems with roughly the same efficiency [19].

SOECs operate at high temperatures between 650-1,000^oC enabling high efficiencies up to 90% [88], [89]. SOEC is the newest electrolyzer technology and is not yet commercially available. While cost estimates in the literature are rare, fuel cell systems with identical cells are reported to cost \$5,000-\$6,500 per kW_e [52] and it is assumed that SOEC system costs are currently at the high end of this range.

Many academic and industry experts expect SOEC to become the most broadly applicable PtG technology by 2030 as prices decrease [18].

Table 4. Comparison of AEC, PEMEC, and SOEC characteristics.

	AEC		PEMEC		SOEC	
Electrolyte	Aq. Potassium hydroxide		Polymer membrane		Yittria--stabilized Zirconia	
Operating Temp. (℃)	40-90	[92]	20-100	[92]	650-1,000	[93], [94]
Gas Purity (%)	>99.5	[95]	99.99	[96]	99.9	[18]
Lower Dynamic Range	10-40 %	[96]	0-10 %	[19], [97]	>30 %	[18]
System Response	Seconds	[98]	Milliseconds	[98]	Seconds	[18]
Cold-start time (min)	<60	[48]	<20	[48]	<60	[18]
Stack Lifetime (h)	60,000-90,000	[48]	20,000-60,000	[48]	10,000	[a]
Maturity	Mature	[18], [19]	Commercial	[92]	Demonstration	[18], [92]
Efficiency	62-82%	[92]	67-82%	[92]	60-90%	[88], [89]
2018 Capital Cost ($/kW$_e$)	1,080-1,300	[18], [48]	2,170-2,510	[18], [48]	6,500	[b]
2030 Capital Cost [c] ($/kW$_e$)	813	[18]	921-1790	[18]	1140-4,600	[18], [19]

[a] Industry experts interviewed estimated SOEC lifetimes to be significantly longer than 10,000 h [18]. However, there is little evidence in the literature proving longer lifetimes.
[b] Indirect from SOFC costs reported in [52].
[c] Projected capital costs from interviewed industry and academic experts [18].

All electrolysis systems have low maintenance costs compared to capital and electricity costs. Alkaline electrolysis O&M costs are approximately 1.5% of total capital expenditure (including initial capital cost and stack replacement costs) [49], [50]. Stack replacement occurs every 10 years over the system's 30-year operational lifetime [19], [49]. Each stack replacement cost is assumed to be \$840/kW$_e$ and is paid in monthly installments throughout the previous stack's lifetime with an 8% annual credit on payments. Modeled electrolysis systems have a 0.8 capacity factor. The O&M cost shown in Table 1 includes maintenance fees as well as stack replacement costs.

1.3.6 Methanation

Methane, the major component of natural gas, is a ubiquitous energy carrier in modern society. In the United States the natural gas distribution network contains 2.44 million miles of pipe, 400 underground storage facilities, and 1,400 compressor stations [99]. Most methane fuel used today is derived from fossil fuels but production from alternative sources has increased in recent years. Methanation is the process of producing methane and water from carbon oxides, usually CO_2, and molecular hydrogen. Two types of methanation systems are used commercially: catalytic and biological.

Biological methanation is often cited as having lower capital costs for very small systems while catalytic methanation is the more mature reactor technology and is widely used for larger systems [100]. Catalytic methanation of hydrogen occurs at temperatures between 200 and 550°C and pressures between 1 and 100 bar. The methanation process includes several chemical reactions, which are summarized by the following overall reactions: carbon dioxide hydrogenation (reaction (4)), water-gas shift (reaction (5)), and Boudouard reactions (reaction (6)) [19], [101]. The major methanation reaction (reaction (4)) is strongly exothermic.

$$CO_2(g) + 4H_2(g) \leftrightarrow CH_4(g) + 2H_2O(g) \quad (4)$$

$$CO_2(g) + H_2(g) \leftrightarrow CO(g) + H_2O(g) \quad (5)$$

$$2CO_2(g) \leftrightarrow C(s) + CO_2(g) \quad (6)$$

A typical industrial adiabatic fixed bed methanation system uses a series of 2 to 5 reactors with intercooling between reactors to maintain proper operating temperatures. These systems typically produce methane with 95-98% purity at efficiencies near 80% [19], [100], [102], [103]. Nickel is the most popular catalyst for the reactor beds because of its high selectivity and low material cost [19]. Catalyst cost fluctuates with the market value of nickel but is estimated to be 1.6-3.1 cents per 1000 scf_{NG} in methanation systems [104].

The endothermic electrolysis reaction in SOECs is known to pair well with the exothermic catalytic methanation process. This thermal coupling of the processes increases overall efficiency [105]. Additional considerations should be made for systems that do not operate at steady state conditions. For an electrolyzer with intermittent hydrogen production, a methanation reactor with rapid start up and shut down or significant hydrogen storage is required. Because hydrogen storage is very expensive, a dynamic methanation reactor is often the more economical choice [19], [106].

Capital cost estimates in the literature for catalytic methanation systems ranged from $170 to $640/$kW_{RNG}$ [19], [96]. In the relevant literature eight methanation plant capital cost values were reported together with a plant size description that are listed in Table 5.

Three plants reference methanation systems that produced RNG from renewable sources, and five plants described systems that produce synthetic natural gas (SNG) from nonrenewable sources. The capital and levelized costs were calculated for each plant and the values were plotted against plant size in Figure 4. The equation of the best fit line for capital cost values is shown in Table 1.

Table 5. Methanation plant sizes and capital costs found in the literature. Values reported are scaled to 2018$ as the original values were reported from 2004 to 2014.

Plant Type	Methanation Plant Size (MW_{NG})	Total Plant Cost (MM$, 2018)	Levelized Methanation Cost (2018$/$kW_{NG}$)	Source
RNG	5	2.7 [a]	5.4×10^{2} [a]	[107]
RNG	14.8	4.23 [a]	2.86×10^{2} [a]	[108]
RNG	110	19 [a]	1.8×10^{2} [a]	[107]
SNG	390	41 [b]	1.1×10^{2} [b]	[109]
SNG	410	44 [b]	1.1×10^{2} [b]	[109]
SNG	470	48 [b]	1.0×10^{2} [b]	[109]
SNG	510	51 [b]	1.0×10^{2} [b]	[110]
SNG	910.	109 [b]	1.20×10^{2} [b]	[104]

[a] Historical annual EUR-to-USD exchange rates and USD inflation values were used to calculate costs in 2018$.

[b] Historical annual USD inflation values were used to calculate costs in 2018$.

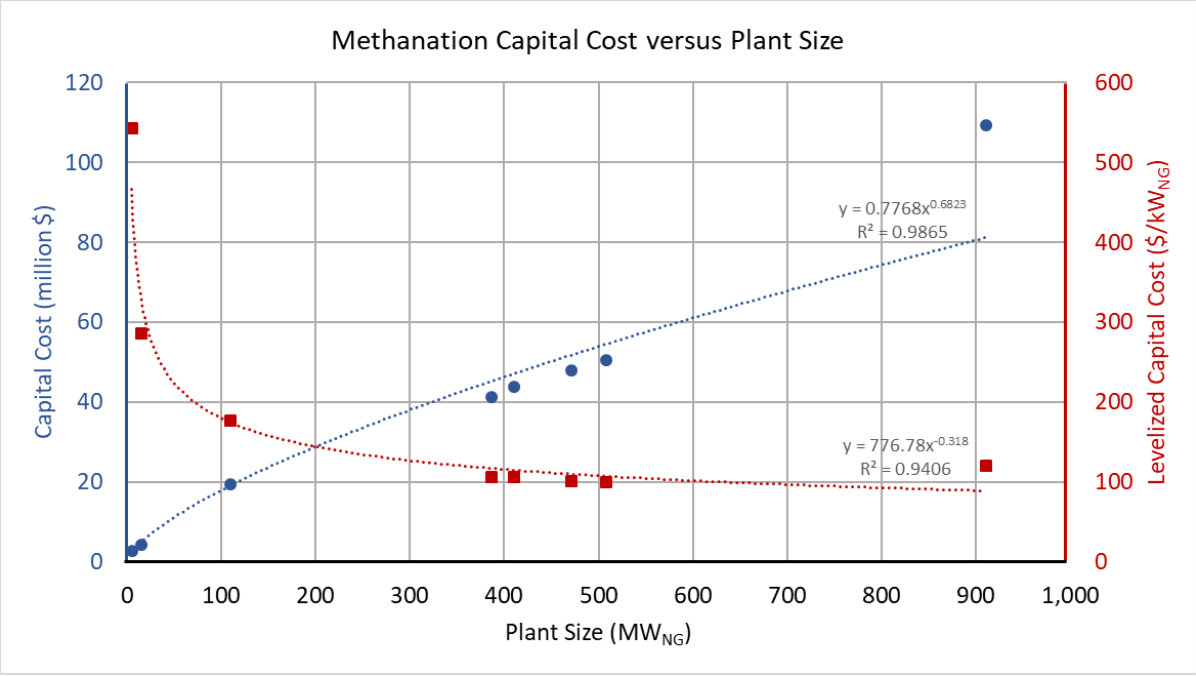

Figure 4. Best-fit lines for total and levelized methanation system capital cost versus plant size.

Methanation operating and maintenance costs in the literature are rare. One study showed O&M costs to be 8.35% of capital costs assuming that there is no cost for acquiring carbon dioxide [51]. This percentage is used to calculate methanation O&M costs in this study.

1.3.7 Solid Oxide Fuel Cell Systems

There has been a great deal of work demonstrating and developing the benefits of various alternative distributed energy resources [28], [85], [111]–[114]. Most fueled DER systems in operation today use internal combustion engines (ICEs) or microturbines. At the small scale, typical ICE and microturbine DERs have electrical efficiencies of 27-41% and 22-28%, respectively [52]. Unlike ICEs and Microturbines the electrical efficiency of fuel cells does not strongly correlate with size as they produce electricity directly from the chemical energy stored in fuels, i.e. hydrogen or natural gas. As such, even small-scale fuel cell systems have electrical efficiencies of 40-60% [115]. Solid oxide fuel cell systems integrate well with the existing natural gas infrastructure and are most often used for stationary power generation [115], [116]. In addition to high electrical efficiencies, SOFCs have high fuel flexibility, nearly zero criteria pollutant emissions, operate silently with few moving parts, and produce high quality waste heat that can be used for reclamation as electricity, heat, steam, or chilled water [115], [117]–[119]. In the case of coupled anaerobic digestion, the excess heat can be used to maintain digester temperature. In the United States space heating and cooling account for 54% of residential site energy consumption, and water heating accounts for an additional 18% [120]. Thus, DER SOFC systems can help meet heating and cooling loads as well as electricity demands when installed in residential communities. At the end of 2006, Osaka Gas Co., Ltd. developed and installed compact SOFC power generation units into four houses [121]. By April 2012 ,the company launched the first commercial residential SOFC-CHP system “Ene Farm type S” [121]. AC power from these SOFC generator units varied from 50 W to 700 W depending on electric demand [121]. Similar technologies are used by the ene.field project, the largest European case study of micro-CHP smart energy solutions for private homes [122]. Over 1,000 fuel cell

micro-CHP systems were installed under ene.field in ten European member states as of the programs end in 2017 [123]. Several recent studies have tested and modeled solid oxide fuel cells for more complex residential and commercial distributed energy and energy storage applications [28], [88], [111], [112], [124], [125].

A complex system of physical, chemical, and electrochemical interactions dictates fuel cell operation. The specific processes vary slightly between fuel cell types, but all directly convert chemical energy stored in fuels to electricity using an electrolytic cell (Figure 5). In an ideal SOFC fuel enters the cell's anode compartment and an oxidant, typically air, enters the cathode compartment where oxygen is reduced. The electrolyte transports oxygen ions from the cathode to the anode where they react with hydrogen to form water. The electrons freed during the oxygenation of hydrogen at the anode flow through the external load to the positively charged cathode and produce the useful electrical current. SOFCs operate at high temperatures of 500-1,000 °C and use a solid ceramic (metal oxide) electrolyte, typically yittria-stabilized zirconia, for which the fuel cell is named [115].

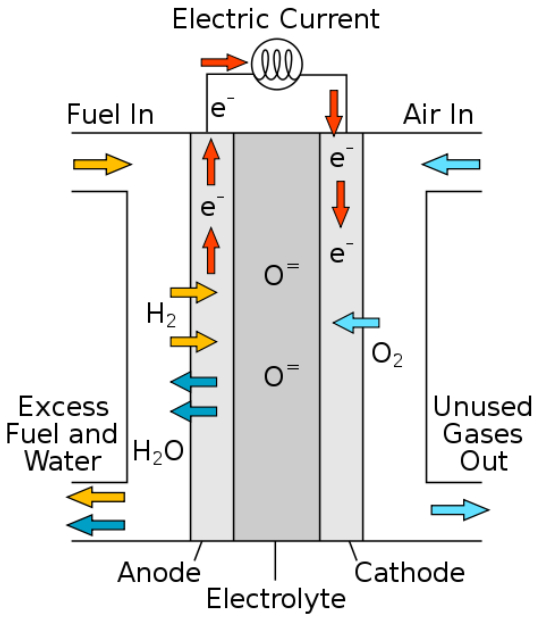

Figure 5. Schematic of an SOFC electrolytic cell [126].

The Nernst potential describes the concentration- and temperature-dependent thermodynamic limit of cell voltage that drives electricity generation. Voltage losses are subtracted from the Nernst potential and the remaining value is multiplied by the current to calculate electrical power produced by the cell. As applied to an SOFC, the Nernst potential equation is

$$E = E^o + \frac{R_U T}{2F} \ln\left(\frac{P_{H_2}}{P_{H_2O}}\right)_{anode} + \frac{R_U T}{2F} \ln\left(P_{O_2}^{1\backslash 2}\right)_{cathode}.$$

Assuming that the pressures in the anode and cathode compartments are the same, this expression reduces to

$$E = E^o + \frac{R_U T}{2F} \ln\left(\frac{X_{H_2} X_{O_2}^{\frac{1}{2}}}{X_{H_2O}} P_{cathode}^{\frac{1}{2}}\right)$$

where E is the Nernst potential in volts, E^o is the ideal reversible cell potential in volts, R_U is the universal gas constant in $\frac{kJ}{kmol \cdot K}$, T is the electrolyte temperature in Kelvin, F is Faraday's constant in $\frac{coulombs}{mol_e}$, P_i is the partial pressure of species i normalized by atmospheric pressure, and X_i is the mole fraction of species i.

SOFCs typically operate on natural gas, but a great deal of work has been performed to characterize the performance of SOFC systems fueled by hydrogen, biogas, and even ammonia [84], [116], [127]–[129]. Regardless of fuel type, fuels must be cleaned by removing sulfur, siloxanes and chlorine compounds before use in an SOFC or an ICE [76], [130]. Prior to use in SOFCs, biogas must be upgraded to standards used for ICEs to avoid carbon deposition and carbon-induced electrode catalyst degradation [76]. One study used AspenPlus™ software to model an SOFC operating on cleaned biogas for 7,000 hours, achieving a system electrical efficiency of 55% [117]. Papurello, et al. recorded the stable performance of an SOFC operating on simulated biogas (60% CH_4 and 40% CO_2 by volume) for over 200 hours [64]. In a 2015 paper, the same group operated an SOFC on cleaned biogas from the AD of OFMSW for 400 hours without significant carbon deposition [64], [76]. Additionally, several

experiments have concluded that SOFCs can operate on biogas containing less than 45% CH_4 [64], [76], [117], and one 2017 experiment even validated a dynamic SOFC model operated on biogas [131].

Currently, nearly all commercial SOFC units only operate at steady-state conditions and like most power systems are designed only considering system performance at steady-state operation [132]. Experimental testing has shown that SOFC stacks can operate dynamically. However, thermal cycling that occurs during start-up and shut-down as well as interruptions in the fuel supply accelerate fuel cell degradation mechanisms [124], [133], [134]. Modeling dynamic operation is essential to understanding experimental transient system performance and utilizing such performance characterization. In the past 15 years, several transient SOFC modeling approaches [132] and SOFC power and temperature control strategies for rapid load following have been described in the literature [85], [113], [135], [136].

As SOFCs are newly commercialized, reports on SOFC capital costs vary widely. However, most reports estimated the cost of an SOFC system including installation to be \$5,000-6,500 per kW_e [52], [53]. Lower levelized costs are cited for systems above 50 kW in size and if increased SOFC production volume is accounted for [137], [138]. As fuel cell systems are easily scalable like most other distributed energy technologies, their cost is relatively constant for all system sizes. An SOFC capital cost of \$5,000 per kW_e is used in subsequent calculations. The SOFC O&M cost equation presented in Table 1 assumes a capacity factor of 0.8, a stack replacement cost of \$1,500, a stack lifetime of 5 years, and that replacement payments are made monthly over the previous stack lifetime. This report uses data from the experimental operation of a BlueGEN 1.5 kW SOFC from SOLIDpower SpA to verify SOFC steady-state and dynamic efficiency and behavior.

1.3.8 Axial Compressors and Centrifugal Blowers

The Simulink-based SOFC model previously developed at the NFCRC included an industrial-scale axial compressor (AC) model, an example of which is shown in Figure 6, to cool the model SOFC system.

The BlueGEN uses a backward-curved single intake centrifugal blower (CB), ebm-papst model NRG 118 shown in Figure 8, which is typical of smaller-scale fuel cell systems.

Axial compressors produce a continuous flow of pressured gas and are characterized by alternating rotating and static airfoil stages [139]. Air flows parallel to the axis of rotation along the outer edge of cylindrical airfoil stages. The rotor stage blades exert torque on the fluid and increase fluid velocity tangential to the compressor stage rotation, and thus, increase fluid angular momentum. Stationary stages remove this angular momentum by converting kinetic energy to pressure energy as fluid velocity decreases. Alternating stages are added in series until desired pressures are obtained.

Compressor performance is characterized by a compressor map, which allows for determination of operating conditions. A typical compressor map shows pressure rise on the y-axis as a ratio of static pressures at the inlet and outlet stagnation points (i.e. points where fluid velocity is zero and all kinetic energy has been transformed to pressure energy) and mass flow along the x-axis. Figure 7 shows an example compressor map. Efficiency contours are overlaid on performance curves corresponding to rotational speeds. A surge line identifies the maximum pressure ratio for each mass flow at which there is a steep decline in compressor performance.

Axial compressors are integral in large gas turbines such as jet engines, high speed ship engines, and small-scale power stations. Axial compressors exhibit high pressure ratios, high efficiency and large mass flow rate in relation to their cross-sectional size. They can, however, be complex and expensive compared to other compressor types due to their multi-stage design.

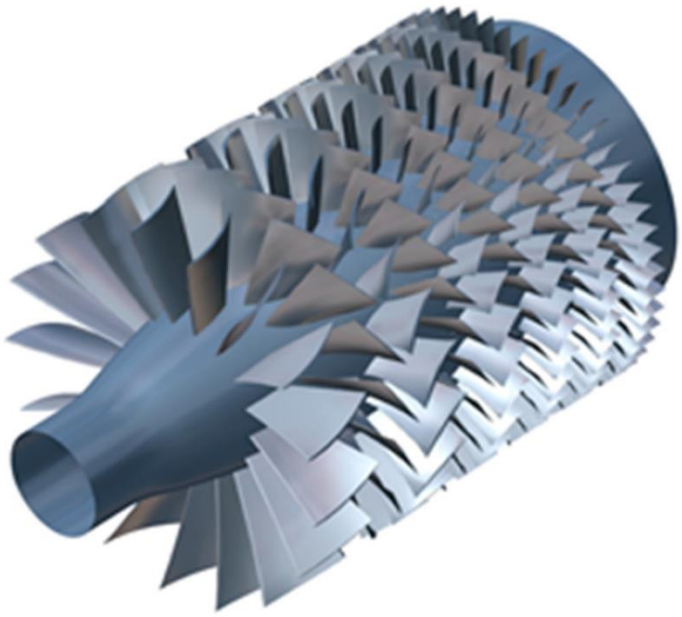

Figure 6. Example axial compressor configuration [140].

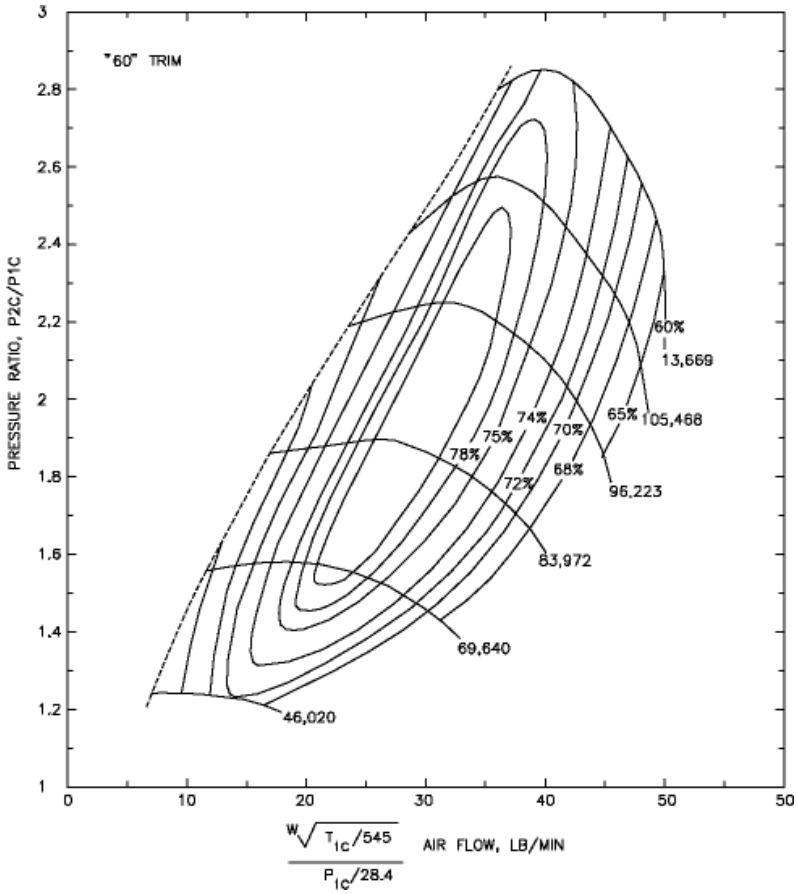

Figure 7. Garrett T04E-60 example axial compressor map [141].

Centrifugal blowers (also called radial blowers) are the most common type of blower used by the HVAC industry [142]. They are extremely quiet and both simpler and cheaper to manufacture than axial compressors [142]. Centrifugal blowers are composed of fan blades mounted on a cylindrical hub rotating on a driveshaft within the fan housing. Air enters through the center of the hub parallel to the axis of rotation and is accelerated outward by the hub's rotating blades. The rotating fan blades impart kinetic energy to the air increasing its speed and volume. Fan housing directs the exiting airflow into a single stream. Centrifugal blowers are constant displacement devices, meaning that at a constant fan speed a constant volume of air moves through the blower resulting in air flow with constant velocity.

Figure 8. ebm-papst model NRG 118 centrifugal fan used in the BlueGEN SOFC system [143].

Blower performance is described using two characterization curves: a pressure-volume curve and a brake horsepower curve. The pressure-volume curve characterizes the static pressure change for each impeller speed in RPM. The brake horsepower curve identifies the break power for each fluid flow rate. For single speed blower, such as the NRG 118, power consumption is nearly constant for all flow rates in the small range of operative impeller speeds. Horsepower curves are used to relate static pressure change, impeller speed, and volume flow rate at nearly constant power consumption. The NRG 118 has a maximum power consumption of 56 W and operates according to the characteristic curves in Figure 9 and Figure 10 [143].

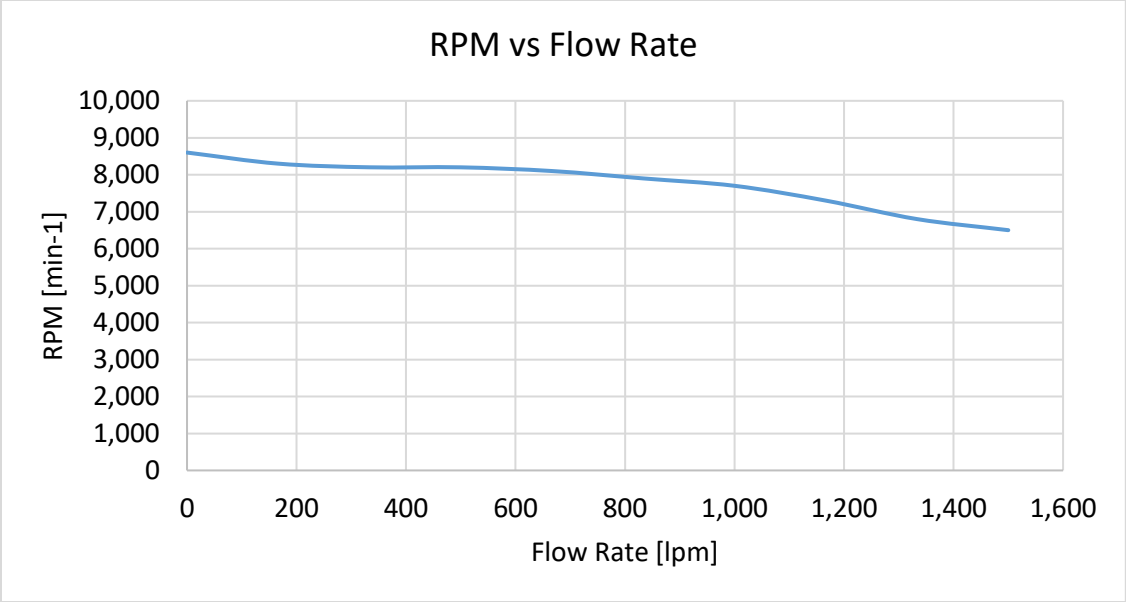

Figure 9. ebm-papst model NRG 118 centrifugal blower characteristic curve showing motor RPM over air flow rate [143].

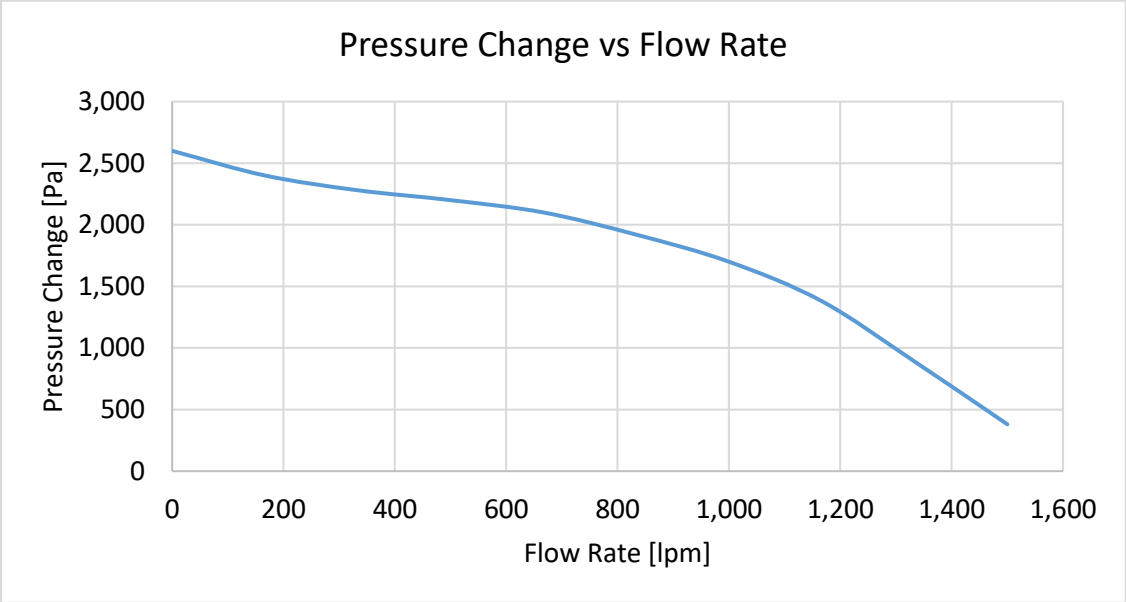

Figure 10. ebm-papst model NRG 118 centrifugal blower characteristic curve showing the pressure difference between air flowing out of and into the blower over air flow rate [143].

1.3.9 Natural Gas Pipeline Injection

Injection of RNG into the natural gas distribution grid allows for the use of natural gas pipelines and infrastructure for the transport and storage of renewable fuels. If a renewable fuel is to be injected into the natural gas distribution grid, it must be processed to comply with quality requirements

established by the local gas utility. California has the most stringent gas quality standards (see Rule No. 30 by the Southern California Gas Company (SCG)) when compared to other states and European countries [144]–[146]. Strict standards correlate with increased biogas upgrading costs [145]. Northern California's major utility provider, Pacific Gas and Electric Company, estimates the cost of interconnection to the natural gas pipeline for a gas producer to be $1,500,000-3,000,000 in California (compared to $75,000-500,000 in other states) [147], [148]. SCG, the natural gas utility company servicing Oak View, requires three engineering studies totaling over $200k over the course of one year before an injection project can be approved [149]. The California Public Utilities Commission estimates a cost of $1.2-1.9 million to build a point of receipt facility with a monthly operating cost of $3,500 [147]. Parker, et al. presents functions (found in Table 1) describing capital and O&M costs for pipeline injection of RNG in California that are corroborated by the costs cited by utility companies [37]. These pipeline injection cost equations assume a 30-year economic lifetime.

Injection of hydrogen into the natural gas grid is currently being done in several countries, mainly in Europe [150]. Scientific literature has reported that 5-20% hydrogen would be tolerable for most residential and commercial end-use appliances [99]. In 2015 researchers at University of California at Irvine in partnership with SCG installed the first hydrogen pipeline injection project in California [151], [152]. Electrolysis from excess solar electricity produces renewable hydrogen that is injected into a natural gas pipeline directly upstream of the campus's power plant [151]. Hydrogen pipeline injection is assumed to have the same costs as RNG pipeline injection.

CHAPTER 2: METHODOLOGY

In order to accomplish the goal of evaluating the renewable fuel energy potential for the design area, the renewable potential must first be established. Renewable resources considered in this work are wind, solar, and municipal waste streams.

Historically, wind speeds in the Huntington Beach area have not been high enough to support wind power generation [153], [154]. As a result, the wind resource is assumed to be infeasible. Available solar radiation was defined using Typical Meteorological Year 3 data [155].

Quantified waste stream information was provided by the operators of the Oak View waste transfer station (OVWTS). The following sections describe the transformation of these renewable energy streams into renewable fuel quantities.

After the renewable resources have been quantified, different renewable fuel production, conversion, and use as renewable natural gas or fuel for renewable electricity production is be explored. As part of this effort, dynamic SOFC operation on natural gas and clean biogas were explored. These efforts included operating an SOFC at steady-state and dynamically on natural gas, using experimental data to verify and adjust an SOFC model, and simulating SOFC dynamic operation on clean biogas. Ultimately, pathways for utilizing renewable fuel energy potential were selected that involved only steady-state SOFC operation on hydrogen fuel and renewable natural gas.

2.1 Energy Conversion Pathways

Six production and use paths consisting of combinations of solar PV, electrolysis, SOFC, and natural gas pipeline injection technologies are evaluated for energy efficiency, cost-effectiveness, and ability to meet Oak View energy demand. Methanation was also considered. However, hydrogen production was not large enough in any scenario to accurately calculate methanation costs. Figure 11 contains flowcharts of energy flow pathways through the Oak View community for each path considered. All six paths produce either RNG or electricity. Odd numbered paths terminate with RNG

injection into the natural gas grid, and even numbered paths conclude with electricity generation via SOFC. Table 6 summarizes the technologies used in each path. This study assumed an electrolysis efficiency of 72%, a methanation efficiency of 80%, and an SOFC electrical efficiency of 60%.

(a) Path 1: PV-PI

(b) Path 2: PV-SOFC

(c) Path 3: AD-PI

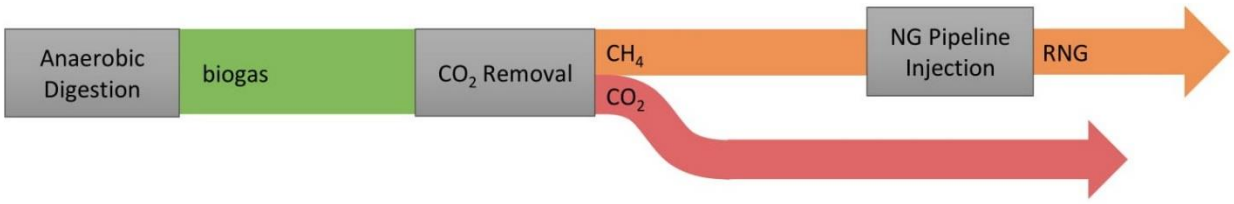

(d) Path 4: AD-SOFC

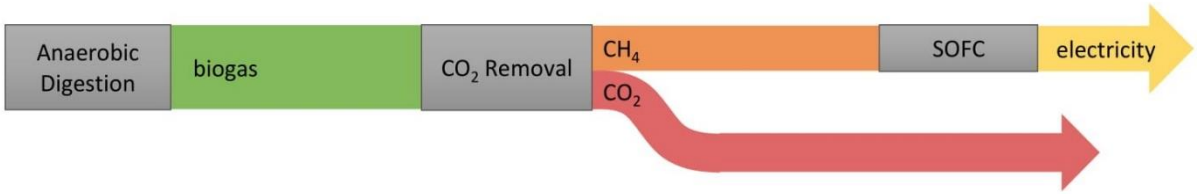

(e) Path 5: PV&AD-PI

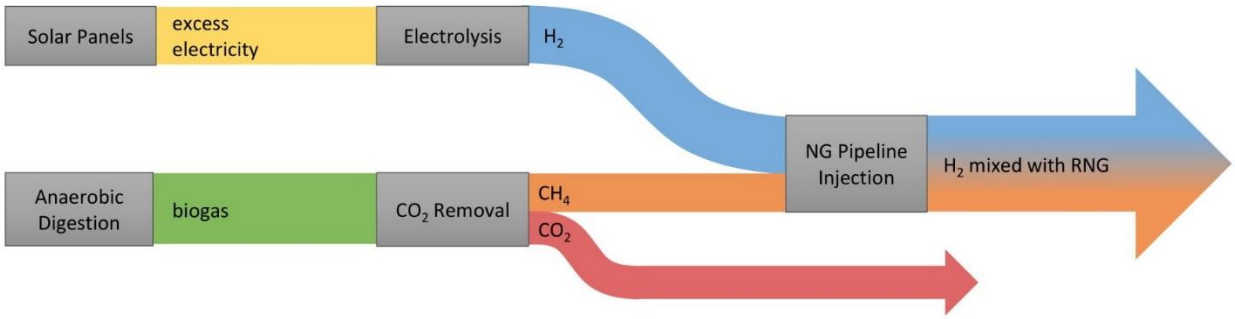

(f) Path 6: PV&AD-SOFC

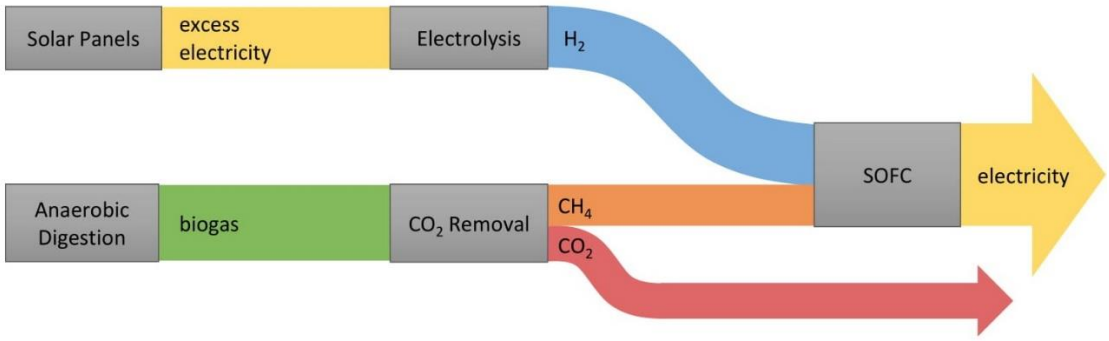

Figure 11. Flowcharts showing the energy and material flow through the production, conversion, storage, and end use for all six pathways. Width of lines are not drawn to scale and do not include inefficiencies and energy losses.

Table 6. Technologies used in all six production, conversion, storage, and end use paths considered.

Path #	Path Name	Included Technologies					Path Description
		Solar PV (PV)	Anaerobic Digestion (AD)	Electrolysis (EC)	SOFC	NG Pipeline Injection (PI)	
1	PV-PI	✓	X	✓	X	✓	Natural gas pipeline injection of H_2 fuel from excess solar electricity.
2	PV-SOFC	✓	X	✓	✓	X	Electricity production via SOFC using H_2 fuel from excess solar electricity.
3	AD-PI	X	✓	X	X	✓	Natural gas pipeline injection of CH_4 fuel from anaerobic digestion.
4	AD-SOFC	X	✓	X	✓	X	Electricity production via SOFC using CH_4 fuel from anaerobic digestion.
5	PV&AD-PI	✓	✓	✓	X	✓	Natural gas pipeline injection of H_2 fuel from excess solar electricity and CH_4 fuel from anaerobic digestion.
6	PV&AD-SOFC	✓	✓	✓	✓	X	Electricity production via SOFC using H_2 fuel from excess solar electricity and CH_4 fuel from anaerobic digestion.

The final pathway considered in this work assumes that AD is not locally adopted, but the organic waste is diverted to a preexisting digester. In this case, the cost of shipping the waste and paying a tipping fee must be weighed against potential revenue from generating renewable fuel. This option is considered as the final scenario as interviews with waste transfer station operators indicate that this is the most likely pathway to occur.

Note that gasification of organic waste and methanation of renewable hydrogen were both originally considered. Despite being able to produce a hydrogen rich stream, gasification was not considered after discussions with waste transfer station operators due to the quality and moisture content of the waste feedstock. Methanation was omitted due to a reduction in renewable fuel energy, but more importantly. More importantly, the renewable hydrogen production results are small relative to the capacity of methanation systems reported in the literature [102]–[105].

2.2 Experimental Verification and Optimization of SOFC Model

A BlueGEN 1.5 kW SOFC from SOLIDpower was installed and operated as part of a dynamic CHP energy generation system in a simulated ZNE home setting. Experimental performance measures were used to verify a MATLAB Simulink model previously developed at the NFCRC for SOFC operation on

natural gas fuel [24]. The model was then used to simulate the BlueGEN performance operating on clean biogas (60% CH_4 and 40% CO_2).

2.2.1 SOFC Installation and Operation

The simulated ZNE electricity generation system included the 1.5 kW SOFC, a simulated residential electric load and PV profiling system, a waste heat rejection system, and an energy flux monitoring and logging system. The SOLIDpower BlueGEN fuel cell system used an external reformer and a planar electrochemical cell design. The PV profiling system simulated a dynamic electricity load, the waste heat rejection system contains a cooling loop, and the energy flux monitoring system included all data acquisition equipment and processes. A mass flow meter on the natural gas supply pipeline was used to record the amount of natural gas consumed by the system. Waste heat was measured using two thermometers: one measuring the temperature of water produced by the SOFC heat exchanger and one measuring the temperature of water returning to the SOFC heat exchanger from the cooling loop.

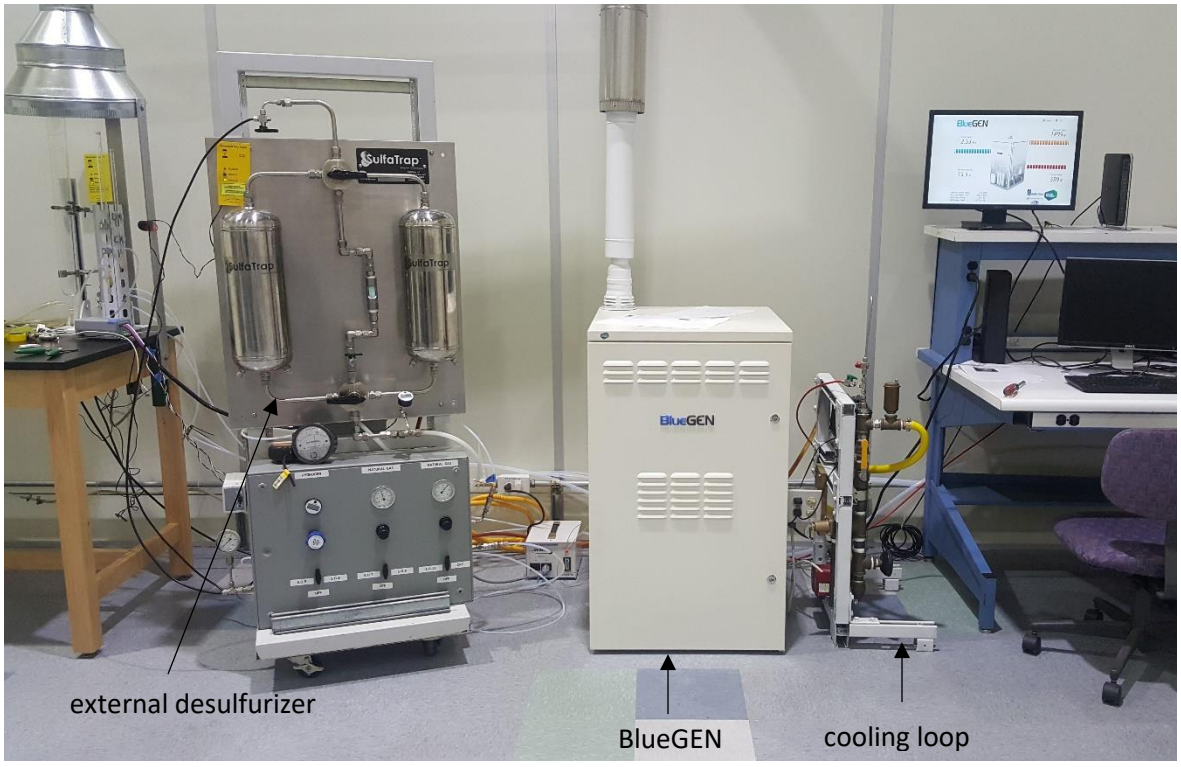

Figure 12. BlueGEN installation at the NFCRC.

Electrical power demand data recorded at 5-minute intervals for a single-family residence in Irvine, CA, over one week was used to approximate residential electricity demand. The weekday electricity demand profiles were averaged to produce a mean weekday power demand curve, shown in Figure 13. Available solar radiation was defined using National Solar Radiation Data Base data [156]. The roof space suitable for PV installation was measured using Google Earth Pro [157], and the installation capacity was calculated assuming 108 ft^2 per kW installed PV capacity. The dynamic solar PV electricity production was obtained using HOMER Pro software.

The SOFC load profile was selected to complement electricity production of a rooftop PV installation on a day in July 2016 in Irvine, CA and to maximize electricity production when solar meets residential demand and to minimize electricity production when solar does not meet residential demand. This was accomplished by matching the net electrical demand while constrained to 33-100% of the fuel cell's design power output and a 0.5 kW per hour ramp rate. The resulting SOFC power profile (Figure 14) specified 0.5 kW steady state operation during the night and midday with spikes to 1.5 kW operation during morning and evening demand peaks. The morning spike was shorter than the evening spike. These power profiles are plotted in Figure 13.

The combined time-resolved PV and fuel cell electricity production nearly meet all residential demand. The large spikes between 7:00 and 9:00 pm could be partially met by increasing the SOFC to its maximum power output during these hours. However, during nearly all daylight hours the minimum SOFC power summed with solar production generates significantly more power than demanded. This overproduction could be stored using a battery and used later to meet the unmet evening demand. Additionally, all sharp demand peaks greater than the total power production could be met using the same battery storage system.

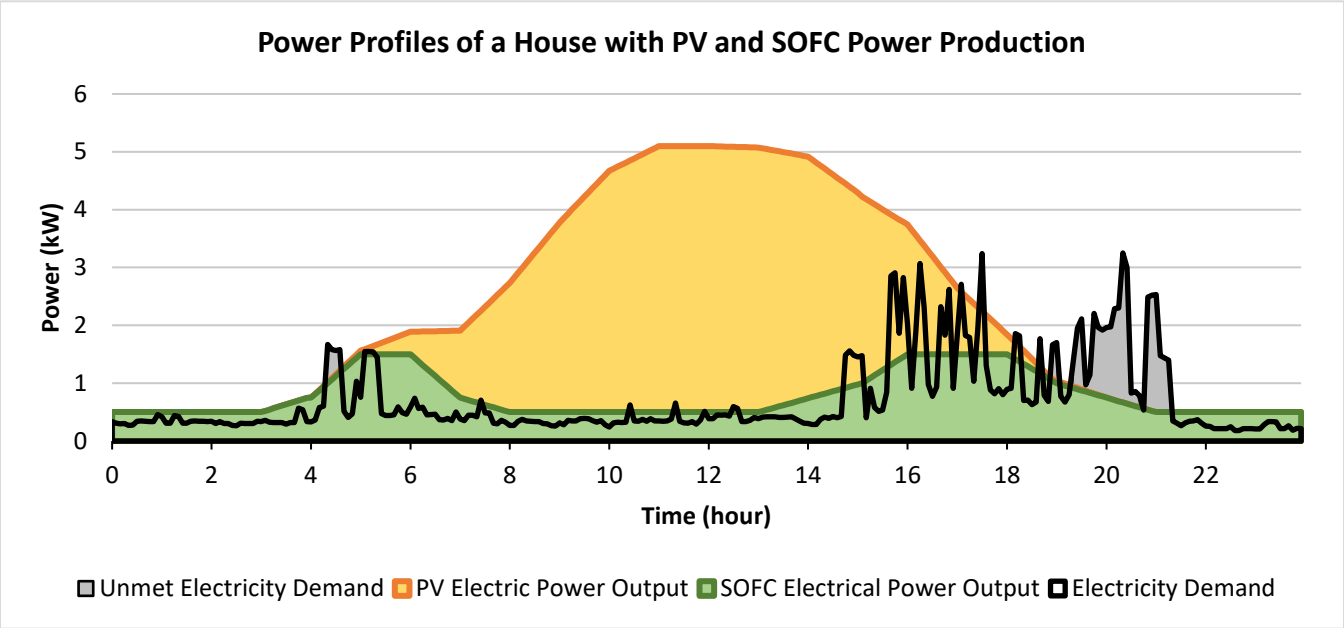

Figure 13. Averaged example single-family residence weekday electrical power demand overlaid on SOFC and PV electricity production.

The BlueGEN was operated at steady state conditions at the maximum power output of 1.5 kW for 4,578 hours (191 days) between December 7, 2016 and June 16, 2017. The BlueGEN was then run at steady state conditions at 0.5 kW (33% of its maximum capacity) for 48 hours. Then the fuel cell was programmed to follow a dynamic power profile simulating a night-time and mid-day baseload of 0.5 kW and ramping up to and down from two periods of steady-state 1.5 kW power production to meet morning and evening demand peaks. The morning peak is comprised of a two-hour ramp to 1.5 kW, one hour of steady-state operation at 1.5 kW, and a two-hour ramp down to 0.5 kW. The evening peak is

comprised of a three-hour ramp to 1.5 kW, two hours of steady-state operation at 1.5 kW, and a three-hour ramp down to 0.5 kW. The BlueGEN was operated dynamically using this power profile, shown in Figure 14, for 528 hours (22 days). The BlueGEN was then returned to steady state operation at its maximum power output of 1.5 kW for 839 hours (approximately 35 days) before initiating the three-day shutdown procedure. The BlueGEN was in operation for a total of 5,995 hours (approximately 250 days). Static and dynamic operating performance is characterized using experimental results. These data are used to define the accuracy of model results and dynamic operating performance under an example residential load.

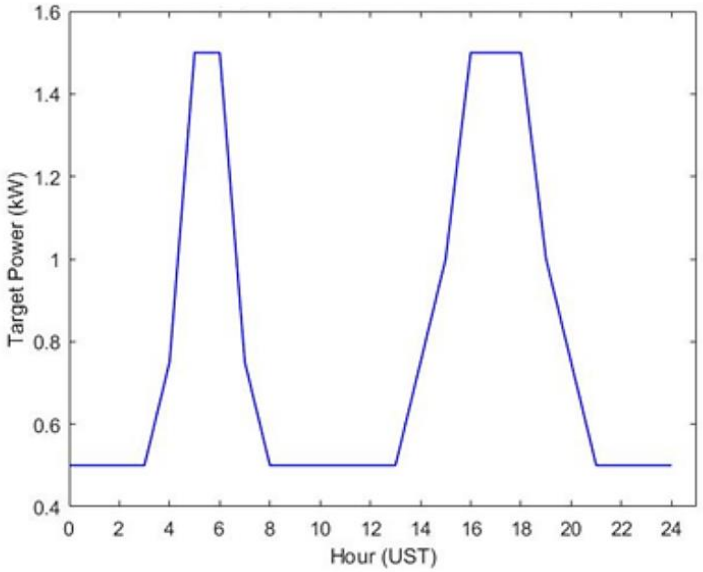

Figure 14. BlueGEN dynamic power profile.

2.2.2 SOFC Dynamic Model Verification with Natural Gas Fuel

A MATLAB Simulink model previously developed at the NFCRC was modified to simulate the BlueGEN's performance [24]. The original code used an axial compressor (AC) model to simulate air flow through the SOFC system and is referenced in the following sections as the SOFC-AC model. Five parameters were recorded for both steady-state and dynamic operation: stack voltage, stack current, cathode gas exit temperature, anode tail oxidizer gas temperature, and air flow. From these parameters,

stack power was also calculated. The experimental measurements reported by these six parameters were used to validate model output.

The Simulink code models anode supported cells in a single stack to reach the desired power output. The BlueGEN system uses four cell stacks. Thus, the model stack current was multiplied by four and the model stack voltage was divided before to obtain values comparable to the actual BlueGEN system. Significant input parameters of the simulation include a 1.5 kW desired net power output, a specified power current density of 230 mW/cm^2, and a fuel utilization rate of 85%. Other model assumptions are shown in Table 7.

Table 7. Initial SOFC-AC simulation (a) electrochemical and (b) physical parameters for natural gas operation.

(a)	***Electrochemical Parameters***	
	System net power output	*1.5 kW*
	Steam-to-carbon ratio	*2.0*
	Fuel utilization	*0.85*
	Current density	*230 mW/cm^2*
	External CH_4 reformation fraction	*0.80*
	Activation current density	*1000 A/m^2*
	Limiting current density	*6000 A/m^2*
	Cathode exchange current density	*5300 A/m^2*
	Electrolyte conductivity	*6.19 $W/m \cdot K$*
(b)	***Physical Parameters***	
	Blower pressure ratio	*1.2*
	Stack temperature difference	*50 K*
	Anode thickness	240e-6 m
	Cathode thickness	60e-6 m
	Membrane thickness	8e-6 m
	Active area per cell	3.481e-3 m^2

The previously developed Simulink SOFC model dynamic axial compressor was replaced with a steady-state centrifugal blower (CB) in this work. The updated code with a centrifugal blower model is referenced as the SOFC-CB model throughout this thesis. The centrifugal blower model developed operates at 56 W, a pressure difference of 2350 Pa, and a volume flow rate of 130 LPM as described by the NRG 118 characteristic curves in Figure 9 and Figure 10 and the ebm-papst blower specification sheet [158]. Model parameters including SOFC power density, fuel utilization, cell component thicknesses and specific heats, heat exchanger volume, and operating temperature, were varied

systematically in an attempt to match other model outputs to experimental BlueGEN operation data for both dynamic and steady-state operation.

2.2.3 Dynamic Simulation of SOFC Operation of Biogas Fuel

The initial Simulink model with an axial compressor was also used to model BlueGEN operation on simulated biogas (60% CH_4 and 40% CO_2). No model parameters were altered, and the model was not optimized for operation on this new fuel. Operation parameters of the model operating on simulated biogas are compared to operational parameters of the same model operating on natural gas.

2.3 Community Assessment of Renewable Energy Assets

Southern California has high solar irradiance and is a good location for solar PV power production [159]. Historically, wind speeds in the Huntington Beach area have not been high enough to support wind power generation [153], [154].

A waste collection and distribution facility located in Oak View was the only source of large-scale biomass resources within Oak View. The Oak View waste transfer facility (OVWTF) collects municipal solid waste and plans to separate and divert the OFMSW to a nearby anaerobic digester in the next few years [160]. It currently accepts commercial, residential, and construction waste as well as recyclable materials. Anaerobic digestion of municipal wastewater was not considered as there is no processing facility in the community.

2.2.4 Community PV Penetration Scenarios and PtG Technology Sizing

In order to determine the excess solar energy, both the community load and solar PV system must be known. Concurrent work using the URBANopt [161]community energy simulation tool based on the OpenStudio [162] and EnergyPlus [163] building energy simulation tools was used to generate a community scale energy use profile for the Oak View community. The models predicted that the

community will use over 25.8 GWh per year, yielding an average electrical demand of 2.95 MW, and a peak demand of 4.81 MW.

Solar PV capacity was predicted by using the solar PV design tool Helioscope to determine the maximum solar potential for all 310 buildings within the design area [164]. Based on this work, it is projected that up to 14.6 MW of solar PV generation can be installed across the Oak View community. After conversations with solar project developers, a second scenario in which only relatively large-scale installations are pursued (> 100 kW) was considered, reducing solar PV capacity to 6.5 MW. This second scenario is considered the "Utility" scenario due to the selection criteria for any solar PV system yielding system sizes that are more favorable to utility ownership within the community.

Net solar electricity generation was calculated by summing the positive differences of total community solar electricity production and total community electricity demand for each hour over the year. The unmet load was calculated similarly as the absolute value of the sum of all negative differences of total community solar electricity production and total community electricity demand for each hour over the year. It was assumed that electricity generated within Oak View could be consumed at any load location in Oak View without incurring grid transportation losses.

2.2.5 Community Biogas Potential from Anaerobic Digestion of OFMSW

A waste collection and distribution facility located in Oak View was the only source of large-scale biomass resources within Oak View. This facility collects municipal solid waste and plans to separate and divert OFMSW to a nearby anaerobic digester in the next few years [160]. Anaerobic digestion of municipal wastewater was not considered as there is no processing facility in the community.

During a meeting with OVWTS officials in May 2017, it was stated that the Oak View transfer station processed approximately 200,000 tons of waste annually in 2016 [160]. About 39% of total waste processed was organic, and 25% of the total waste processed was food waste [160]. Table 8 shows the assumed composition of waste processed at the facility annually.

Table 8. Quantity of waste processed annually in 2016 at the Oak View waste transfer station categorized by type.

Waste Material	MSW Processed by OVWTS (tpy)	Percentage of Total
Non-Organic MSW	122,000	61%
Organic MSW	78,000	39%
Food Waste	50,000	25%
Yard Waste & Other Organics	28,000	14%
Total	200,000	100%

Publicly available data on municipal waste generated in Huntington Beach were compiled and used to calculate the percentage of waste processed by the OVWTS that can be attributed to the residents of Oak View [165], [166]. The average biogas yield of food and yard waste for full-scale wet OFMSW digesters cited in a 2008 report by the California Integrated Waste Management Board was 3.59 ft^3 per ton (0.112 m^3 per kg) feedstock [167]. The amount of biogas produced from OFMSW generated by Oak View residents was calculated assuming a biogas density of 1.15 kg/m^3 and composition of 60% CH_4 and 40% CO_2. Biogas upgrading facilities were assumed to have an efficiency of 90% [37].

2.2.6 Waste Transfer

Four types of heavy-duty vehicles are considered for the transport of all 78,000 tons of organic MSW processed by the OVWTS in 2017: class 7 single unit short-haul (SUSH), class 7 single unit long haul (SULH), class 8 combination short-haul (CSH), and class 8 combination long-haul (CLH). These categories are defined using gross vehicle weight rating (GVWR). Class 7 vehicle GVWRs range from 26,001 to 33,000 lbs. and have a maximum payload capacity of 18,500 lbs. [168]. Class 8 vehicle GVWRs range from 33,001 to 80,000 lbs. and have a maximum payload capacity of 54,000 lbs. [168]. All trucks are assumed to be 2017 diesel-powered models. Payload capacity, annual miles traveled per vehicle, miles per gallon diesel (MPG_{diesel}), and annual criteria pollutant emissions modeled using AFLEET for the four truck types are compared in Table 9 [86].

Table 9. Properties of and annual criteria pollutant emissions from the annual operation of one vehicle in each truck category [86], [168].

Truck Class	**7**		**8**	
Truck Description, 2017 Model	Single Unit Short-Haul	Single Unit Long-Haul	Combination Short-Haul	Combination Long-Haul
Maximum Payload (lbs.)	18,500	18,500	54,000	54,000
Annual Miles Per Vehicle	16,500	23,000	65,000	170,000
MPG_{diesel}	7.4	6.6	7.4	7.3
MPGGE	6.4	5.7	6.4	6.3
Annual Fuel Consumption (GGE/year)	2,573.0	4,044.0	10,137.8	26,877.4
Annual CO_2 Emissions Per Vehicle (US Tons)	31.7	49.8	124.8	330.9

Once the vehicle has arrived at the established AD, it is assumed that a tipping fee is required to dump the organic waste. The tipping fee is the cost per ton of feedstock deposited, or "tipped", by a transport truck at an existing anaerobic digester. The tipping fee is the price the anaerobic digestion facility must charge for accepting feedstock in order to recover the costs associated with the AD facility. The current work does not determine current tipping fees but looks to establish a ceiling on the maximum allowable tipping fee when considering the costs, incentives for, and value of renewable natural gas.

If the AD derived RNG is used to replace diesel fuel, then RNG sales can be supported using Low Carbon Fuel Standard (LCFS) and Renewable Identification Number (RIN) credits. The LCFS credit price is found for compressed RNG being used as a substitute for diesel fuel using the assumption that RNG has carbon intensity score of 11.26 g CO_2e/MJ [169], the LFCFS credit trading price is $154 [170], the EER value is 1 for compressed natural gas used in a heavy-duty compression ignition engine [171], and the compliance year is 2020. The resulting LCFS credit price is $13.09/MMBTU [171]. For RNG that is not used as vehicle fuel, P_{LCFS} is zero. The RIN waiver credit for cellulosic RNG (D3) is $18.39/MMBTU [172]. Considering that a high RNG price can be offset by these credits, the maximum allowable tipping fee such that the eventual RNG cost does not surpass the cost of conventional natural gas is shown in Equation (2).

$$P_{tip} = P_{NG} - P_{fuel} + P_{LCFS} + P_{RIN} \quad (2)$$

where P_{tip} is the tipping cost in $/ton OFMSW, P_{NG} is the market price of natural gas, P_{fuel} is the price of diesel fuel used to truck OFMSW from Huntington Beach to Perris per MMBTU, P_{LCFS} is the Low Carbon Fuel Standard (LCFS) credit price for low carbon transportation fuel, and P_{RIN} is the Renewable Identification Number (RIN) credit price.

CHAPTER 3: RESULTS

3.1 BlueGEN Experimental Results and Initial SOFC Model Verification using Natural Gas Fuel

Due to a calibration error during the BlueGEN installation process, natural gas consumption rate of the experimental system was not recorded accurately during dynamic operation. Thus, efficiency could not be calculated accurately. As such, the experimental data presented in this thesis was recorded and reported by SOLIDpower using the BlueGEN's built-in sensors. The uncertainty of these measurements was not reported by SOLIDpower and so is not presented in this Thesis.

The initial model characterization results comparing BlueGEN experimental data recorded and reported by SOLIDpower and data from the initial Simulink SOFC Axial Compressor (SOFC-AC) model during dynamic operation on natural gas fuel are described in this section. The simulated natural gas composition is 95% CH_4, 1% CO, 3% N_2, and 1% CO_2, in accordance with reported utility concentrations in California [173], [174].

Experimental and model values are compared for six benchmark quantities: stack power, stack current, stack voltage, air volume flow rate, cathode exit temperature (CET), and anode tail gas oxidizer (ATO) temperature. Modeling results are also shown for load power, efficiency, and stack temperature difference. The experimental data from June 19, 2017, is the most complete of all dynamic run days and is used for comparison with all model outputs except for air flow rate. Experimental air flow data was most complete on June 27, 2017 and is used for comparison to model air flow output.

Figure 15 shows the experimental and model stack power profiles over the 24-hour test period. The experimental stack power is approximately 0.15 kW larger than the model stack power over the entire profile. The model stack power is not significantly different from the power demand, which indicates that the Simulink model is not accurately simulating losses due to blower and other component internal power consumption that would increase stack power above system power in a real system.

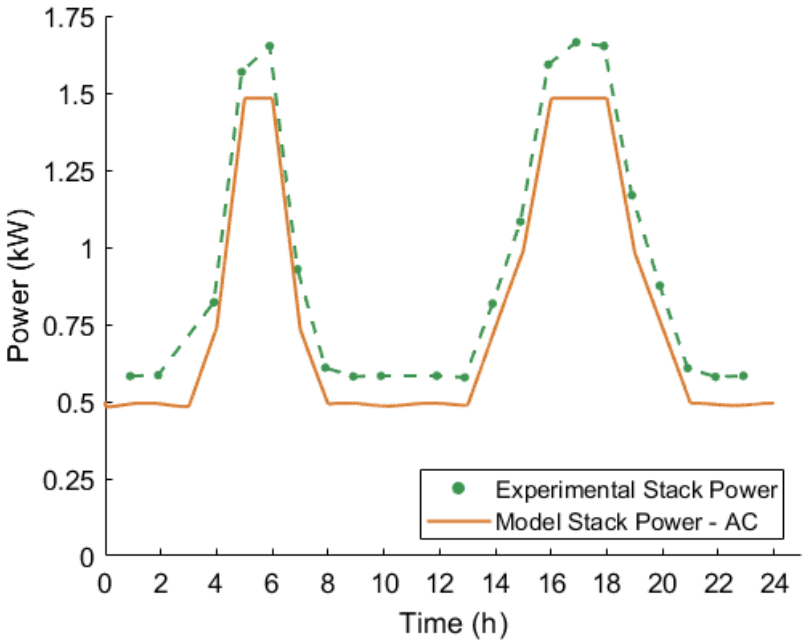

Figure 15. BlueGEN experimental and SOFC-AC model dynamic stack power profiles and system power demand.

The model load power, the amount of power available to meet demand, does not converge to the input demand values as shown in Figure 16. The model converges stack power to power demand and calculates load power by subtracting the blower power consumed from the stack power. This results in a power output lower than the power demand. The model load power during steady-state 1.5 kW operation is 1.48 kW, and the load power during 0.5 steady-state operation is 0.49 kW.

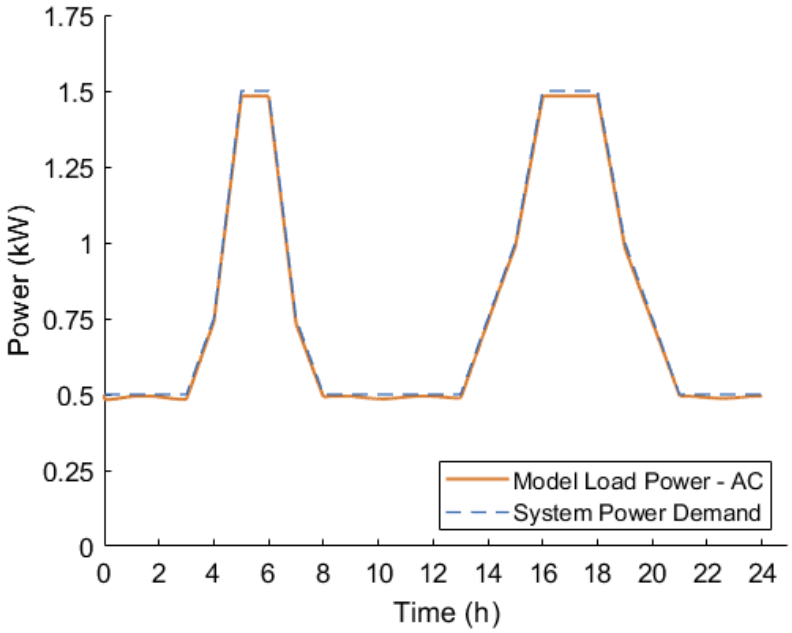

Figure 16. SOFC-AC model dynamic load profile plotted against system power demand.

Figure 17 compares the BlueGEN experimental and SOFC-AC model stack current 24-hour dynamic operation profiles. The average experimental stack current for steady-state operation at 1.5 kW is 40.2 A, and the average experimental stack current while operating at 0.5 kW is 13.0 A. The Simulink model average stack current at 1.5 kW SOFC steady-state operation is 38.4 A, and average stack current at 0.5 kW is 12.3 A. The model stack current is within 5% of the experimental value over the entire 24-hour dynamic profile.

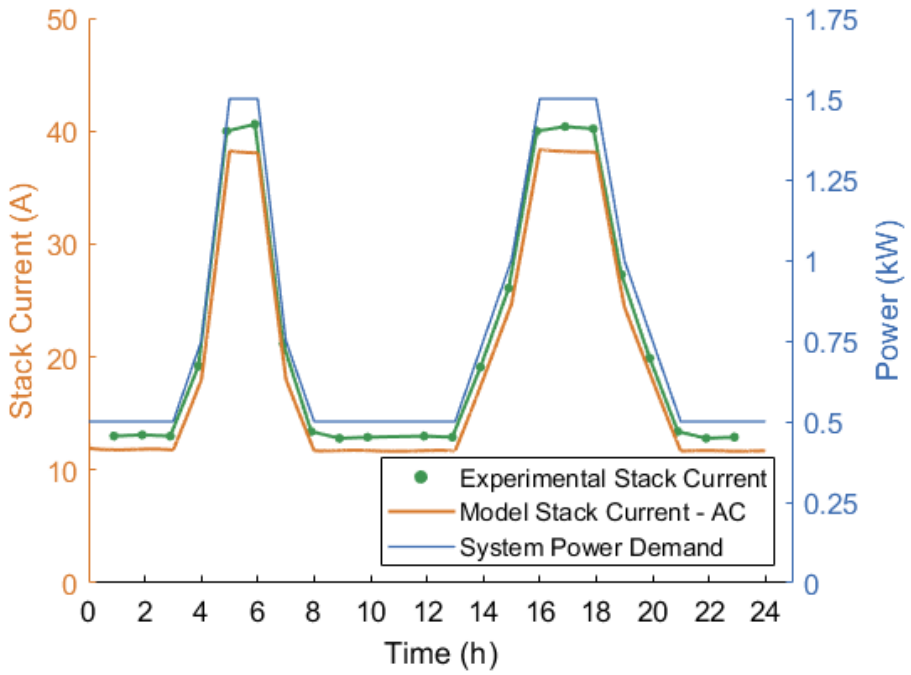

Figure 17. BlueGEN experimental and SOFC-AC model dynamic stack current profiles plotted against system power demand.

Figure 18 shows the BlueGEN stack voltage 24-hour profile during dynamic operation. Again, the model and experimental data exhibit similar trends. Experimental stack voltage ranges from 39.2 to 45.3 V. The experimental stack voltage is lowest at 1.5 kW power generation and highest at 0.5 kW power generation. The model stack voltage follows the same trend and is within 5% of the experimental value over the entire 24-hour dynamic profile.

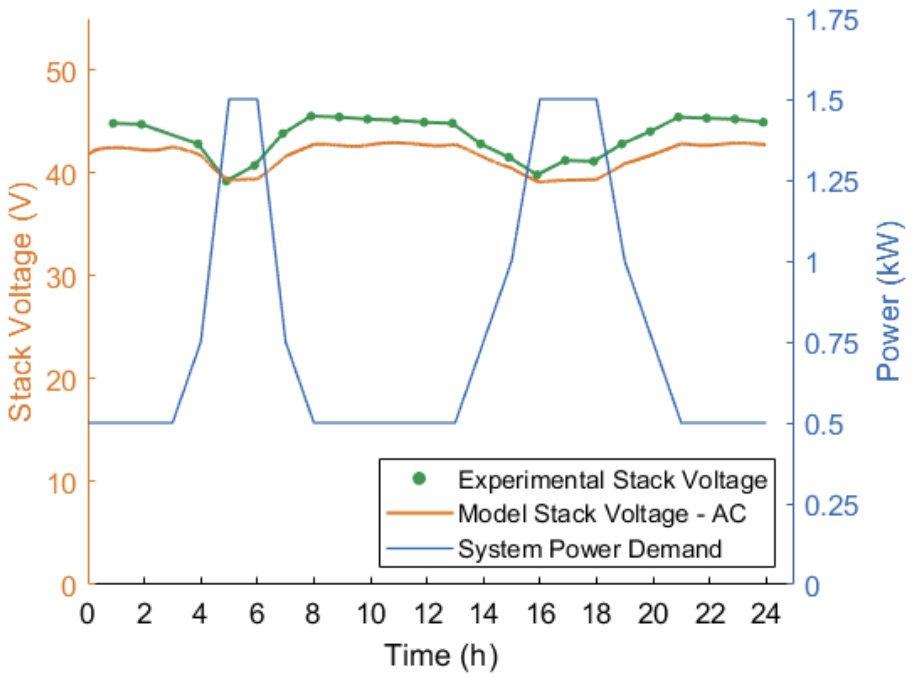

Figure 18. BlueGEN experimental and SOFC-AC model dynamic stack voltage profiles plotted against system power demand.

Figure 19 compares the experimentally recorded BlueGEN airflow and the model simulated airflow. The experimental air volume flow rate is nearly constant with an average of 130 LPM for all electricity generation values tested. The axial compressor model adjusts air flow to maintain stack temperature as the load varies during dynamic operation of the SOFC. Air flow values for the axial compressor model are 114 - 406 LPM. Model air flow is highest when power production is highest and lowest when power production is lowest. Thus, the axial compressor model does not accurately model air flow in the BlueGEN during dynamic operation.

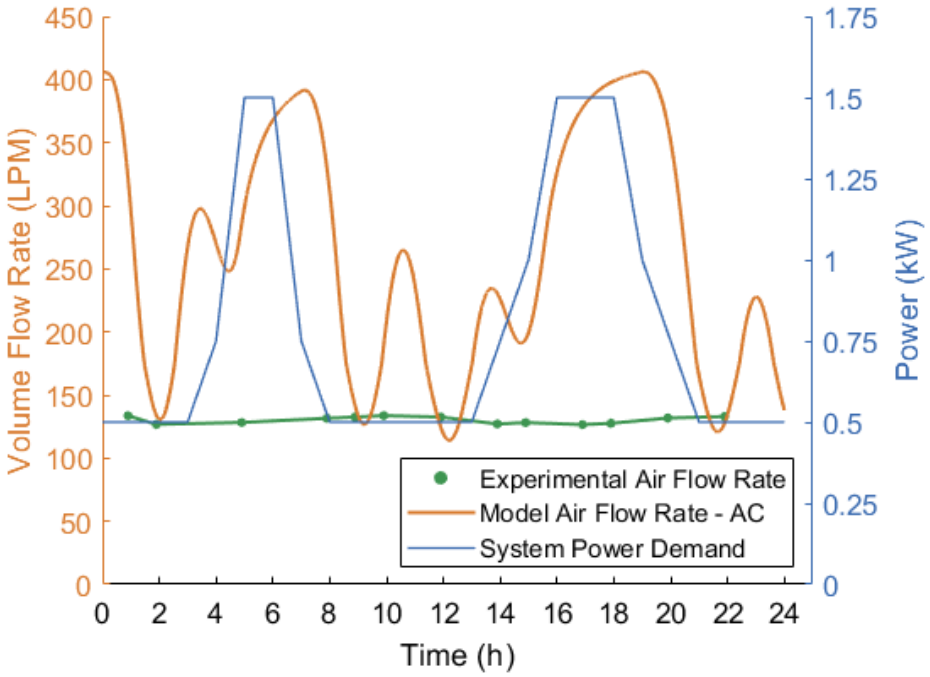

Figure 19. BlueGEN experimental and SOFC-AC model dynamic air flow rate profiles plotted against system power demand.

Figure 20 plots the experimental and model cathode exit temperatures over the 24-hour dynamic period. In this figure, the two data sets exhibit similar trends. Both show temperature increases during the ramp up to 1.5 kW electrical output and decrease during the ramp down to 0.5 kW. This verifies the model's general dynamics as a high and low CETs correspond to times of high and low air flow, respectively. The difference between experimental and model values increases over the 24-hour period suggesting that the model fuel cell system is accruing an error over time. However, the model CET is always within 10% of the experimental CET.

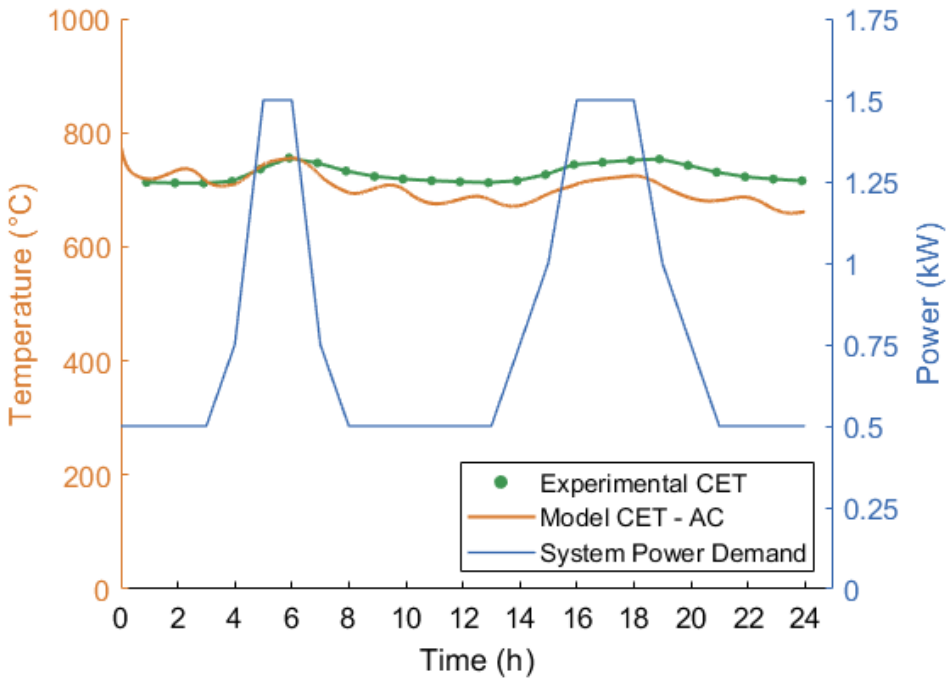

Figure 20. BlueGEN experimental and SOFC-AC model dynamic cathode exit temperature profiles plotted against system power demand.

Figure 21 compares the model and experimental anode tail gas oxidizer temperatures during SOFC system dynamic operation. The experimental and model ATO temperatures show inverse trends – the model ATGO temperature decreases while the experimental value increases and vice versa. The maximum percent difference between experimental and model values is nearly 21%. The model ATO temperature is larger than the experimental ATO temperature at all times.

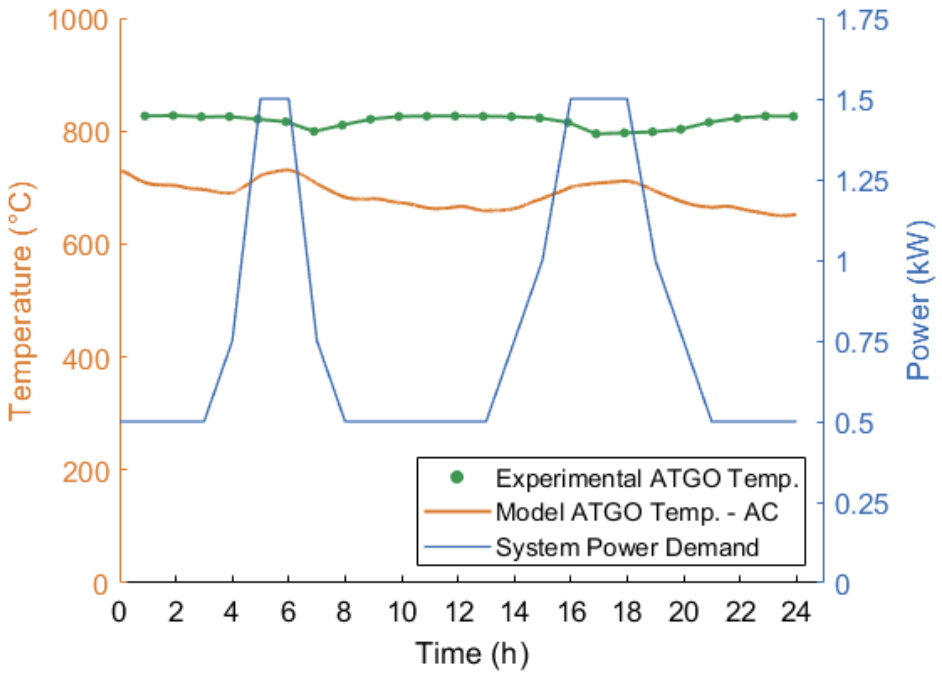

Figure 21. BlueGEN experimental and SOFC-AC model dynamic anode tail gas oxidizer temperature profiles plotted against system power demand.

Figure 22 shows the SOFC-AC model dynamic efficiency profile plotted with the system power demand profile. Due to a calibration error during the BlueGEN installation process, natural gas consumption of the system was not recorded accurately during dynamic operation. Thus, experimental efficiency cannot be calculated accurately. During steady-state operation the BlueGEN efficiency was approximately 40% during 0.5kW electricity generation and approximately 60% during 1.5 kW electricity generation. Initial 1.5 kW steady-state system efficiency was 63% but degraded over the first few months of operation to a steadier 60% efficiency value. Model efficiencies during dynamic operation are 67-74%, significantly higher than those experimentally observed. The model efficiency is lowest during 1.5 kW steady-state operation and highest during 0.5 kW steady-state operation; the system efficiency is high when the blower produces less air flow and consumes less power. This is the inverse trend that is expected for a system using a steady-state blower. The constant air flow produced by a steady-state blower results in a cooler stack during periods of low power generation when the stack produces less heat. System efficiency correlates strongly with temperature in SOFCs and the efficiency is expected to

increase when operating at higher partial load conditions (as voltage increases for lower stack currents) and decrease at lower partial load conditions (as parasitic loads consume an increasing share of the stack power to counterbalance the increased stack efficiency). The high model efficiency improvements observed at lower power levels are likely due to this counterbalancing of effects over time together with the impact of system thermal mass, which impacts air flow requirements and the main blower parasitic load.

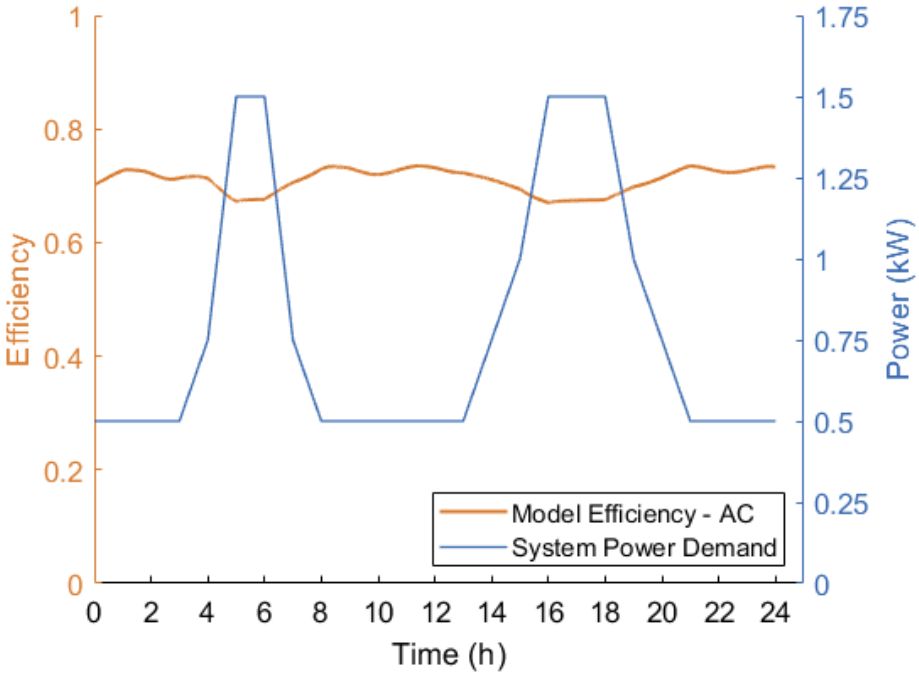

Figure 22. SOFC-AC model dynamic efficiency profile plotted against system power demand.

The initial results show good correlation between the model and experimental results. Values that do not correlate well, including air flow rate, ATO temperature, and efficiency are investigated further in section 4.2.

3.2 SOFC Model with Steady-State Centrifugal Blower using Natural Gas Fuel

Because the air flow rates and blower power and some related temperatures were not well predicted by the previous model, it was deemed necessary to create a more accurate model of the

system blower. Note that the original SOFC system model contained an axial compressor for producing cathode air flow, which is not expected to well simulate a centrifugal fan like that of the experiment.

To inform the replacement of the axial compressor (AC) model with a centrifugal blower (CB) model, the axial compressor model performance was first characterized. The initial SOFC Simulink model uses compressor parameters that a pressure difference of 1270 Pa while consuming 17 W of power. The compressor has an isentropic efficiency of 65% with an air flow rate of 397 LPM during steady-state 1.5 kW operation. Centrifugal blower efficiency is calculated according to the equation below:

$$\eta = \frac{1}{P} \cdot dp \cdot q$$

where η is the unitless efficiency, P is the power in Watts, dp is the total pressure increase in the blower in Pascals, and q is the air flow volume delivered by the blower in cubic meters per second [175]. As shown by Figure 19 the recorded air flow of the BlueGEN during dynamic operation is nearly constant. The centrifugal blower operating point is characterized by a power consumption of 56 W, a frequency of 8,000 rpm, a volume flow rate of 130 LPM, and a pressure increase of 2350 Pa based on experimental data and fitting of the NRG 118 characteristic curves [143]. Substituting these values into the efficiency equation, the NRG 118 efficiency is calculated to be 9.1%.

The Simulink axial compressor model was replaced with a steady-state centrifugal blower model exhibiting the performance parameters of the NRG 118 discussed above. The steady-state 1.5 kW operation results comparing AC and CB models are summarized in Table 10. The CB model produces a 1.56 kW stack power, much closer to the 1.65 kW recorded experimentally than the 1.50 kW AC model result. The CB model steady-state stack current is 43.8 A, an 8% error from the experimental value, and the CB steady-state stack voltage is 35.6 V, a 13% error from the experimental value. Errors for the AC stack current and voltage are 6% and 3%, respectively. The CB model air flow rate is 130 LPM, the same as the experimentally recorded value, while the AC air flow rate is over three times larger than the experimentally recorded value. Both the cathode exit temperature and the ATO temperature in the CB

model are very high compared to experimental and AC model results. The CB model CET is 1040℃ while the experimental CET is 756℃. The CB model ATO temperature is 906℃ compared to the experimental value of 817℃.

Table 10. Comparison of the steady-state 1.5 kW power output experimental results and the SOFC-AC and SOFC-CB model results for the six benchmark quantities.

Parameter	BlueGEN Experiment	SOFC-AC Model	SOFC-CB Model
Stack Power (kW)	1.65	1.50	1.56
Stack Current (A)	40.6	38.1	43.8
Stack Voltage (V)	40.7	39.3	35.6
Air Flow Rate (LPM)	130	397	130
CET (℃)	756	777	1040
ATO Temp. (℃)	817	748	906

Dynamic SOFC-CB model results are shown in Figure 23 which compares the 24-hour dynamic (a) stack power, (b) system load power, (c) stack current, (d) stack voltage, (e) air flow rate, (f) CET, (g) ATO temperature, (h) temperature difference across the stack, and (i) efficiency profiles of the initial SOFC-AC model and the SOFC-CB model. Both SOFC system models are operating on natural gas fuel.

The CB model results in an increased blower power and, therefore, stack power compared to that of the AC model as shown in Figure 23(a). The stack power increase is constant for all load powers. The CB model stack power is 0.02 kW less than the experimental stack power at 0.5 kW power generation but is just over 0.1 kW lower than the experimental stack power at 1.5 kW power generation. This implies that there is additional equipment within the SOFC system not considered by the model that consumes and that consumes more power at high load power than at low load power.

Figure 23(b) shows the SOFC-AC model output power to be less than the system's power demand. The initial model converges stack power to power demand and calculated load power by subtracting blower power from stack power. Thus, producing a load power that does not meet power demand. The SOFC-CB model is updated to converge stack power to the sum of power demand and blower power so that load power equals the system power demand.

Figure 23(c) displays stack current profiles of the two blower models and the experimental setup. The AC model stack current is less than the experimental value at each steady-state load power

tested. The CB model shows increased stack current that matches experimental stack current at 0.5 kW load power and during the morning power production peak. During the afternoon peak, the CB model stack current is larger than the experimental stack current and increases over time at steady-state conditions while the experimental value remains constant.

Figure 23(d) compares stack voltage profiles of the two blower models and the experimental setup. The CB model stack voltage is less accurate than the AC model stack voltage compared to the experimental values. However, both model stack voltages match the experimental values well. The maximum percent error of the CB model stack voltage is 10%.

Air flow rate profiles are compared in Figure 23(e). The CB model air flow rate is constant and matches the experimental air flow rate.

Figure 23(f) shows CET for both blower models. The AC model CET matches the experimental CET well. The CB model CET is significantly higher than the experimental CET and shows exaggerated increases during periods of increased power production. This is likely due to the lower air flow in the SOFC-CB model compared to that in the SOFC-AC model. As air flow is often used to regulate stack temperature, decreased air flow would result in high anode and cathode exit temperatures as there is less (relatively) cool air for other species to exchange heat with.

The CB model ATO temperature profile exhibits the same inversed trend as the AC model compared the experimental values as shown in Figure 23(g). However, the CB model shows an increase in average ATO temperature that more closely matches experimental results.

Figure 23(h) graphs the dynamic stack temperature difference profiles of the two models. Real dynamic SOFCs are expected to have a stack temperature difference of 50-150℃. The initial SOFC-AC model showed relatively little variation in stack temperature difference ranging from 31-75℃. The SOFC-AC model was programmed to manipulate blower power and therefore, air flow, to ensure stack temperature differences in this range. The initial SOFC-CB model showed extremely large variations in

stack temperature difference ranging from 86-311℃. These results are for the initial SOFC-CB model results before optimization. Stack temperature difference values of greater than 150℃ would be too large for physical SOFC materials to accommodate and would not be acceptable in a real system. This is addressed and corrected in section 3.3.

Figure 23(i) compares efficiency profiles of the two blower models during dynamic operation. The CB model and AC model efficiencies exhibit the same dynamic trend. The CB model efficiency is lower than the AC model efficiency and closer to observed values of the BlueGEN system. Both model efficiencies show less range during dynamic operation than does the experimental system.

(a)

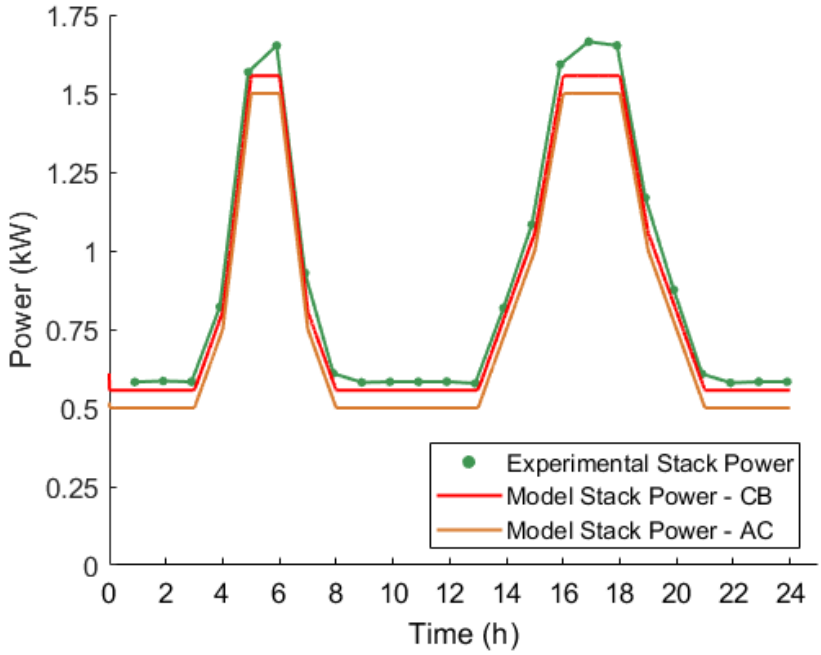

(b)

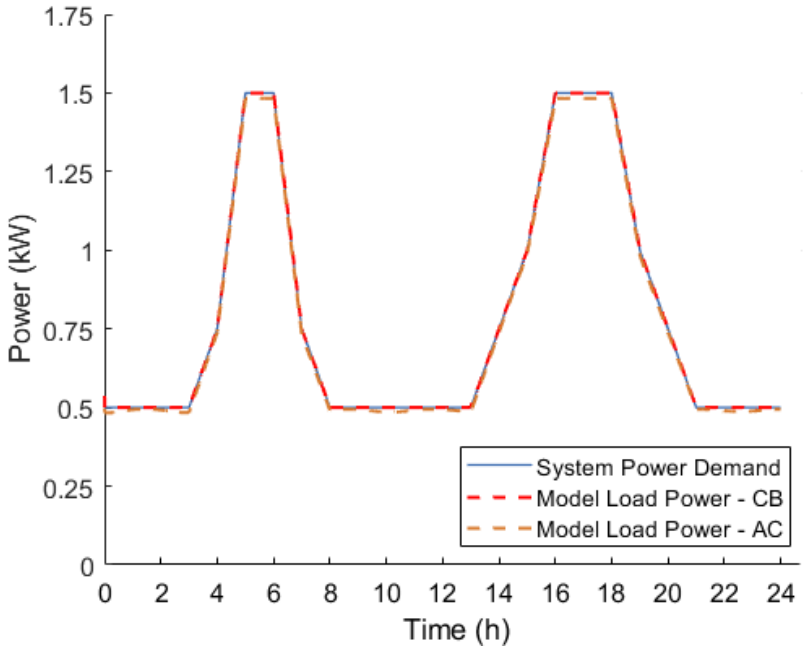
Power (kW)
Time (h)
System Power Demand
Model Load Power - CB
Model Load Power - AC

(c)

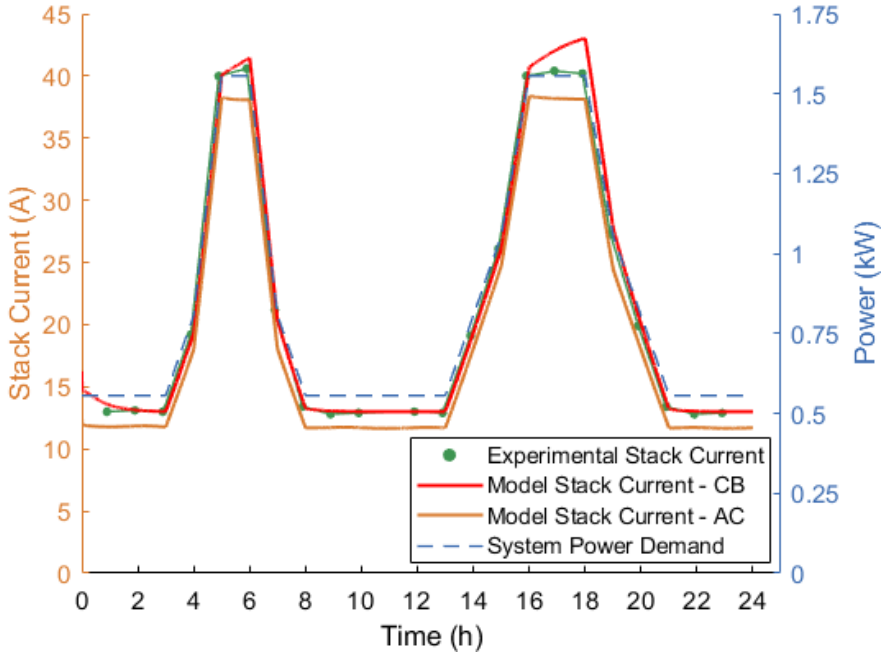
Stack Current (A)
Power (kW)
Time (h)
Experimental Stack Current
Model Stack Current - CB
Model Stack Current - AC
System Power Demand

(d)

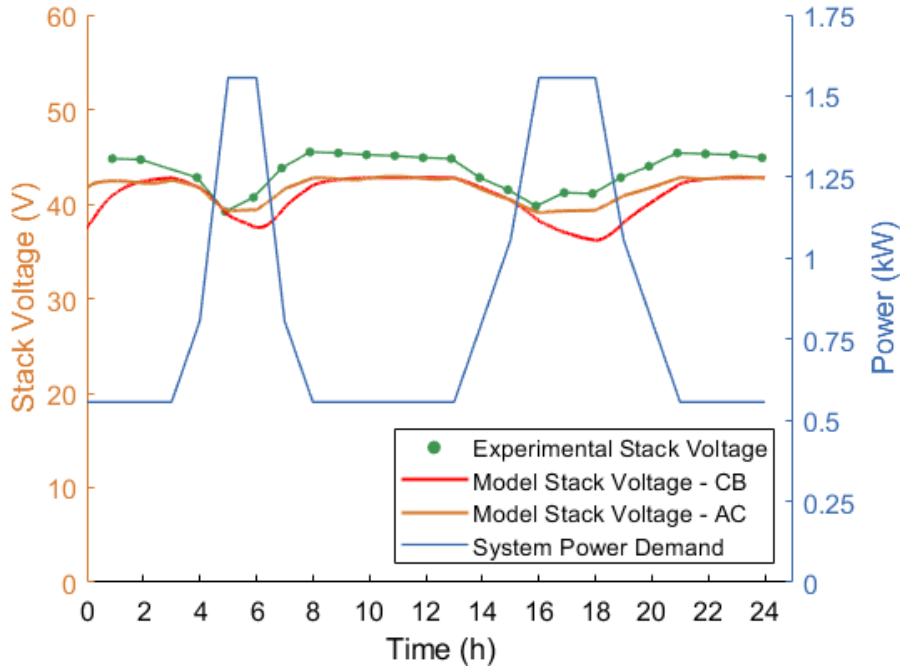
Stack Voltage (V)
Power (kW)
Time (h)
Experimental Stack Voltage
Model Stack Voltage - CB
Model Stack Voltage - AC
System Power Demand

(e)

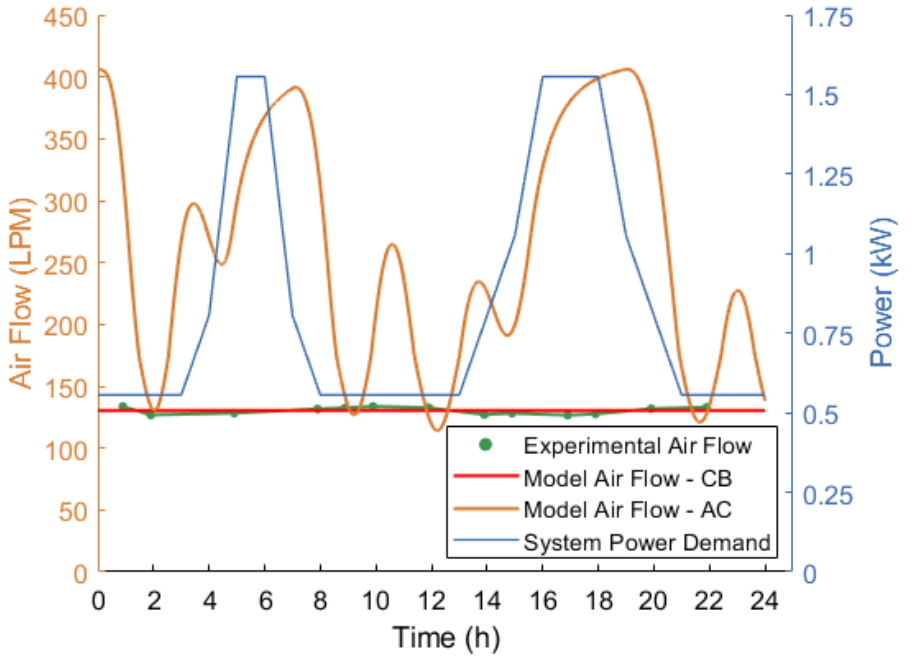
Air Flow (LPM)
Power (kW)
Time (h)
Experimental Air Flow
Model Air Flow - CB
Model Air Flow - AC
System Power Demand

(f)

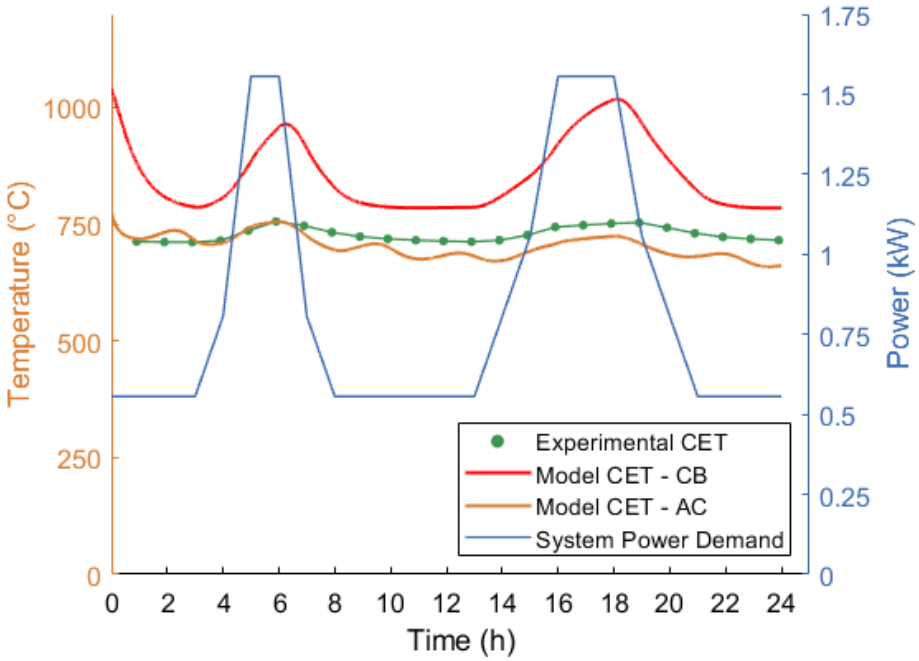
Temperature (°C)
Power (kW)
Time (h)
Experimental CET
Model CET - CB
Model CET - AC
System Power Demand

(g)

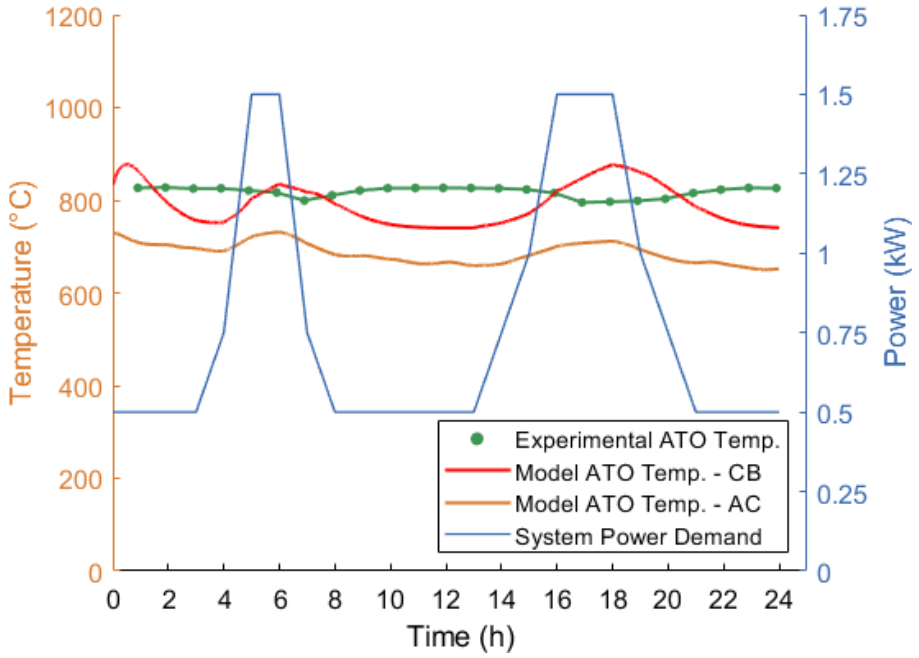
Temperature (°C)
Power (kW)
Time (h)
Experimental ATO Temp.
Model ATO Temp. - CB
Model ATO Temp. - AC
System Power Demand

(h)

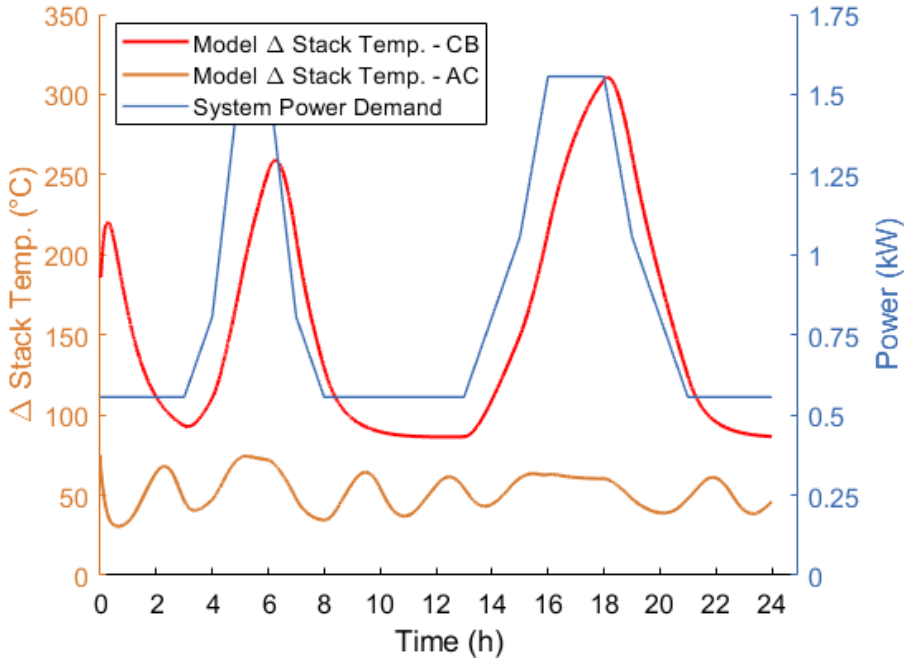

(i)

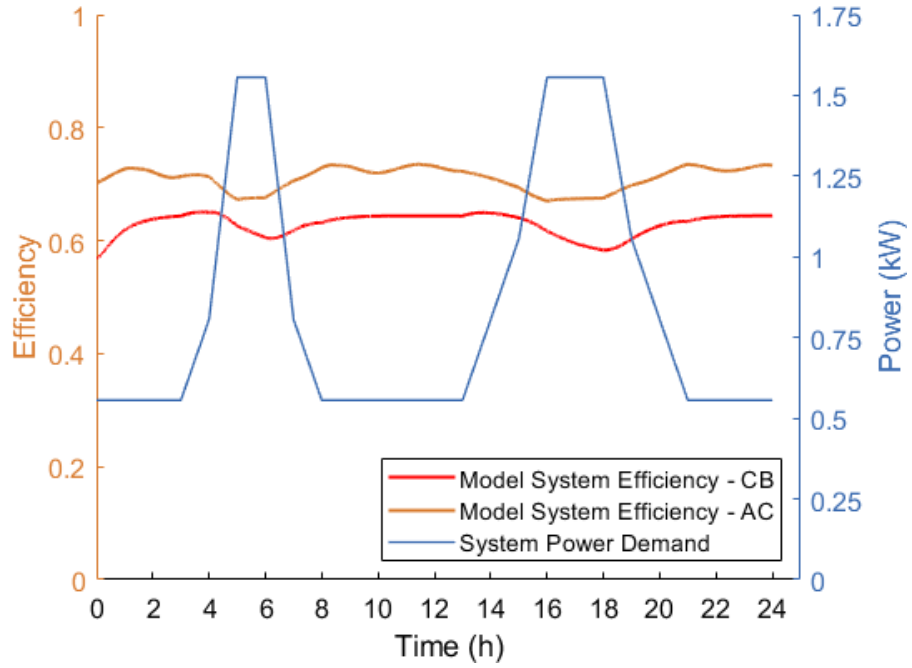

Figure 23. Dynamic (a) stack power, (b) system load power, (c) stack current, (d) stack voltage, (e) air flow rate, (f) CET, (g) ATO temperature, (h) stack temperature difference, and (i) efficiency profile comparison for 1.5 kW SOFC-AC and SOFC-CB models operating on natural gas fuel and plotted against system power demand.

3.3 Optimized BlueGEN Model with Steady-State Centrifugal Blower using Natural Gas Fuel

Several other model parameters are systematically tested to lower the CET and ATO temperature to more closely match the experimental data. The most successful SOFC-CB model run uses a power density of 235 mW/cm^2, a stack temperature difference of 10°C, and increased component specific heats as inputs. The stack temperature difference input parameter does not set a constant value. Instead, the model uses this parameter to calculate the stack's initial average operating temperature.

The system's thermal mass was increased by raising specific heat input values of system components including the cell electrolyte, the fuel separator plates, external reformers, plenum fuel recirculation chambers, and heat exchangers. The input values used to run the optimized SOFC-CB model are shown in Table 11. Increased thermal mass resulted in a lower cathode exit temperature, ATO temperature, and stack temperature difference for the optimized SOFC-CB model compared to the initial SOFC-CB model that are closer to experimental results.

Table 11. Specific heat values for various SOFC system components used in the optimized SOFC-CB model.

Model Component	Specific Heat Input $\left(\frac{\mathbf{kJ}}{\mathbf{kg\,K}}\right)$
electrolyte	0.80
fuel separator plates	0.80
External reformer	0.30
Plenum fuel recirculation chambers	0.70
Heat exchangers	0.68

The 1.5 kW steady-state operation performance for the six benchmark parameters for this BlueGEN CB Model are shown in Table 12. CET shows the largest percent difference between model and experimental values at 6.2%. All steady-state parameters match experimental values within an acceptable tolerance.

Table 12. 1.5 kW steady-state operation results of the optimized BlueGEN SOFC-CB model compared to experimental values.

Parameter	BlueGEN Experiment	Opt. SOFC-CB Model	% Difference
Stack Power (kW)	1.65	1.57	4.8%
Stack Current (A)	40.6	39.5	2.7%
Stack Voltage (V)	40.7	39.7	2.5%
Air Flow Rate (LPM)	130	130	< 1%
CET (℃)	756	803	6.2%
ATO Temp. (℃)	817	826	1.1%

The optimized SOFC-CB model dynamic operation shows an increased blower power and, therefore, stack power compared to the AC model results as shown in Figure 24(a). The optimized BlueGEN SOFC-CB model has the same blower power as the initial SOFC-CB model but an increased internal power consumption. The initial SOFC-AC model had a total internal power consumption of 56 kW – the same as the blower power. The final SOFC-CB model has an internal power consumption of 70 W, more than the 56 W blower power. Total internal power consumption was added to the model as a user input and is constant for all load power outputs. Experimental measurements show that this is not the case for the BlueGEN which has an average internal power consumption of 0.16 kW at 1.5 kW load power and 0.08 kW at 0.5 kW load power. The variable nature of internal power consumption of the BlueGEN is not accurately represented in the SOFC-CB model. However, a constant internal power consumption gives a good approximation of observed behavior.

Figure 24(b) again shows the AC model output power to be less than the system power demand. The optimized and initial SOFC-CB models converge to the same load power that is equal to the system power demand.

Figure 24(c) displays stack current profiles of the optimized SOFC-CB model, the initial SOFC-AC model, and the BlueGEN dynamic operation experiment. The optimized BlueGEN SOFC-CB model shows a slightly lower stack current that more accurately matches the experimental data compared to the initial SOFC-CB model. Both SOFC-CB models have larger stack current profiles than the SOFC-AC model mostly due to their increased blower power and stack power.

Figure 24(d) compares stack voltage profiles of the optimized SOFC-CB model, the initial SOFC-AC model, and the experimental BlueGEN measurements. Both models show very similar stack voltage values that are slightly lower than the experimental values. The optimized SOFC-CB model stack voltage is always within 5% of the experimental value.

Air volume flow rate profiles are compared in Figure 24(e). The SOFC-AC model shows a highly variable air flow rate ranging from 114 - 406 LPM. The final SOFC-CB model air flow rate is constant at 130 LPM and matches the experimental air flow rate.

Figure 24(f) shows CET profiles for both blower models and the experimental system. The optimized SOFC-CB CET is much smaller and closer to experimental values compared to the initial SOFC-CB model results. The SOFC-AC CET values are closer to experimental results, but both SOFC-AC and final SOFC-CB model CET profiles are acceptable approximations of the experimental measurements.

The CB model ATO temperature profile exhibits the same inversed trend as that of the AC model compared the experimental values as shown in Figure 24(g). However, the final SOFC-CB model shows an increased average ATO that closely matches that of the experimental results.

Figure 24(h) shows the stack temperature difference of the initial SOFC-AC model and the final SOFC-CB model. The optimized SOFC-CB model stack temperature difference profile shows dynamic behavior with low stack temperature differences of about 67℃ at 0.5 kW load power and high stack temperature differences of about 128℃ at 1.5 kW load power as expected in a real system with a centrifugal blower. The maximum stack temperature difference in the optimized SOFC-CB model was 141℃.

Figure 24(i) compares dynamic efficiency profiles of the relevant models. The final SOFC-CB model shows lower system efficiencies than does the initial SOFC-AC model. The optimized SOFC-CB model maximum efficiency is 64%, very near the experimental BlueGEN maximum efficiency of 63%. However, the model showed only small variations in efficiency during dynamic operation with 62% being

the lowest efficiency value. This contrasts observations of efficiency for the experimental setup, which had dynamic efficiency values of 40-63%. The model prediction of a slightly too high efficiency is likely due to the model's lower internal power consumption at 1.5 kW load power. The stack temperature difference profiles show that the SOFC-CB model decreases heating in proportion to load power. The dynamic efficiency behavior of the real BlueGEN system may be caused by constant fuel heat addition at all power outputs or by oversized system components. This may account for lack of decreased model efficiency at fractional load powers compared to observed steady-state values.

(a)

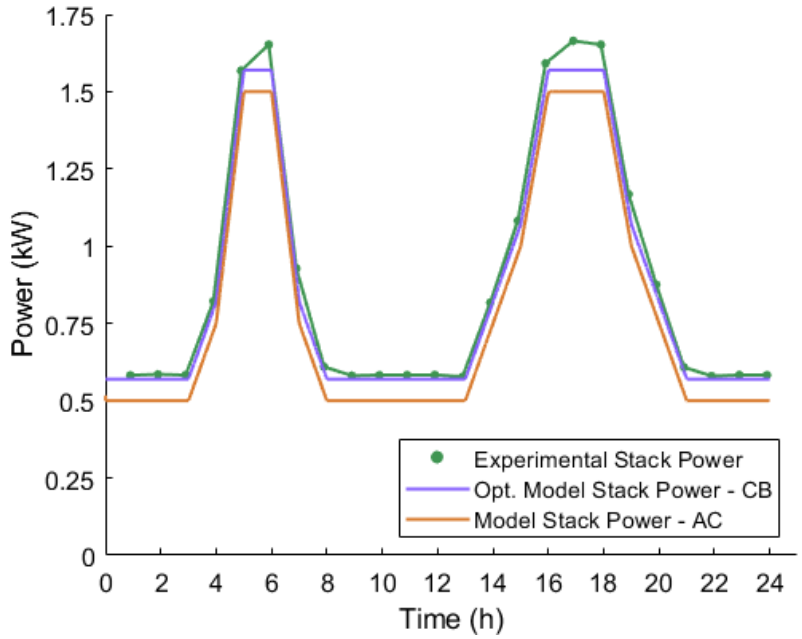

(b)

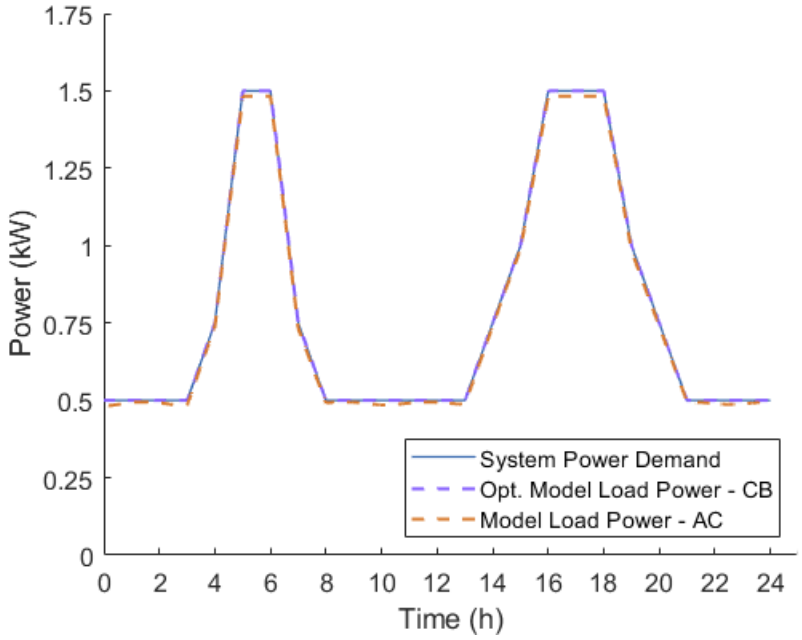
Power (kW)
Time (h)
System Power Demand
Opt. Model Load Power - CB
Model Load Power - AC

(c)

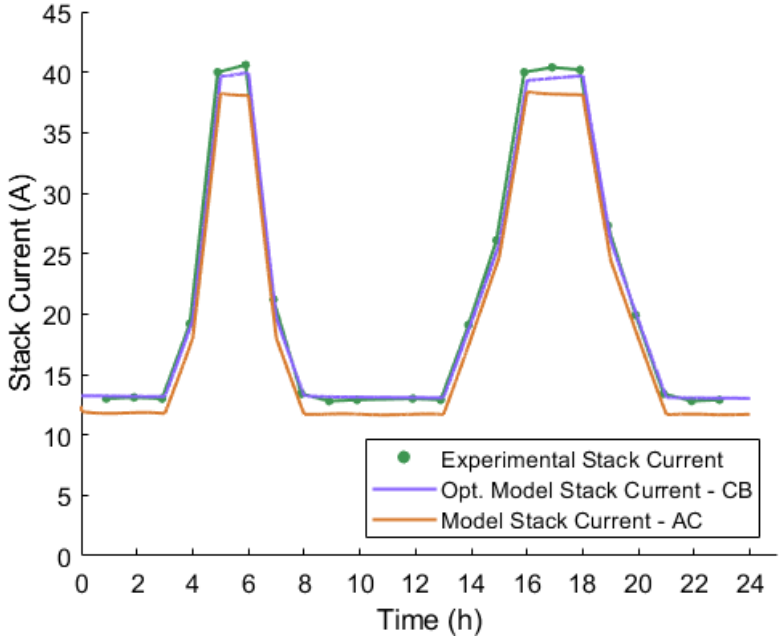
Stack Current (A)
Time (h)
Experimental Stack Current
Opt. Model Stack Current - CB
Model Stack Current - AC

(d)

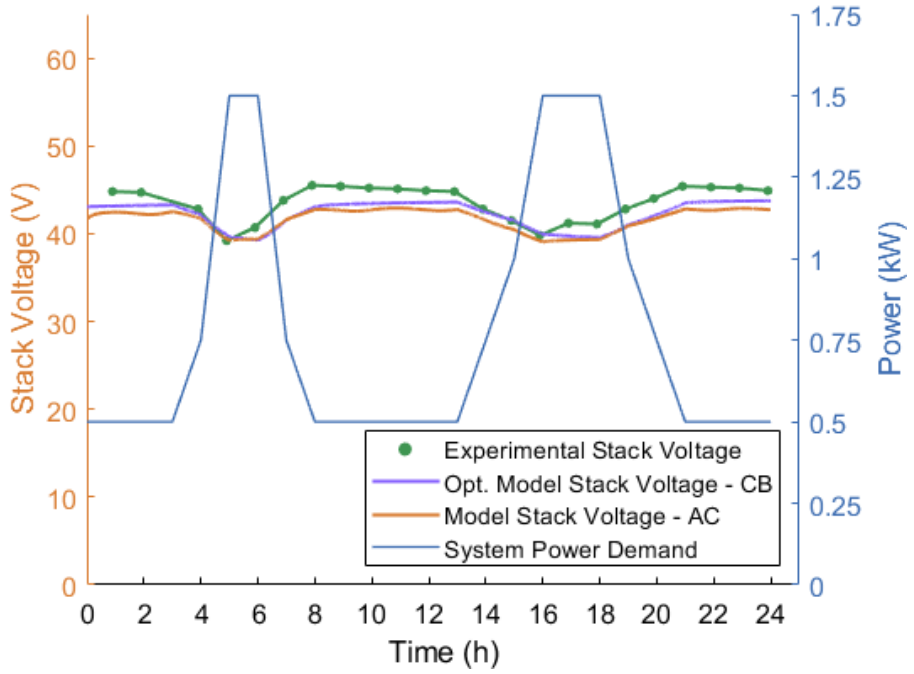
Stack Voltage (V)
Power (kW)
Time (h)
Experimental Stack Voltage
Opt. Model Stack Voltage - CB
Model Stack Voltage - AC
System Power Demand

(e)

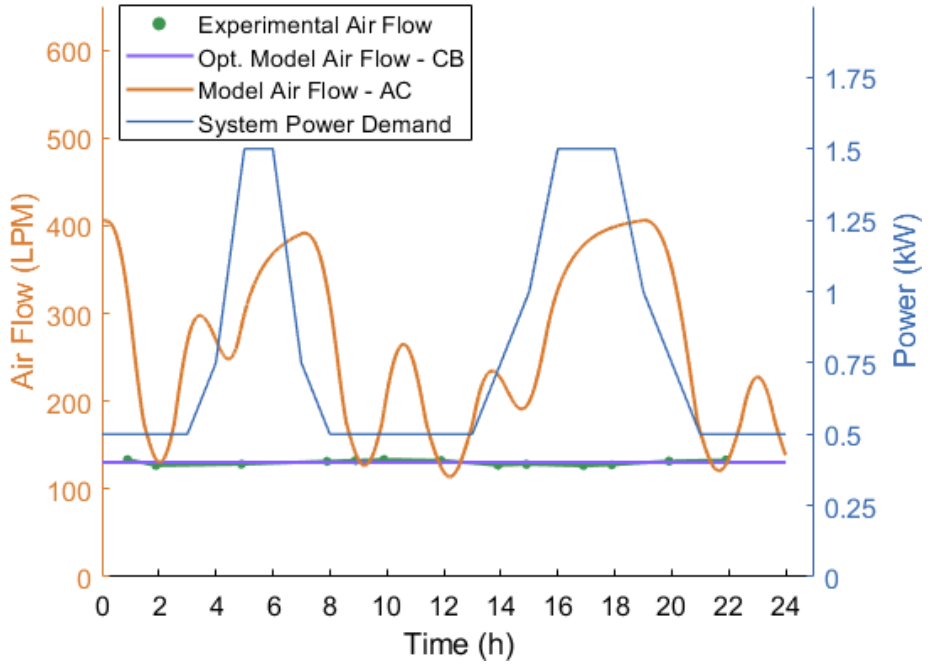
Air Flow (LPM)
Power (kW)
Time (h)
Experimental Air Flow
Opt. Model Air Flow - CB
Model Air Flow - AC
System Power Demand

(f)

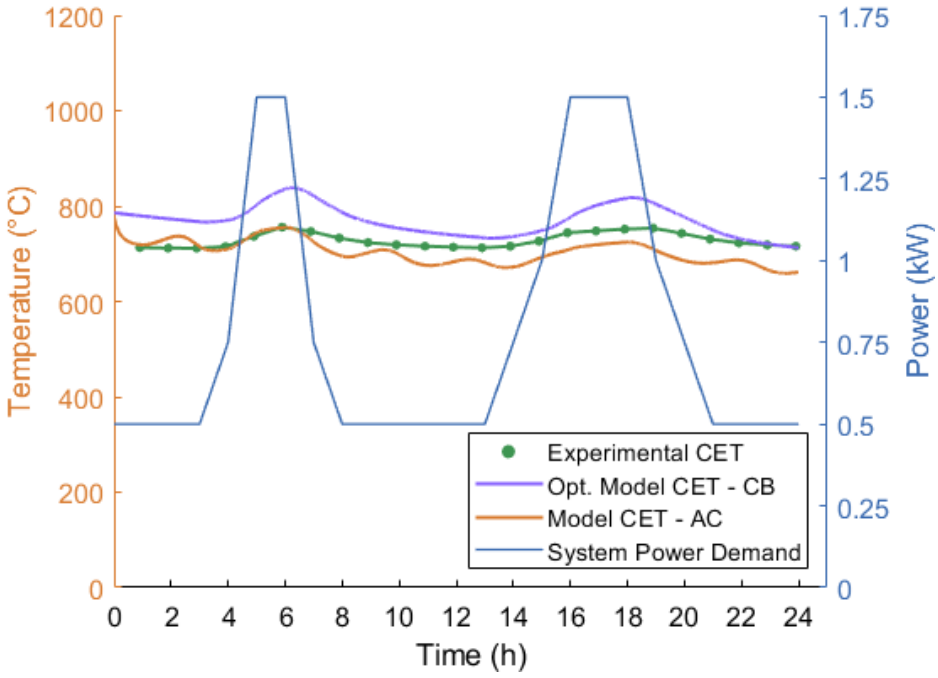
Temperature (°C)
Power (kW)
Time (h)
Experimental CET
Opt. Model CET - CB
Model CET - AC
System Power Demand

(g)

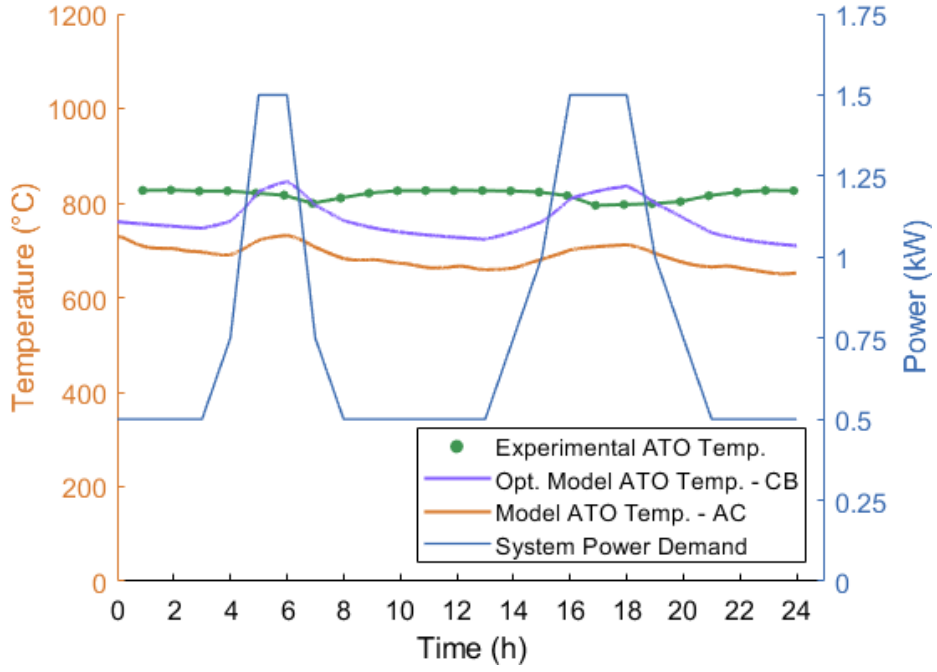
Temperature (°C)
Power (kW)
Time (h)
Experimental ATO Temp.
Opt. Model ATO Temp. - CB
Model ATO Temp. - AC
System Power Demand

(h)

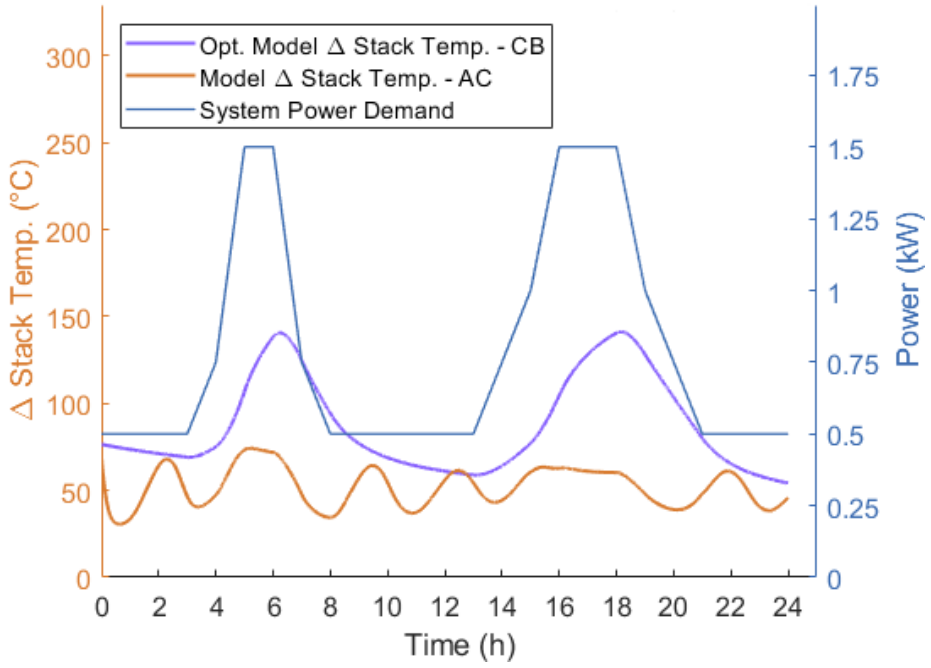

(i)

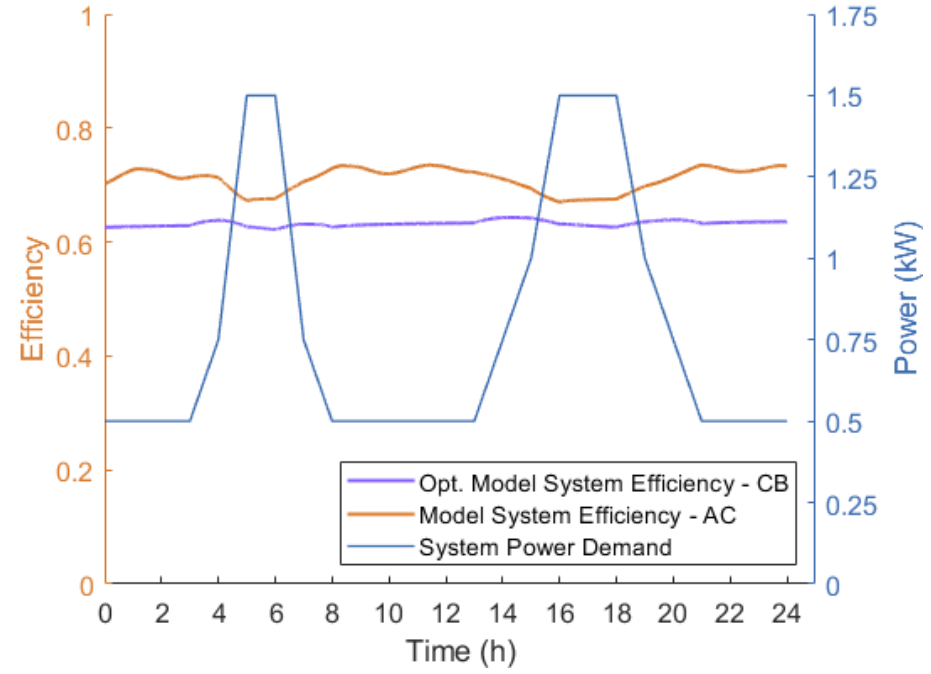

Figure 24. Dynamic (a) stack power, (b) system load power, (c) stack current, (d) stack voltage, (e) air flow rate, (f) CET, (g) ATO temperature, (h) stack temperature difference, and (i) efficiency profile comparison for the optimized 1.5 kW SOFC-CB model, the original SOFC-AC model, and the experimental BlueGEN data.

3.4 Initial SOFC-AC Model Operation on Biogas

The optimized BlueGEN SOFC-CB model failed when run on simulated biogas fuel. There was insufficient time to resolve this challenge, so the initial SOFC-AC model is used to characterize SOFC dynamic performance operating on biogas fuel for this thesis. Figure 25 compares the initial Simulink model 24-hour dynamic (a) stack power, (b) stack current, (v) stack voltage, (d) air flow rate, (e) CET, (f) ATO temperature, and (g) efficiency profiles for a 1.5 kW SOFC operating on biogas and natural gas fuels. Simulated dynamic operation on both biogas and natural gas produced nearly identical stack power, CET, ATO temperature, and efficiency profiles.

The initial modeling results show no difference in stack power (Figure 25(a)) between the natural gas and biogas cases. The use of biogas, a fuel with a lower LHV than natural gas, should decrease the maximum voltage produced by the chemical potential across the electrolyte. Thus, lowering the Nernst potential. In order to meet the same power output with both fuels, the biogas-fueled system must use a larger current. As expected the biogas-fueled simulated SOFC system stack current (Figure 25(b)) is slightly higher than that of the natural gas-fueled simulation while its stack voltage (Figure 25(c)) is slightly lower. The maximum air flow in the biogas-fueled model is 424 LPM. This is a 4.4% increase maximum air flow compared to the natural gas-fueld case. Both CET and ATO temperatures are slightly lower in the biogas-fueled system as biogas's larger volume of inert gases requires more gas to pass through the SOFC system for the same power output. This means that the same amount of energy is heating a larger volume of gas in the biogas-fueled system, and so the gas temperature is lower. Additionally, the larger volume flow rate increases the pumping requirements in the biogas-fueled system which decreases efficiency slightly as shown in Figure 25(g).

(a)

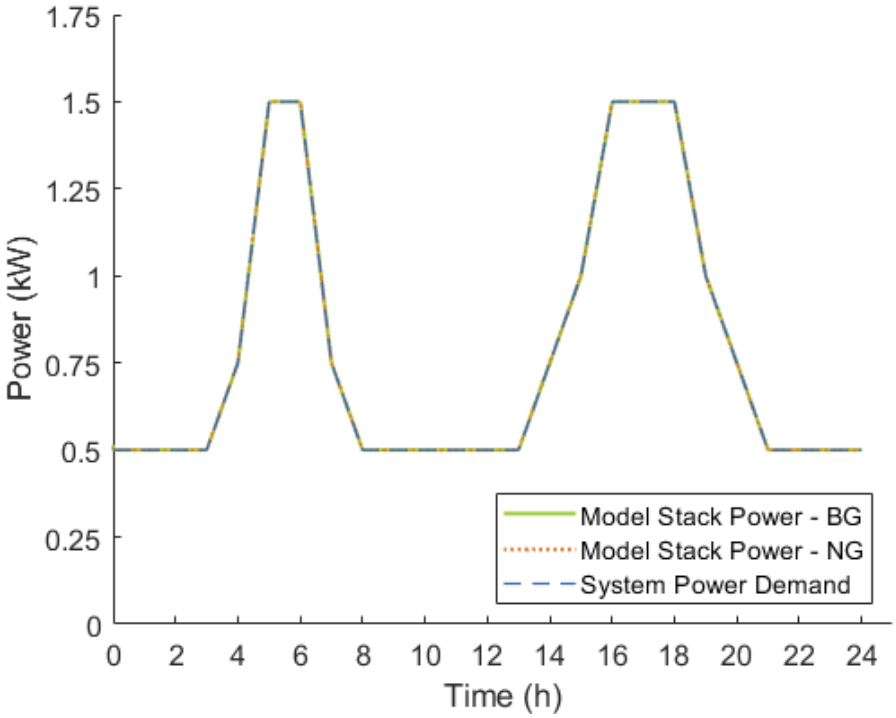
Power (kW)
Time (h)
Model Stack Power - BG
Model Stack Power - NG
System Power Demand

(b)

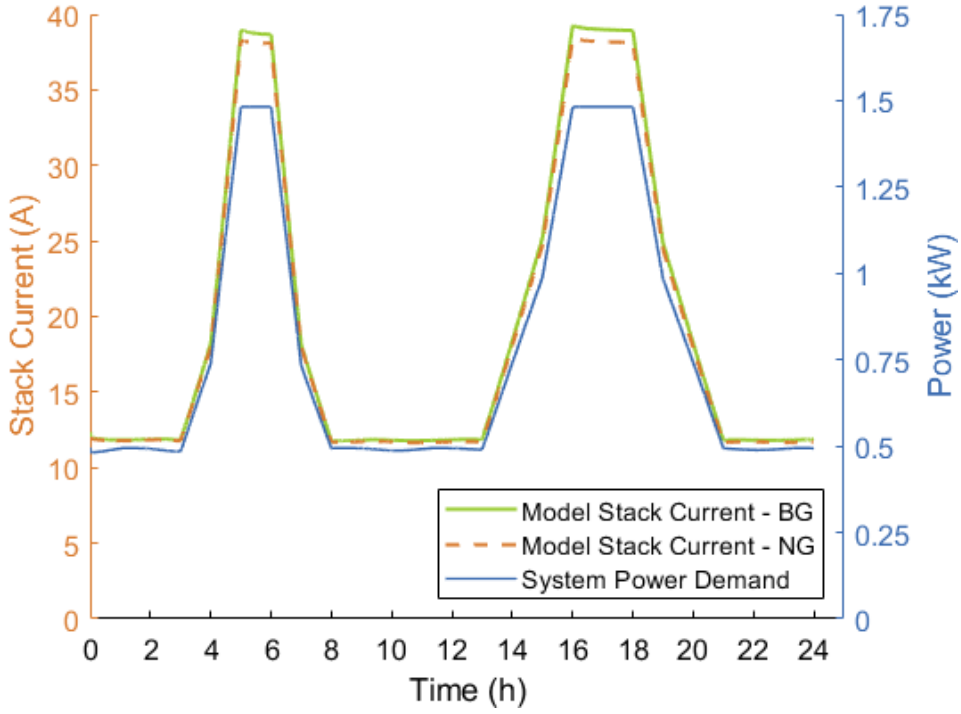
Stack Current (A)
Power (kW)
Time (h)
Model Stack Current - BG
Model Stack Current - NG
System Power Demand

(c)

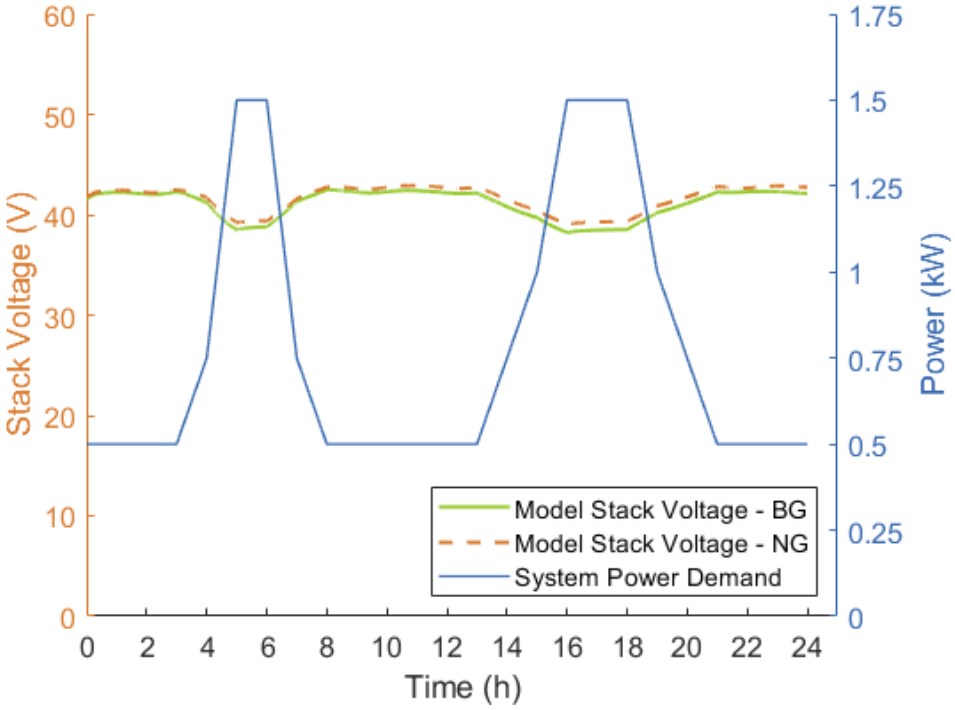
Stack Voltage (V)
Power (kW)
Time (h)
Model Stack Voltage - BG
Model Stack Voltage - NG
System Power Demand

(d)

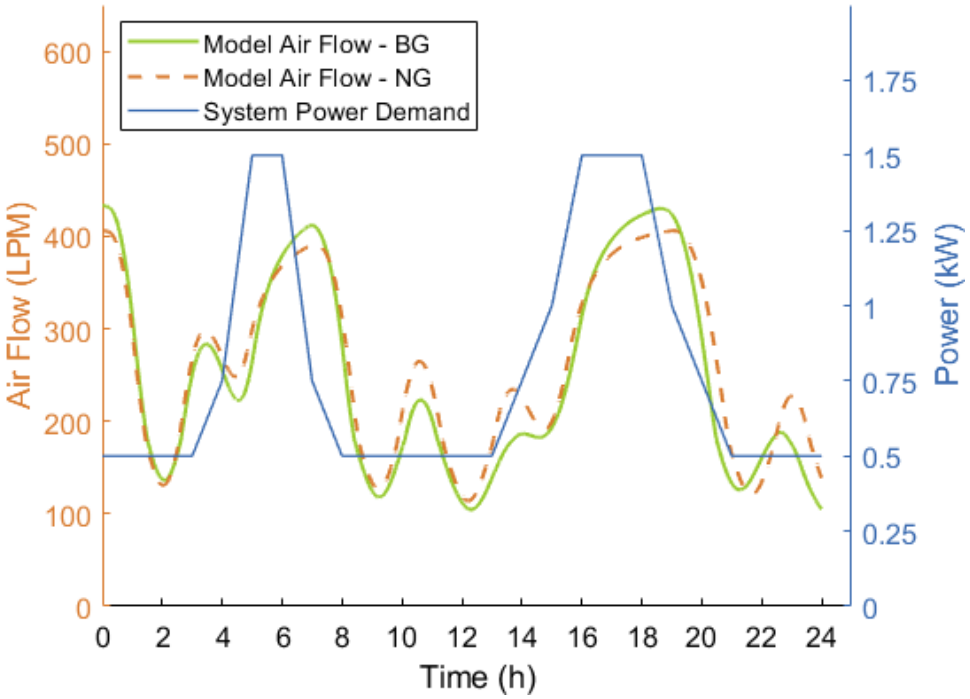
Air Flow (LPM)
Power (kW)
Time (h)
Model Air Flow - BG
Model Air Flow - NG
System Power Demand

(e)

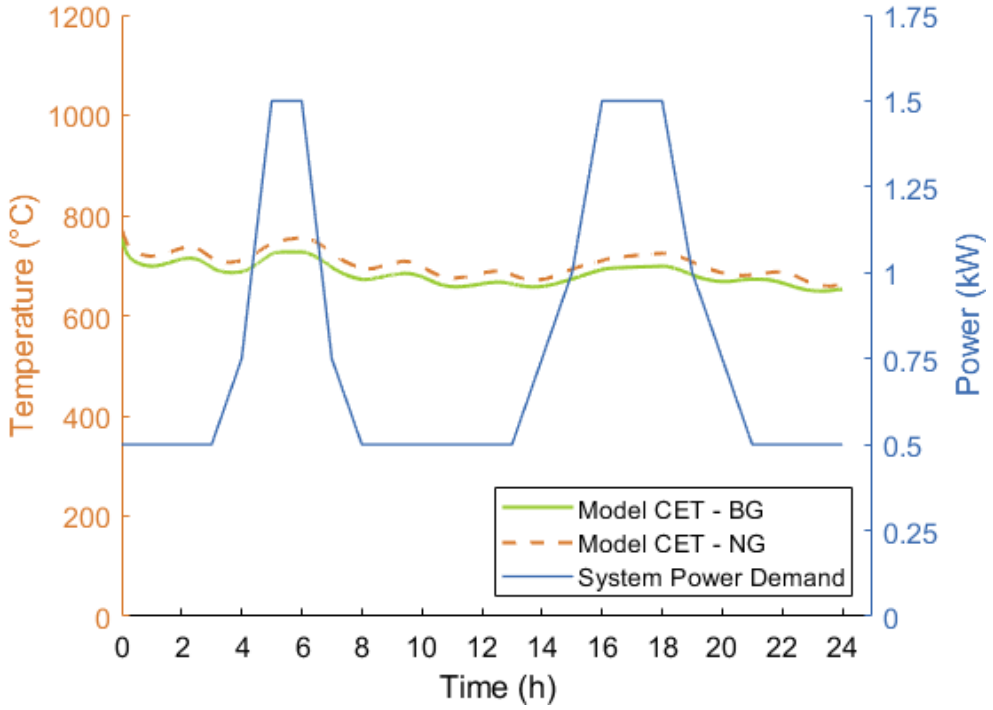
Temperature (°C)
Power (kW)
Time (h)
Model CET - BG
Model CET - NG
System Power Demand

(f)

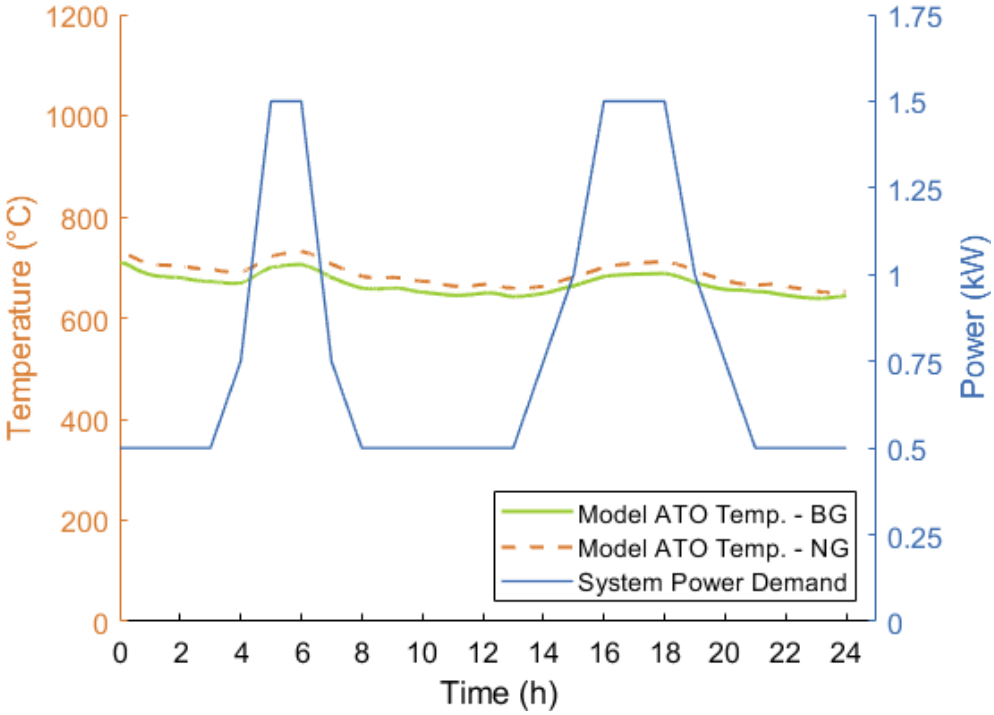
Temperature (°C)
Power (kW)
Time (h)
Model ATO Temp. - BG
Model ATO Temp. - NG
System Power Demand

(g)

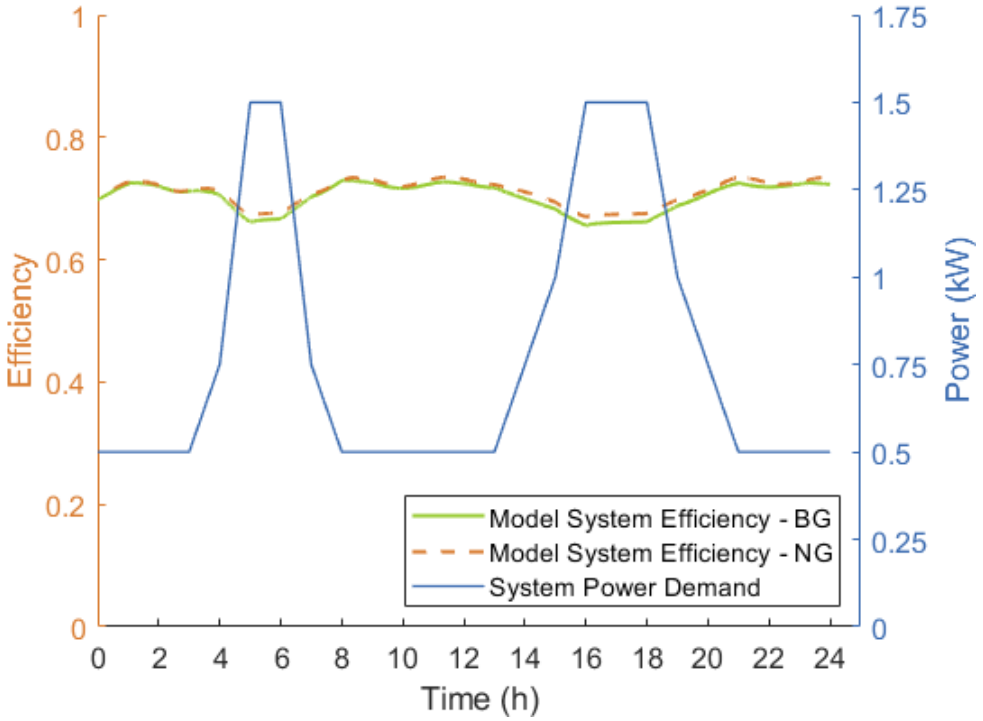

Figure 25. Dynamic (a) stack power, (b) stack current, (v) stack voltage, (d) air volume flow rate, (e) CET, (f) ATO temperature, and (g) efficiency profile comparison for a 1.5 kW SOFC operating on biogas and natural gas fuels plotted against system power demand.

Current-voltage curves for SOFC-AC model operation on natural gas and biogas fuels are shown in

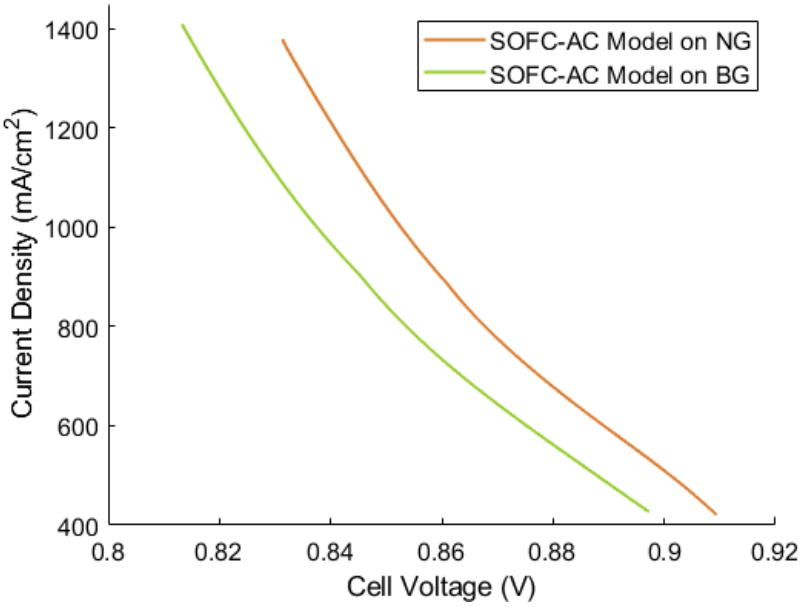

Figure 26. As expected, biogas-fueled model voltage is lower than natural gas-fueled model voltage. The presence of CO_2, a non-reacting species, in biogas lowers the Nernst potential of the electrochemical reaction. The difference between natural-gas model and biogas model stack voltage is nearly constant with an average value of 0.0029 V.

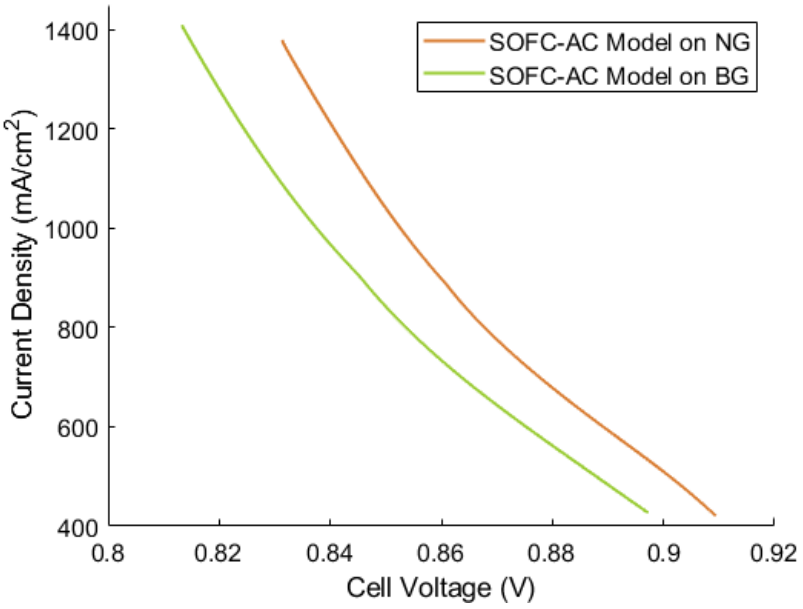

Figure 26. Current density versus voltage curve for SOFC-AC model operation on natural gas and biogas fuels.

3.5 Solar PV Scenarios

The Max and Utility scenarios are characterized by 14.6 MW and 6.5 MW solar PV installations, respectively, as shown in Table 13. The PV installation in the Maximum scenario meets 52% of the Oak View electrical demand, and the PV installation in Utility scenario meets 40% of the modeled Oak View electrical demand. The Maximum scenario uses a 10 MW AEC electrolyzer, while the utility scenario requires a 3.26 MW AEC electrolyzer.

Table 13. Total community excess solar electricity and (b) electrolyzer and battery sizes for both solar PV size scenarios.

Scenario	Solar PV Capacity (MW)	Electrolyzer Capacity (MW_e)	Excess PV Electricity (MWh/year)	Community Load Met by Solar PV	Community Load Unmet by Solar PV (MWh/year)
Maximum	14.6	10	11,600	52%	8,300
Utility	6.5	3.26	1,450	40%	10,300

According to California's Department of Resources Recycling and Recovery, residential sources in Huntington Beach produced 22,184 tons of organic municipal waste, comprised of mostly food and yard waste, annually in 2016 [165]. Table 14 shows the residential waste produced by Huntington Beach residents in 2016 categorized by material type.

Table 14. All residential waste generated by the City of Huntington Beach in 2016 separated by material category according to California's Department of Resources Recycling and Recovery [165].

Material Category	Total Residential Tons	Percent Residential Total
All Paper	9,258	18.7%
All Glass	1,067	2.2%
All Metal	1,448	2.9%
All Electronics	569	1.1%
All Plastic	4,723	9.5%
All Food	9,836	19.9%
All Yard Waste	6,312	12.7%
All Manure	0	0.0%
All Other Organic	6,036	12.2%
All Inerts and Other	6,322	12.8%
All Household Hazardous Waste	247	0.5%
All Special Waste	1,719	3.5%
Mixed Residue	2,010	4.1%
Total	49,547	100%

To develop a design to achieve sustainable ZNE that is replicable for similar communities that may or may not have a waste handling facility, the per capita biogas potential of community resident generated OFMSW is calculated. The population of Huntington Beach in 2016 was 194,322 people [166]. Oak View's 10,000 residents comprise 5.1% of Huntington Beach residents. Thus, the residential organic waste generation of Huntington Beach per capita was 0.11 tons annually, and Oak View residents generated 1,100 tons of organic waste per year, 1.2% of the OFMSW processed at the OVWTS 2017. City-wide and per capita biogas and RNG production potentials are summarized in Table 15Table 15. Digestion of all OMSW processed by the OVWTS would generate 200,000 MMBTU/y of renewable natural gas.

Table 15. Biogas and RNG production potential by source and corresponding OFMSW mass digested.

OFMSW Source	OFMSW (tpy)	Biogas (mil. ft^3/y)	RNG (MMBTU/y)
All Processed at the OVWTS	78,000	340	200,000
All Huntington Beach Residents	22,000	38	51,000
All Oak View Residents	1,100	0.055	2,400
Per Capita in Oak View	0.11	0.0000055	0.24

The 78,000 tons/y includes Oak View waste. This value was used to determine renewable gas potential for the Oak View waste transfer station. However, results specific to the Oak View community in Section 3.6 and community specific results in Section 3.8 only allow for waste associated with the community.

3.6 Path Results

The renewable fuel or electricity production of all paths is shown in Table 16. Path 1 describes natural gas pipeline injection of hydrogen fuel generated via electrolysis from excess solar PV electricity. Electrolysis generates 28,500 MMBTU/y of hydrogen fuel in the Maximum scenario and 3,600 MMBTU/y of hydrogen in the Utility scenario.

In path 2, hydrogen produced via electrolysis of excess solar electricity is used to operate an SOFC. Under the maximum solar PV scenario with nearly 15 MW of solar PV capacity, a 570 kW steady state SOFC can be supported. Reducing PV capacity to the utility scenario reduces SOFC capacity to 72 kW.

Path 3 describes the injection of RNG produced via anaerobic digestion into the natural gas pipeline. Both scenarios produce 2,400 MMBTU/y of RNG in this path. In path 4, waste associated with the community would produce enough RNG to support a 47 kW SOFC operated at steady state.

Path 5 describes the pipeline injection of the mixture of hydrogen fuel from electrolysis and RNG from anaerobic digestion. The injected fuel in the Utility scenario is comprised of 95% RNG and 5% hydrogen, well below the concentration limit accepted by many European countries and has a total energy content of 5,900 MMBTU annually. The injected fuel in the Maximum scenario is comprised of

8% RNG and 92% hydrogen on an energy basis, a concentration above the limit accepted by natural gas pipelines in any country and has a total energy content of 28,500 MMBTU annually. Further investigation into the natural gas pipeline capacity and flow rate at the proposed injection site are required to assess the final hydrogen concentration percentage after pipeline injection and the viability of this pathway.

Path 6 describes the steady-state electrical output of an SOFC fueled by the mixture of hydrogen from electrolysis and RNG from anaerobic digestion. Total electric power production is 119 kW in the Utility scenario and is 570 kW in the Max scenario.

Table 16. Fuel quantities injected into the natural gas pipeline in paths 1, 3, and 5, and steady state SOFC power output for paths 2, 4, and 6 for both solar PV size scenarios.

Path	Fuel Source	Fuel Type	Fuel Injected into NG Pipeline (MMBTU/y)		Steady-State SOFC Power Output (kW)	
			Utility Scenario	Max Scenario	Utility Scenario	Max Scenario
Path 1	EC	H_2	3,600	28,500	-	-
Path 2	EC	H_2	-	-	60.	570
Path 3	AD	RNG	2,400	2,400	-	-
Path 4	AD	RNG	-	-	47	47
Path 5	AD	RNG	3,600	28,500	-	-
	EC	H_2	2,400	2,400		-
	All	RNG & H_2	5,900	30,900	-	-
Path 6	AD	RNG	-	-	47	47
	EC	H_2	-	-	72	570
	All	RNG & H_2	-	-	119	617

3.7 OFMSW Trucking Results

The total number of required vehicle roundtrips was found by rounding up the quotient of the annual weight of OFMSW by vehicle weight capacity. The number of vehicles required for transport was calculated by dividing the number of roundtrips by typical annual miles traveled per vehicle according to the AFLEET tool. Fractional numbers of vehicles were rounded up to the nearest whole. However, calculations assumed only the minimum number of total miles required to transport all OMSW and result in conservative estimates of criteria pollutant emission and fuel consumption.

Both class 7 vehicle types have the same maximum payload and would need to travel over 1.36 million miles over more than 10 thousand roundtrips between Oak View and Perris, CA. Based on annual

miles per vehicle, the class 7 SUSH fleet would consist of at least 83 vehicles, and SULH 60 vehicles. Class 8 vehicles would travel over 3.5 thousand roundtrips, requiring 8 total CSH or 3 CLH vehicles. The class 8 CLH fleet would consume the least amount of diesel fuel and produce the least amount of all criteria pollutants of all examined vehicles. The percent fuel energy consumed as diesel fuel during transportation compared to the fuel energy that could be produced from the OFMSW via anaerobic digestion ranges from 4.2% for the class 8 CLH fleet, to 14.0% for the class 7 SULH fleet. Fuel consumption for each fleet is shown in Table 16. Accounting for the energy loss attributed to trucking OFMSW with combination long-haul trucks, the total annual RNG energy potential from anaerobic digestion is 191,600 MMBTU/y. Only 2,400 MMBTU/y can be attributed to Oak View waste.

Table 17. Properties of vehicle fleets required to transport OMSW for four heavy-duty vehicle types.

Truck Class		**7**		**8**	
Truck Description, 2017 Model		Single Unit Short-Haul	Single Unit Long-Haul	Combination Short-Haul	Combination Long-Haul
Total Vehicle Roundtrips Per Year		10,247	10,247	3,511	3,511
Total Annual Miles Travelled by Fleet		1,364,900	1,364,900	467,665	467,665
Number of Vehicles in Fleet		82.7	59.3	7.2	2.8
Fleet Annual Fuel Consumption	Fleet Fuel Consumption (GGE/year)	212,787	239,809	72,992	75,257
	Energy content of Diesel Consumed (MMBTU)	24,279	27,363	8,329	8,587
	RNG (via AD) Energy Consumed in Transport of OFMSW	12.4%	14.0%	4.3%	4.2%

3.8 Cost Analysis

The cost analysis in this section considered the full organic throughput at the Oak View waste transfer station. When only the Oak View waste contribution is considered, costs are economically infeasible. By considering all OFMSW throughput at the studied location, better economies of scale are realized. The capital and annual O&M cost of each included technology in all six energy paths is listed in Table 19. For all Maximum scenario paths, 47% of PV installations were assumed to be located in the residential area of Oak View, while all else was assumed to be in commercial and industrial areas. For all Utility scenario paths, PV installations were assumed to be all commercial rooftop. For all pathways,

initial capital cost was assumed to be covered through debt with a life of 10 years and an annual interest rate of 8% and is shown in Table 19. Note that only solar PV capital cost associated with solar energy used for fuel production was included in this analysis. Solar energy used for fuel production was 56% and 17.4% for the maximum and utility solar scenarios, respectively.

Table 18. Capital and O&M cost of each technology included in Maximum and Utility scenario paths.

	Tech.	Utility Scenario		Max Scenario	
		Capital Cost ($)	O&M Cost ($/y)	Capital Cost ($)	O&M Cost ($/y)
Path 1	PV	3,547,298	3	15,957,200	28
	AEC	3,915,467	187,294	11,976,000	572,866
	H_2 PI	422,154	20,753	1,011,281	42,979
	Total	7,884,918	208,051	28,944,481	615,873
Path 2	PV	3,547,298	3	15,957,200	28
	AEC	3,915,467	187,294	11,976,000	572,866
	SOFC	357,667	45,066	2,862,956	360,732
	Total	7,820,431	232,364	30,796,156	933,626
Path 3	AD	35,500,000	3,910,261	35,481,204	3,910,261
	BG U	8,280,000	1,371,334	8,280,445	1,371,334
	RNG PI	2,270,000	84,337	2,270,838	84,337
	Total	46,000,000	5,365,931	46,032,487	5,365,931
Path 4	AD	35,481,204	3,910,261	35,481,204	3,910,261
	BG U	8,280,445	1,371,334	8,280,445	1,371,334
	SOFC	19,646,136	2,475,413	19,646,136	2,475,413
	Total	63,407,785	7,757,007	63,407,785	7,757,007
Path 5	PV	3,547,298	3	15,957,200	28
	AEC	1,140,000	187,294	11,976,000	572,866
	AD	35,500,000	3,910,261	35,481,204	3,910,261
	BG U	8,280,000	1,371,334	8,280,445	1,371,334
	RNG PI	2,290,000	84,871	2,404,363	88,450
	Total	67,600,000	5,553,763	74,099,212	5,942,937
Path 6	PV	3,547,298	3	15,957,200	28
	AEC	3,915,467	187,294	11,976,000	572,866
	AD	35,481,204	3,910,261	35,481,204	3,910,261
	BG U	8,280,445	1,371,334	8,280,445	1,371,334
	SOFC	20,003,802	2,520,479	22,509,092	2,836,146
	Total	71,228,217	7,989,371	94,203,941	8,690,633

BG U is biogas upgrading.

Table 19. Total cost of loan for path capital costs.

	Total Loan Cost (mil. $)	
	Utility Scenario	Max Scenario
Path 1: PV-PI	8	31
Path 2: PV-SOFC	8	33
Path 3: AD-PI	49	49
Path 4: AD-SOFC	68	68
Path 5: PV&AD-PI	57	79
Path 6: PV&AD-SOFC	76	100

All values are rounded to two significant figures.

LCOE values were calculated for each path on a per kWh or per MMBTU basis. Values in Table 20include the total loan cost, all O&M costs, and the cost of diesel fuel required to truck all OFMSW from Huntington Beach to Perris and assume 30-year lifetimes for the energy generation systems. LCOEs for paths 2, 4, and 6 assume a 0.5% electricity production degradation per year. LCOEs for paths 1, 3, and 5 do not include any degradation of the renewable fuel production rate over time. Table 20shows the levelized cost of renewable fuel energy for paths 1, 3, and 5 and LCOE of electrical energy produced via SOFC from renewable fuels for paths 2, 4, and 6.

The average residential and commercial cost of natural gas in California in 2017 was $12.04 and $8.45 per MMBTU, respectively [43]. The average price of residential and commercial electricity in 2017 from Southern California Edison, the local provider in Huntington Beach, was $0.1660/kWh and $0.1441/kWh, respectively [44].

The lowest levelized cost of renewable fuel is $36.79/MMBTU in path 3, the anaerobic digestion only case, of both scenarios. The highest levelized cost of renewable fuel is $136.94/MMBTU in path 1, a small-scale power-to-gas system, of the Utility scenario. At the larger Max scenario-scale system, LCOE of renewable fuel is still high at $57.62/MMBTU. In path 5, the renewable fuel LCOE is $38.40/MMBTU in the Utility scenario and $39.12/MMBTU in the Max scenario. LCOE for renewably generated gas in Oak View is 3-11 times larger than the 2017 average residential natural gas price in California.

The lowest levelized cost of electricity is $0.32/kWh, which occurs in path 4, the anaerobic digestion only case, of both scenarios. The LCOE in path 6, the PV and AD case, of both scenarios is $0.33\kWh, and the LCOE in Path 2 of the Max scenario is $0.43/kWh. The highest levelized cost of electricity is $0.88/kWh in path 2 of the Utility scenario. Levelized costs of electricity generated in Oak View are 2-5 times larger than the 2017 SCE average residential electricity price.

Table 20. Levelized cost of renewable fuel energy for paths 1, 3, and 5 and electrical energy produced via SOFC from renewable fuels for paths 2, 4, and 6. Anaerobic digestion facilities are sized to use all OFMSW processed at the OVWTS as feedstock.

	Utility Scenario		Max Scenario	
	Fuel Energy Cost ($/MMBTU)	Electrical Energy Cost ($/kWh$_e$)	Fuel Energy Cost ($/MMBTU)	Electrical Energy Cost ($/kWh$_e$)
Path 1: PV-PI	$136.94	-	$57.62	-
Path 2: PV-SOFC	-	$0.88	-	$0.43
Path 3: AD-PI	$36.79	-	$36.79	-
Path 4: AD-SOFC	-	$0.32	-	$0.32
Path 5: PV&AD-PI	$38.40	-	$39.12	-
Path 6: PV&AD-SOFC	-	$0.33	-	$0.33

Using a diesel sale price of $3.18/gal [176], the minimum cost of diesel fuel required to truck OFMSW from Oak View to Perris is $1.04/MMBTU of RNG produced. P_{NG} was set to the average residential cost of natural gas in California in 2017, $12.04/MMBTU [43]. The resulting tipping cost for OFMSW to produce RNG for vehicle fuel is $41.61/ton and for other end uses is $28.79/ton. Assuming a fully loaded class 8 CLH full truckload, RNG cost parity is achieved when the total tipping fee is $1,123. If the RNG is not used for vehicle fuel, the tipping fee must decrease to $777 per truckload. Thus, tipping fees much less than these would be required for profitability.

The payback period in years of each path of the Maximum scenario was calculated according to the formula:

$$Payback\ Period\ in\ years = \frac{total\ loan\ cost}{average\ annual\ net\ cash\ flow}$$

$$= \frac{total\ loan\ cost}{average\ annual\ generated\ income - average\ annual\ O\&M\ costs}.$$

Payback period calculations do not consider the electricity production degradation, inflation, or changes in electricity and natural gas prices, and the solar electricity capital and O&M costs in all paths is again

scaled to only include the costs of excess electricity production. All six paths of the Maximum scenario have negative net annual cash flows if the natural gas sale price is set to $12.04/MMBTU, the average residential cost of natural gas in California in 2017 [43], and the electricity sale price is set to $0.1660/kWh, the average price of residential and commercial electricity in 2017 from Southern California Edison [44]. All six paths operate at a loss annually and so can never pay pack the initial loan investment at these prices. Vishwanathan, et al. approximated a payback period of 7.0 years for a high-efficiency CHP natural gas generator in Los Angeles based on 2016 average electricity prices [177]. In order to compare RNG and renewable electricity prices to current natural gas and electricity prices, Table 21(a) shows the required renewable fuel and electricity sales prices to obtain payback periods of 7, 10, 20, and 30 years. To yield a payback period of 7 years, the RNG sale price would need to be 5.2-15 times larger than the 2017 California residential average and the electricity sale price would need to be 3.0-6.8 times larger than the 2017 SCE average residential price as shown in Table 21(b).

Table 21. (a) Renewable fuel and electricity sale prices required for pathway payback periods of 10, 20, and 30 years. (b) The number of times larger the fuel/electricity sale price would need to be compared to the 2017 average residential prices in order to produce payback periods of 10, 20, and 30 years.

(a)

Payback Period (years):			**7 years**	**10 years**	**20 years**	**30 years**
Fuel/Electricity Cost	Path 1	($/MMBTU)	176	130	76	58
	Path 2	($/kWh)	1.1	0.84	0.51	0.40
	Path 3	($/MMBTU)	63	52	40	36
	Path 4	($/kWh)	0.51	0.42	0.32	0.29
	Path 5	($/MMBTU)	77	62	44	38
	Path 6	($/kWh)	0.58	0.48	0.35	0.31

(b)

Payback Period (years):		**7 years**	**10 years**	**20 years**	**30 years**
Times larger than 2017 average residential sale price	Path 1	15	11	6.3	4.8
	Path 2	6.8	5.1	3.1	2.4
	Path 3	5.2	4.4	3.3	3.0
	Path 4	3.0	2.5	1.9	1.8
	Path 5	6.4	5.1	3.7	3.2
	Path 6	3.5	2.9	2.1	1.9

3.9 Net Energy Analysis

The subsequent energy analysis only considers results for the scenario where OMFSW would be trucked out of the Oak View community. This scenario was selected as most likely to occur considering the current decision to move waste to this location combined with local desires to not install an anaerobic digester in Oak View. Table 22Table 22 shows the percent net electrical demand in Oak View after accounting for the minimum 4.2% RNG energy loss as diesel fuel consumption during trucking. Only electricity-producing paths 2, 4, and 6 are considered for this analysis and are directly compared to Oak View's modeled electrical demand to calculate percent demand met by renewable electricity production.

The results shown in Table 22(a) consider only RNG produced from OFMSW attributed to Oak View residents. An SOFC operating on net RNG fuel energy would meet 2.3% of community electrical demand. The power produced from hydrogen fuel made via electrolysis of excess solar electricity would meet 3.3% of electrical demand in the Utility scenario, and 26% in the Max scenario. The percent total community electrical demand that would be met by the power produced from all renewable fuels (path 6) and solar PV is 46% in the Utility scenario and 80% in the Max scenario. The largest amount of energy produced exclusively from renewable fuels is 29% in the Max scenario path 6.

The results for cases that consider renewable fuels generated from all OFMSW processed at the OVWTS are shown in Table 22(b). An SOFC operating on this RNG would meet 190% of community electrical demand. The percent total community electrical demand that would be met by power produced from all renewable fuels (path 6) and solar PV is 240% in the Utility scenario and 270% in the Max scenario.

Table 22. Percent modeled community electrical demand met by renewable electricity and fuel generation for two anaerobic digestion feedstock cases: (a) Oak View residential OFMSW and (b) all OFMSW currently processed at the Oak View waste transfer station.

(a) Electrical End Use Paths Using Oak View OFMSW

	Utility Scenario		Max Scenario	
	Community Electrical Demand Met by SOFC	Total Demand met by renewables (SOFC + PV)	Community Electrical Demand Met by SOFC	Total Demand met by renewables (SOFC + PV)
Path 2	3.65%	43.7%	29.2%	80.9%
Path 4	2.31%	42.4%	2.31%	54.0%
Path 6	5.96%	46.0%	31.5%	83.2%

(b) **Electrical End Use Paths Using Total OFMSW**

	Utility Scenario		Max Scenario	
	Community Electrical Demand Met by SOFC	Total Demand met by renewables (SOFC + PV)	Community Electrical Demand Met by SOFC	Total Demand met by renewables (SOFC + PV)
Path 2	3.65%	43.7%	29.2%	80.9%
Path 4	192%	232%	192%	244%
Path 6	195%	236%	221%	273%

CHAPTER 4: SUMMARY AND CONCLUSIONS

A model for assessing the efficiency and economic viability of community-scale renewable gas generation, conversion, and use to complement residential PV was developed and used to evaluate renewable fuel and electricity production potential in a 10,000 resident example community in Huntington Beach, California. The model shows that the use of environmentally friendly technologies such as community-scale distributed fuel generation and power systems is not economically competitive with current natural gas and natural gas-based electricity prices. However, technological advances in the next decades may make electrolysis and SOFC technologies significantly more competitive. The continued development of intermittent renewable generation systems (i.e. solar and wind) at increasingly high levels of market penetration may also make community-level use of these technologies more competitive as the utility grid network is required to store increasingly larger amounts of excess renewable energy for long periods of time. Additionally, government incentives may be enough to make these technologies more competitive. Current analyses suggest that this could occur in the present day for anaerobic digestion, especially in larger scales.

Transient SOFC performance on natural gas and clean biogas were explored in the effort to model renewable fuel and electricity generation in the community. These efforts included operating an SOFC both at steady-state and dynamically on natural gas, using experimental data to verify and adjust an SOFC model, and simulating SOFC dynamic operation on clean biogas. The optimized SOFC-centrifugal blower model shows good correlation to experimental results for stack power, stack current, stack voltage, and air volume flow rate. Model cathode exit temperatures are consistently higher than but within 6.2% of the experimental values, while model and experimental anode tail gas oxidizer profiles exhibit inverse trends. The modeled efficiency profile is similar to experimental efficiency measurements for steady-state operation but does not accurately match dynamic experimental efficiency measurements. Overall, the dynamic simulation satisfactorily captures the BlueGEN steady-

state and transient performance. Because of the limited commercial availability of dynamic and biogas-friendly SOFC systems, ultimately only pathways for utilizing renewable fuel energy potential that involved steady-state SOFC operation on hydrogen and renewable natural gas fuels were selected for efficiency and financial analysis.

This analysis is unable to achieve zero-net-energy for the studied community. The largest percent total community electrical demand is met by the Maximum scenario path 6, which includes PV electricity production, RNG production from anaerobic digestion, and hydrogen fuel production from electrolysis and meets over 80% of the modeled total community electrical demand. In this case 52% of the community's total electrical demand is met by solar PV, 26% by SOFC operation on renewable hydrogen produced using excess solar, and 3% by SOFC operation on RNG produced from anaerobic digestion of OFMSW. When solar capacity is maximized, yearly hydrogen production for the entire community is 2.85 MMBTU/y of hydrogen fuel via electrolysis and 0.24 MMBTU/y of RNG via anaerobic digestion of residential OFMSW.

The levelized cost of energy for renewable fuel production for analyzed pathways is $37-137/MMBTU. These prices are driven primarily by the high capital costs associated with the relatively small anaerobic digestion system operating on community-sourced OFMSW. The LCOE for renewable electricity production is $0.32-0.43/kWh. The lowest levelized cost of electricity of the cases analyzed occurs in path 4 (AD-SOFC case) of both scenarios, while the LCOE of path 6 (PV&AD-SOFC case) in both scenarios is only $0.01 higher. The lowest LCOE of RNG for each scenario occurs in path 3 (AD-PI case). Path 1 (PV-EC case) and path 2 (PV-SOFC case), in which only hydrogen fuel production is considered, yield the highest cost of fuel and electricity. LCOE cost trends correlate well with those exhibited by the required sale prices of electricity and renewable fuel when system payback period is set to match that of current high-efficiency natural gas power generation plants.

To yield a payback period of 7 years, the sale price of renewable gaseous fuel generated in the community would need to be $176/MMBTU of hydrogen in path 1 (PV-EC case), $63/MMBTU of RNG in path 3 (AD-PI case), and $77/MMBTU of RNG in path 5 (PV&AD-PI case). These prices correspond to 15, 5.2, and 6.4 times the 2017 average California residential natural gas price. These results suggest that neither renewable gaseous fuel production from the small-scale electrolysis of solar energy or from the anaerobic digestion of OFMSW can be economically competitive with natural gas without extensive subsidies or incentives. However, by supplementing more energy dense feedstocks like fat, oil, grease, and manure with OFMSW existing digesters could increase RNG production in a way that is currently economically feasible.

The sale price of renewable electricity generated in the community would need to be $1.12/kWh in path 2 (PV-SOFC case), $0.51/kWh in path 4 (AD-SOFC case), and $0.58/kWh in path 6 (PV&AD-SOFC case) to yield a power generation plant payback period of 7 years. These prices correspond to 6.8, 3.0, and 3.5 times the 2017 SCE residential electricity price making renewable electricity production about twice as economically competitive as renewable gaseous fuel production in all pathways analyzed. The biogas-fueled SOFC system in path 4 and the biogas- and hydrogen-fueled SOFC system in path 6 were the most economically competitive of all scenarios analyzed. Biogas-fueled SOFC power generation plants using fuel from the anaerobic digestion of more energy dense feedstocks would be even more economically competitive with current electricity prices.

These results suggest that zero-net-energy communities are not possible using currently available commercial renewable fuel and electricity generation technologies. However, excess solar electricity and organic wastes from residential communities can provide significant energy for larger utility-scale systems that amass resources from multiple communities. The results encourage the present trend of installing residential solar PV and building industrial-scale power plants. Further research could validate SOFC transient performance with biogas fuel operation to allow for allow

sustainable load-following electricity production or to could consider additional sources of renewable power and organic waste, including wind and wastewater, to more accurately assess the potential of designing a zero-net-energy residential community.

REFERENCES

[1] C. P. U. Commission, “2020 Planning and Information for California ZNE Homes: Frequently Asked Questions,” 2016. .

[2] R. B. C. Weisenmiller *et al.*, “2019 Building Energy Efficiency Standards: building energy efficiency standars for residential and nonresidential buildings,” 2019.

[3] California Public Utilities Commission, “Commercial & Residential: California’s ZNE Action Plans,” *Zero Net Energy California*. [Online]. Available: https://www.capath2zne.org/. [Accessed: 01-Oct-2018].

[4] N. Bautista, “08/28/18- Senate Floor Analysis for Bill No. SB 100,” Sacramento, 2018.

[5] *AB-398 California Global Warming Solutions Act of 2006: market-based compliance mechanisms: fire prevention fees: sales and use tax manufacturing exemption.* 2018.

[6] California Public Utilities Commission, “California Solar Initiative (CSI) - Go Solar California.” .

[7] H. Geller, P. Harrington, and A. H. Rosenfeld, “Polices for increasing energy efficiency : Thirty years of experience in OECD countries,” vol. 34, pp. 556–573, 2006.

[8] R. Darghouth, G. Barbose, and R. Wiser, “The impact of rate design and net metering on the bill savings from distributed PV for residential customers in California,” vol. 39, pp. 5243–5253, 2011.

[9] E. Funkhouser, G. Blackburn, C. Magee, and V. Rai, “Business model innovations for deploying distributed generation : The emerging landscape of community solar in the U . S . &,” *Chem. Phys. Lett.*, vol. 10, pp. 90–101, 2015.

[10] A.-F. Marique and S. Reiter, “A simplified framework to assess the feasibility of zero-energy at the neighbourhood / community scale,” vol. 82, pp. 114–122, 2014.

[11] J. Keirstead, N. Samsatli, N. Shah, and C. Weber, “The impact of CHP (combined heat and power) planning restrictions on the efficiency of urban energy systems,” *Energy*, vol. 41, no. 1, pp. 93–103, May 2012.

[12] S. Mashayekh, M. Stadler, G. Cardoso, and M. Heleno, “A mixed integer linear programming approach for optimal DER portfolio , sizing , and placement in multi-energy microgrids,” *Appl. Energy*, vol. 187, pp. 154–168, 2017.

[13] A. Omu, S. Hsieh, and K. Orehounig, “Mixed integer linear programming for the design of solar thermal energy systems with short-term storage,” *Appl. Energy*, vol. 180, pp. 313–326, 2016.

[14] J. Keirstead, M. Jennings, and A. Sivakumar, “A review of urban energy system models: Approaches, challenges and opportunities,” *Renew. Sustain. Energy Rev.*, vol. 16, no. 6, pp. 3847–3866, 2012.

[15] D. Parra, S. A. Norman, G. S. Walker, and M. Gillott, “Optimum community energy storage for renewable energy and demand load management,” *Appl. Energy*, vol. 200, pp. 358–369, 2017.

[16] M. Obi and R. Bass, “Trends and challenges of grid-connected photovoltaic systems – A review,” *Renew. Sustain. Energy Rev.*, vol. 58, pp. 1082–1094, 2016.

[17] A. Saeedmanesh, M. A. Mac Kinnon, and J. Brouwer, “Hydrogen is essential for sustainability,” *Curr. Opin. Electrochem.*, vol. 12, pp. 166–181, 2018.

[18] O. Schmidt, A. Gambhir, I. Staffell, A. Hawkes, J. Nelson, and S. Few, “Future cost and performance of water electrolysis: An expert elicitation study,” *Int. J. Hydrogen Energy*, vol. 42, no. 52, pp. 30470–30492, Dec. 2017.

[19] M. Götz *et al.*, “Renewable Power-to-Gas: A technological and economic review,” *Renewable Energy*, vol. 85. pp. 1371–1390, 2016.

[20] D. van der Horst, “NIMBY or not ? Exploring the relevance of location and the politics of voiced opinions in renewable energy siting controversies,” vol. 35, pp. 2705–2714, 2007.

[21] S. Ohnishi, M. Fujii, M. Ohata, I. Rokuta, and T. Fujita, “Resources , Conservation and Recycling

Efficient energy recovery through a combination of waste-to-energy systems for a low-carbon city," *"Resources, Conserv. Recycl.*, vol. 128, pp. 394–405, 2018.
[22] Y. Geng, F. Tsuyoshi, and X. Chen, "Evaluation of innovative municipal solid waste management through urban symbiosis : a case study of Kawasaki q," *J. Clean. Prod.*, vol. 18, no. 10–11, pp. 993–1000, 2012.
[23] P. Ghisellini, C. Cialani, and S. Ulgiati, "A review on circular economy : the expected transition to a balanced interplay of environmental and economic systems," *J. Clean. Prod.*, vol. 114, pp. 11–32, 2016.
[24] D. F. McLarty, "Fuel Cell Gas Turbine Hybrid Design, Control, and Performance," University of California Irvine, 2006.
[25] P. Jaramillo and N. Z. Muller, "Air pollution emissions and damages from energy production in the U.S.: 2002–2011," *Energy Policy*, vol. 90, pp. 202–211, Mar. 2016.
[26] Bob Fesmire, "Energy Efficiency in the Power Grid - Renewable Energy World," *ABB Inc.*, 2007. [Online]. Available: https://www.renewableenergyworld.com/articles/2007/07/energy-efficiency-in-the-power-grid-49238.html. [Accessed: 01-Oct-2018].
[27] U. S. D. of E. Lawrence Livermore National Laboratory, "LLNL Flow Charts," 2017. [Online]. Available: https://flowcharts.llnl.gov/. [Accessed: 01-Oct-2018].
[28] K. Nanaeda, F. Mueller, J. Brouwer, and S. Samuelsen, "Dynamic Modeling of a Solid Oxide Fuel Cell Combined Heat and Power System With Thermal Storage for Commercial Building Applications," in *ASME 2009 7th International Conference on Fuel Cell Science, Engineering and Technology*, 2009, pp. 631–640.
[29] The United States Senate, "The American Recovery and Reinvestment Act of 2009: Creating Jobs, Cutting Taxes and Investing in Our Country's Future," 2009.
[30] "A Glimpse of the Future Grid through Recovery Act Funding."
[31] Executive Order, "Planning for Federal Sustainability in the Next Decade, 3 C.F.R. (2015)." [Online]. Available: https://obamawhitehouse.archives.gov/the-press-office/2015/03/19/executive-order-planning-federal-sustainability-next-decade. [Accessed: 01-Oct-2018].
[32] C. Fogel and B. Martha, "Defining ZNE Buildings and ZNE Building Goals in California." IEPR Workshop on ZNE, 2013.
[33] B. Kumar Sahu, "A study on global solar PV energy developments and policies with special focus on the top ten solar PV power producing countries," *Renew. Sustain. Energy Rev.*, vol. 43, pp. 621–634, Mar. 2015.
[34] P. Denholm, M. O'connell, G. Brinkman, and J. Jorgenson, "Overgeneration from Solar Energy in California: A Field Guide to the Duck Chart," 2015.
[35] California Independent Systems Operator (CAISO), "California ISO Fast Facts: What the duck curve tells us about managing a green grid," Folsom, California, 2016.
[36] California Independent System Operator, "Managing Oversupply," 2018. [Online]. Available: http://www.caiso.com/informed/Pages/ManagingOversupply.aspx. [Accessed: 15-Oct-2018].
[37] N. Parker, R. Williams, R. Dominguez-Faus, and D. Scheitrum, "Renewable natural gas in California: An assessment of the technical and economic potential," *Energy Policy*, vol. 111, pp. 235–245, Dec. 2017.
[38] J. Starn, "Negative Prices in Power Market as Wind Solar Cut Electricity," *Bloomberg*, 2018. [Online]. Available: https://www.bloomberg.com/news/articles/2018-08-06/negative-prices-in-power-market-as-wind-solar-cut-electricity. [Accessed: 17-Nov-2018].
[39] California Independent System Operator (CAISO), "Managing Oversupply," 2018. [Online]. Available: http://www.caiso.com/informed/Pages/ManagingOversupply.aspx. [Accessed: 17-Nov-2018].

[40] J. Faust, J., August, L., Bangia, K., Schmitz, R., Galaviz, V., & Leichty, "California Communities Environmental Health Screening Tool, Version 2.0 (CalEnviroScreen 2.0): Guidance and Screening Tool.," 2014.
[41] United States Census Bureau, "American Community Survey (ACS)."
[42] "Findings and Decision for Order for Abatement (Stipulated) - South Coast Air Quality Management District vs. Rainbow Transfer/Recycling, Inc. Case no. 4394-2," Diamond Bar, 2015.
[43] United States Energy Information Administration, "U.S. Natural Gas Summary." [Online]. Available: https://www.eia.gov/dnav/ng/ng_sum_lsum_dcu_nus_a.htm. [Accessed: 13-Sep-2016].
[44] U.S. Energy Information Administration, "Electricity Data," 2018. [Online]. Available: https://www.eia.gov/electricity/data.php. [Accessed: 24-Oct-2018].
[45] Lazard, "Levelized Cost of Energy 2017," 2018. [Online]. Available: https://www.lazard.com/perspective/levelized-cost-of-energy-2017/. [Accessed: 12-Dec-2018].
[46] R. Fu, D. Feldman, R. Margolis, M. Woodhouse, and K. Ardani, "U.S. Solar Photovoltaic System Cost Benchmark: Q1 2017," Denver, 2017.
[47] Lazard, "Levelized Cost of Storage 2017," 2018. [Online]. Available: https://www.lazard.com/perspective/levelized-cost-of-storage-2017/. [Accessed: 22-Oct-2018].
[48] L. Bertuccioli, A. Chan, D. Hart, F. Lehner, B. Madden, and E. Standen, "Development of water electrolysis in the European Union," *Fuel Cells Hydrog. Jt. Undert.*, vol. 83, 2014.
[49] J. Jacobs, "Economic Modeling of Cost Effective Hydrogen Production From Water Electrolysis by Utilizing Iceland's Regulating Power Market," 2016.
[50] E. I. Zoulias and N. Lymberopoulos, "Techno-economic analysis of the integration of hydrogen energy technologies in renewable energy-based stand-alone power systems," *Renew. Energy*, vol. 32, no. 4, pp. 680–696, Apr. 2007.
[51] J. Baier, G. Schneider, and A. Heel, "A Cost Estimation for CO2 Reduction and Reuse by Methanation from Cement Industry Sources in Switzerland," *Front. Energy Res.*, vol. 6, p. 5, Feb. 2018.
[52] K. Darrow, R. Tidball, J. Wang, and A. Hampson, "Catalog of CHP Technologies," 2017.
[53] M. Chatsko, "Bloom Energy Is the Newest Fuel Cell Stock, but Is Its Technology Already Outdated?," *The Motley Fool*, 2018. [Online]. Available: https://www.fool.com/investing/2018/09/05/bloom-energy-is-the-newest-fuel-cell-stock-but-is.aspx. [Accessed: 12-Oct-2018].
[54] L. M. Fraas, "History of Solar Cell Development," in *Low-Cost Solar Electric Power*, Cham: Springer International Publishing, 2014, pp. 1–12.
[55] M. Hosenuzzaman, N. A. Rahim, J. Selvaraj, M. Hasanuzzaman, A. B. M. A. Malek, and A. Nahar, "Global prospects, progress, policies, and environmental impact of solar photovoltaic power generation," *Renew. Sustain. Energy Rev.*, vol. 41, pp. 284–297, Jan. 2015.
[56] California Energy Commission, "Total System Electric Generation," 2018. [Online]. Available: https://www.energy.ca.gov/almanac/electricity_data/total_system_power.html. [Accessed: 15-Oct-2018].
[57] United States Energy Information Administration, "California State Energy Profile." [Online]. Available: https://www.eia.gov/state/print.php?sid=CA. [Accessed: 01-Oct-2018].
[58] J. Leadbetter and L. G. Swan, "Selection of battery technology to support grid-integrated renewable electricity," *J. Power Sources*, vol. 216, pp. 376–386, Oct. 2012.
[59] P. K. Smith *et al.*, "Life Prediction Model for Grid-Connected Li-ion Battery Energy Storage System: Preprint."
[60] I. Hadjipaschalis, A. Poullikkas, and V. Efthimiou, "Overview of current and future energy storage technologies for electric power applications," *Renew. Sustain. Energy Rev.*, vol. 13, no. 6–7, pp.

1513–1522, Aug. 2009.
[61] M. Beaudin, H. Zareipour, A. Schellenberglabe, and W. Rosehart, “Energy storage for mitigating the variability of renewable electricity sources: An updated review,” *Energy Sustain. Dev.*, vol. 14, no. 4, pp. 302–314, Dec. 2010.
[62] H. Chen, T. N. Cong, W. Yang, C. Tan, Y. Li, and Y. Ding, “Progress in electrical energy storage system: A critical review,” *Prog. Nat. Sci.*, vol. 19, no. 3, pp. 291–312, Mar. 2009.
[63] I. H. Son *et al.*, “Silicon carbide-free graphene growth on silicon for lithium-ion battery with high volumetric energy density,” *Nat. Commun.*, vol. 6, no. 1, p. 7393, Dec. 2015.
[64] D. Papurello, A. Lanzini, L. Tognana, S. Silvestri, and M. Santarelli, “Waste to energy: Exploitation of biogas from organic waste in a 500 Wel solid oxide fuel cell (SOFC) stack,” *Energy*, vol. 85, pp. 145–158, Jun. 2015.
[65] United States Environmental Protection Agency, “AgSTAR: Biogas Recovery in the Agriculture Sector.” [Online]. Available: https://www.epa.gov/agstar. [Accessed: 01-Oct-2018].
[66] X. M. Guo, E. Trably, E. Latrille, H. Carrère, and J.-P. Steyer, “Hydrogen production from agricultural waste by dark fermentation: A review,” *Int. J. Hydrogen Energy*, vol. 35, no. 19, pp. 10660–10673, Oct. 2010.
[67] M. J. Park, J. H. Jo, D. Park, D. S. Lee, and J. M. Park, “Comprehensive study on a two-stage anaerobic digestion process for the sequential production of hydrogen and methane from cost-effective molasses,” *Int. J. Hydrogen Energy*, vol. 35, no. 12, pp. 6194–6202, Jun. 2010.
[68] R. Saidi *et al.*, “Biohydrogen production from hyperthermophilic anaerobic digestion of fruit and vegetable wastes in seawater: Simplification of the culture medium of Thermotoga maritima,” *Waste Manag.*, vol. 71, pp. 474–484, Jan. 2018.
[69] G. Antonopoulou, H. N. Gavala, I. V. Skiadas, K. Angelopoulos, and G. Lyberatos, “Biofuels generation from sweet sorghum: Fermentative hydrogen production and anaerobic digestion of the remaining biomass,” *Bioresour. Technol.*, vol. 99, no. 1, pp. 110–119, Jan. 2008.
[70] A. Tabasová, J. Kropáč, V. Kermes, A. Nemet, and P. Stehlík, “Waste-to-energy technologies: Impact on environment,” *Energy*, vol. 44, no. 1, pp. 146–155, Aug. 2012.
[71] M. Kim, Y.-H. Ahn, and R. . Speece, “Comparative process stability and efficiency of anaerobic digestion; mesophilic vs. thermophilic,” *Water Res.*, vol. 36, no. 17, pp. 4369–4385, Oct. 2002.
[72] A. J. Ward, P. J. Hobbs, P. J. Holliman, and D. L. Jones, “Optimisation of the anaerobic digestion of agricultural resources,” *Bioresour. Technol.*, vol. 99, no. 17, pp. 7928–7940, Nov. 2008.
[73] R. Waltenberger and R. Kirchmayr, “Wet and Dry Anaerobic Digestion Processes,” 2013.
[74] I. H. International Commission of Agricultural Engineering (CIGR), M. F. N. Abowei, M. J. Ayotamuno, and C. L. Eze, *Agricultural engineering international : CIGR journal.* International Commission of Agricultural Engineering, 1999.
[75] L. Alibardi and R. Cossu, “Composition variability of the organic fraction of municipal solid waste and effects on hydrogen and methane production potentials,” *Waste Manag.*, vol. 36, pp. 147–155, Feb. 2015.
[76] D. Papurello, A. Lanzini, P. Leone, M. Santarelli, and S. Silvestri, “Biogas from the organic fraction of municipal solid waste: Dealing with contaminants for a solid oxide fuel cell energy generator,” *Waste Manag.*, vol. 34, no. 11, pp. 2047–2056, Nov. 2014.
[77] M. Herout, J. Malatak, L. Kucera, and T. Dlabaja, “Biogas composition depending on the type of plant biomass used.,” *Res. Agric. Eng.*, vol. 57, no. 4, p. 137, 2011.
[78] E. J. Hengeveld, W. J. T. van Gemert, J. Bekkering, and A. A. Broekhuis, “When does decentralized production of biogas and centralized upgrading and injection into the natural gas grid make sense?,” *Biomass and Bioenergy*, vol. 67, pp. 363–371, Aug. 2014.
[79] Q. Sun, H. Li, J. Yan, L. Liu, Z. Yu, and X. Yu, “Selection of appropriate biogas upgrading technology-a review of biogas cleaning, upgrading and utilisation,” *Renew. Sustain. Energy Rev.*,

vol. 51, pp. 521–532, Nov. 2015.
[80] California Public Utilities Commission, “SB 1122: Bioenergy Feed-in Tariff,” 2019. [Online]. Available: http://www.cpuc.ca.gov/sb_1122/. [Accessed: 10-Mar-2019].
[81] U.S. Energy Information Administration (EIA), “Feed-in tariff: A policy tool encouraging deployment of renewable electricity technologies,” *Today in Energy* . [Online]. Available: https://www.eia.gov/todayinenergy/detail.php?id=11471. [Accessed: 10-Mar-2019].
[82] U. Di Matteo *et al.*, “Energy Contribution of OFMSW (Organic Fraction of Municipal Solid Waste) to Energy-Environmental Sustainability in Urban Areas at Small Scale,” *Energies*, vol. 10, no. 2, p. 229, Feb. 2017.
[83] M. Franchetti and A. Dellinger, “Economic Feasibility of a Municipal Food Waste Collection and Energy Generation Model,” *Energy Technol. Policy*, vol. 1, no. 1, pp. 52–58, Jan. 2014.
[84] Y. Shiratori, T. Oshima, and K. Sasaki, “Feasibility of direct-biogas SOFC,” *Int. J. Hydrogen Energy*, vol. 33, no. 21, pp. 6316–6321, Nov. 2008.
[85] T. Kaneko, J. Brouwer, and G. S. Samuelsen, “Power and temperature control of fluctuating biomass gas fueled solid oxide fuel cell and micro gas turbine hybrid system,” *J. Power Sources*, vol. 160, no. 1, pp. 316–325, Sep. 2006.
[86] Argonne National Laboratory, “Alternative Fuel Life-Cycle Environmental and Economic Transportation (AFLEET) Tool,” 2017. [Online]. Available: https://greet.es.anl.gov/afleet_tool. [Accessed: 30-May-2018].
[87] Google, “Google Maps,” 2018. .
[88] M. Ni, M. K. H. Leung, and D. Y. C. Leung, “Technological development of hydrogen production by solid oxide electrolyzer cell (SOEC),” *Int. J. Hydrogen Energy*, vol. 33, no. 9, pp. 2337–2354, May 2008.
[89] A. Hauch, S. D. Ebbesen, S. H. Jensen, and M. Mogensen, “Highly efficient high temperature electrolysis,” *J. Mater. Chem.*, vol. 18, no. 20, p. 2331, May 2008.
[90] T. L. LeValley, A. R. Richard, and M. Fan, “The progress in water gas shift and steam reforming hydrogen production technologies – A review,” *Int. J. Hydrogen Energy*, vol. 39, no. 30, pp. 16983–17000, Oct. 2014.
[91] J. D. Holladay, J. Hu, D. L. King, and Y. Wang, “An overview of hydrogen production technologies,” *Catal. Today*, vol. 139, no. 4, pp. 244–260, Jan. 2009.
[92] M. Carmo, D. L. Fritz, J. Mergel, and D. Stolten, “A comprehensive review on PEM water electrolysis,” *Int. J. Hydrogen Energy*, vol. 38, no. 12, pp. 4901–4934, Apr. 2013.
[93] M. A. Laguna-Bercero, “Recent advances in high temperature electrolysis using solid oxide fuel cells: A review,” *J. Power Sources*, vol. 203, pp. 4–16, Apr. 2012.
[94] J. A. Kilner, *Functional materials for sustainable energy applications*. Woodhead Pub, 2012.
[95] K. Zeng and D. Zhang, “Recent progress in alkaline water electrolysis for hydrogen production and applications,” *Prog. Energy Combust. Sci.*, vol. 36, no. 3, pp. 307–326, Jun. 2010.
[96] M. Lehner, R. Tichler, H. Steinmüller, and M. Koppe, “Storage Options for Renewable Energy,” in *Power-to-Gas: Technology and Business Models*, Cham: Springer International Publishing, 2014.
[97] M. Carmo, D. L. Fritz, J. Mergel, and D. Stolten, “A comprehensive review on PEM water electrolysis,” *Int. J. Hydrogen Energy*, vol. 38, no. 12, pp. 4901–4934, Apr. 2013.
[98] M. Lehner, R. Tichler, H. Steinmüller, and M. Koppe, “The Power-to-Gas Concept,” Springer, Cham, 2014, pp. 7–17.
[99] M. W. Melaina, O. Antonia, and M. Penev, “Blending Hydrogen into Natural Gas Pipeline Networks: A Review of Key Issues,” Denver, 2013.
[100] J. de Bucy, “The Potential of Power-to-gas: Technology review and economic potential assessment,” 2016.
[101] S. Rönsch *et al.*, “Review on methanation – From fundamentals to current projects,” *Fuel*, vol.

166, pp. 276–296, Feb. 2016.
[102] E. Giglio, A. Lanzini, M. Santarelli, and P. Leone, “Synthetic natural gas via integrated high-temperature electrolysis and methanation: Part I—Energy performance,” *J. Energy Storage*, vol. 1, pp. 22–37, Jun. 2015.
[103] G. Benjaminsson, J. Benjaminsson, and R. B. Rudberg, “Power-to-Gas - A technical review,” Malmö, 2013.
[104] “An Engineering-Economic Analysis of Syngas Storage Final Report,” 2008.
[105] E. Giglio, A. Lanzini, M. Santarelli, and P. Leone, “Synthetic natural gas via integrated high-temperature electrolysis and methanation: Part II—Economic analysis,” *J. Energy Storage*, vol. 2, pp. 64–79, Aug. 2015.
[106] C. Bloch and L. von Broich, “Optimised biogas upgrading by methanation in full scale,” Odense, Denmark, 2017.
[107] Graf, F., M. Götz, M. Henel, T. Schaaf, and R. Tichler, “Abschlussbericht: Techno-ökonomische Studie von Power-to-Gas-Konzepten.,” *Bonn*, 2014.
[108] M. Gassner and F. Maréchal, “Thermo-economic process model for thermochemical production of Synthetic Natural Gas (SNG) from lignocellulosic biomass,” *Biomass and Bioenergy*, vol. 33, no. 11, pp. 1587–1604, Nov. 2009.
[109] D. Gray, S. Salerno, G. Tomlinson, and J. J. Marano, “Polygeneration of SNG, Hydrogen, Power, and Carbon Dioxide from Texas Lignite,” *Carbon N. Y.*, 2004.
[110] D. Gray, S. Salerno, and G. Tomlinson, “Mitretek Technical Report Potential Application of Coal-Derived Fuel Gases for the Glass Industry: A Scoping Analysis,” 2004.
[111] J. D. Maclay, J. Brouwer, and G. S. Samuelsen, “Dynamic modeling of hybrid energy storage systems coupled to photovoltaic generation in residential applications,” *J. Power Sources*, vol. 163, no. 2, pp. 916–925, Jan. 2007.
[112] J. D. Maclay, J. Brouwer, and G. Scott Samuelsen, “Dynamic analyses of regenerative fuel cell power for potential use in renewable residential applications,” *Int. J. Hydrogen Energy*, vol. 31, no. 8, pp. 994–1009, Jul. 2006.
[113] F. Mueller, F. Jabbari, R. Gaynor, and J. Brouwer, “Novel solid oxide fuel cell system controller for rapid load following,” *J. Power Sources*, vol. 172, no. 1, pp. 308–323, Oct. 2007.
[114] G. Gigliucci, L. Petruzzi, E. Cerelli, A. Garzisi, and A. La Mendola, “Demonstration of a residential CHP system based on PEM fuel cells,” *J. Power Sources*, vol. 131, no. 1–2, pp. 62–68, May 2004.
[115] W. G. C. Ryan O’hayre, Suk-Won Cha, “Fuel Cell Fundamentals, 3. Edition,” *Wiley*. 2005.
[116] J. Brouwer, “On the role of fuel cells and hydrogen in a more sustainable and renewable energy future,” *Curr. Appl. Phys.*, vol. 10, no. 2, pp. S9–S17, Mar. 2010.
[117] D. Borello, S. Evangelisti, and E. Tortora, “Modelling of a CHP SOFC System Fed with Biogas from Anaerobic Digestion of Municipal Waste Integrated with Solar Collectors and Storage Unit*,” *Int. J. Thermodyn.*, vol. 28, no. 1, pp. 28–35, 2013.
[118] Q. Wang, H.-H. Wei, Q. Xu, Q. Wang, H.-H. Wei, and Q. Xu, “A Solid Oxide Fuel Cell (SOFC)-Based Biogas-from-Waste Generation System for Residential Buildings in China: A Feasibility Study,” *Sustainability*, vol. 10, no. 7, p. 2395, Jul. 2018.
[119] A. L. Facci, V. Cigolotti, E. Jannelli, and S. Ubertini, “Technical and economic assessment of a SOFC-based energy system for combined cooling, heating and power,” *Appl. Energy*, vol. 192, pp. 563–574, Apr. 2017.
[120] U. S. D. of Energy, “Buildings Energy Data Book Chapter 2: Residential Sector,” *U.S. Department of Energy*, 2012. [Online]. Available: http://web.archive.org/web/20130214025145/http://buildingsdatabook.eren.doe.gov/ChapterIntro2.aspx. [Accessed: 12-Sep-2016].
[121] M. Suzuki, Y. Takuwa, S. Inoue, and K. Higaki, “Durability Verification of Residential SOFC CHP

System," *ECS Trans.*, vol. 57, no. 1, pp. 309–314, Oct. 2013.
[122] "Ene.field - HyER." [Online]. Available: http://hyer.eu/ene-field/. [Accessed: 01-Oct-2018].
[123] COGEN Europe, "ene.field: About." [Online]. Available: http://enefield.eu/category/about/. [Accessed: 26-Oct-2018].
[124] M. Asghari, D. McVay, and J. Brouwer, "Integration of a Solid Oxide Fuel Cell with an Absorption Chiller for Dynamic Generation of Combined Cooling and Power for a Residential Application," *ECS Trans.*, vol. 78, no. 1, pp. 243–255, May 2017.
[125] R. Barrera, S. De Biase, S. Ginocchio, S. Bedogni, and L. Montelatici, "Performance and life time test on a 5 kW SOFC system for distributed cogeneration," *Int. J. Hydrogen Energy*, vol. 33, no. 12, pp. 3193–3196, Jun. 2008.
[126] Sakurambo, "SOFC Fuel Cell." Wikimedia Commons, 2015.
[127] S. Farhad, F. Hamdullahpur, and Y. Yoo, "Performance evaluation of different configurations of biogas-fuelled SOFC micro-CHP systems for residential applications," *Int. J. Hydrogen Energy*, vol. 35, no. 8, pp. 3758–3768, Apr. 2010.
[128] A. Wojcik, H. Middleton, I. Damopoulos, and J. Van herle, "Ammonia as a fuel in solid oxide fuel cells," *J. Power Sources*, vol. 118, no. 1–2, pp. 342–348, May 2003.
[129] J. Van herle, Y. Membrez, and O. Bucheli, "Biogas as a fuel source for SOFC co-generators," *J. Power Sources*, vol. 127, no. 1–2, pp. 300–312, Mar. 2004.
[130] J. Álvarez-Flórez and E. Egusquiza, "Analysis of damage caused by siloxanes in stationary reciprocating internal combustion engines operating with landfill gas," *Eng. Fail. Anal.*, vol. 50, pp. 29–38, Apr. 2015.
[131] G. D'Andrea, M. Gandiglio, A. Lanzini, and M. Santarelli, "Dynamic model with experimental validation of a biogas-fed SOFC plant," *Energy Convers. Manag.*, vol. 135, pp. 21–34, Mar. 2017.
[132] D. Bhattacharyya and R. Rengaswamy, "A Review of Solid Oxide Fuel Cell (SOFC) Dynamic Models," *Ind. Eng. Chem. Res.*, vol. 48, no. 13, pp. 6068–6086, Jul. 2009.
[133] M. C. Tucker, "Dynamic-temperature operation of metal-supported solid oxide fuel cells," *J. Power Sources*, vol. 395, pp. 314–317, Aug. 2018.
[134] M. Hanasaki *et al.*, "SOFC Durability against Standby and Shutdown Cycling," *J. Electrochem. Soc.*, vol. 161, no. 9, pp. F850–F860, Jun. 2014.
[135] M. Taghizadeh, M. Hoseintabar, and J. Faiz, "Frequency control of isolated WT/PV/SOFC/UC network with new control strategy for improving SOFC dynamic response," *Int. Trans. Electr. Energy Syst.*, vol. 25, no. 9, pp. 1748–1770, Sep. 2015.
[136] N. Chettibi and A. Mellit, "Intelligent control strategy for a grid connected PV/SOFC/BESS energy generation system," *Energy*, vol. 147, pp. 239–262, Mar. 2018.
[137] F. Palazzi, N. Autissier, F. M. A. Marechal, and D. Favrat, "A methodology for thermo-economic modeling and optimization of solid oxide fuel cell systems," *Appl. Therm. Eng.*, vol. 27, no. 16, pp. 2703–2712, Nov. 2007.
[138] I. Staffell and R. Green, "The cost of domestic fuel cell micro-CHP systems," *Int. J. Hydrogen Energy*, vol. 38, no. 2, pp. 1088–1102, Jan. 2013.
[139] N. A. and S. A. Glen Research Center, "Axial Compressors," 2015. [Online]. Available: https://www.grc.nasa.gov/www/k-12/airplane/caxial.html. [Accessed: 07-Nov-2018].
[140] T. Ning *et al.*, "Aerodynamic Analysis and Three-Dimensional Redesign of a Multi-Stage Axial Flow Compressor," *Energies*, vol. 9, no. 4, p. 296, Apr. 2016.
[141] "COMPRESSOR MAPS." [Online]. Available: http://turbocharged.com/catalog/compmaps/fig16.html. [Accessed: 07-Nov-2018].
[142] M. Guernsey, G. Chung, and W. Goetzler, "Pump and Fan Technology Characterization and R&D Assessment," Burlington, 2015.
[143] ebm-papst, "EC centrifugal fan - NRG118/0800-3612." [Online]. Available:

https://www.ebmpapst.com/en/products/motors/ecigearmotors/ecigearmotorsdetail.php?pID=252064. [Accessed: 07-Nov-2018].
[144] M. Svensson, “Biomethane Standards: Gas quality standardization of biomethane, going from national to international level,” in *Presentation at European Biomethane Workshop, 11 March 2014, Brussels*, 2014.
[145] C. Coker, “Pipeline Injection Of Biomethane In California,” *Biocycle*, vol. 59, no. 3, p. 32, 2018.
[146] D. Skopec, “Rule No. 30: Transportation of Customer-owned Gas,” Los Angeles, 2018.
[147] COM/CAP/lil, “Decision 15-06-029: Decision regarding the costs of compliance with decision 14-01-034 and adoption of biomethane promotion policies and program,” 2015.
[148] Pacific Gas and Electric Company, “Tariff Schedule Applicable to Gas Service of Pacific Gas and Electric Company,” San Francisco, 2013.
[149] Southern California Gas Company, “Renewable Natural Gas Toolkit,” 2017.
[150] M. Götz *et al.*, “Renewable Power-to-Gas: A technological and economic review,” *Renew. Energy*, vol. 85, pp. 1371–1390, Jan. 2016.
[151] “UC Irvine injects P2G green hydrogen into campus power supply,” *Fuel Cells Bull.*, vol. 2017, no. 1, p. 10, Jan. 2017.
[152] Southern California Gas Company, “Power-to-Gas Technology.” [Online]. Available: https://www.socalgas.com/smart-energy/renewable-gas/power-to-gas. [Accessed: 27-Oct-2018].
[153] AWS Truepower and U.S. National Renewable Energy Laboratory, “California 80-Meter Wind Resource Map,” *WINDExchange*, 2017. [Online]. Available: https://windexchange.energy.gov/maps-data/12. [Accessed: 29-Oct-2018].
[154] Wind Energy Technologies Office of the U.S. Department of Energy, “Wind Resource Assessment and Characterization,” *Office of Energy Efficiency & Renewable Energy Website*. [Online]. Available: https://www.energy.gov/eere/wind/wind-resource-assessment-and-characterization. [Accessed: 29-Oct-2018].
[155] S. Wilcox and W. Marion, “Users Manual for TMY3 Data Sets,” Golden, CO, 1994.
[156] “Alphabetical List by State,” *National Solar Radiation Data Base 1991-2010 Update*. [Online]. Available: https://rredc.nrel.gov/solar/old_data/nsrdb/1991-2010/hourly/list_by_state.html#C. [Accessed: 07-Nov-2018].
[157] GOOGLE EARTH, “‘Irvine.’ 33°38’16.81" N 117°50’14.92" W,” 2018. .
[158] ebm-papst, “Radial Blowers with EC internal-rotor motor: NRG 118 - 230 VAC.” p. 66, 2018.
[159] U.S. National Renewable Energy Laboratory, “Solar Maps,” *Geospatial Data Science*, 2017. [Online]. Available: https://www.nrel.gov/gis/solar.html. [Accessed: 29-Oct-2018].
[160] R. E. Silverman, “Notes from meeting between University of California Irvine and Oak View Waste Transfer Station.” Huntington Beach, 2017.
[161] B. Polly *et al.*, “From Zero Energy Buildings to Zero Energy Districts,” Goldcn, CO, 2016.
[162] R. Guglielmetti, D. Macumber, and N. Long, “OpenStudio: An Open Source Integrated Analysis Platform,” in *Proceedings of the 12th conference of international building performance simulation association*, 2011.
[163] D. B. Crawley *et al.*, “EnergyPlus: creating a new-generation building energy simulation program,” *Energy Build.*, vol. 33, no. 4, pp. 319–331, Apr. 2001.
[164] Folsom Labs, “HelioScope: Advanced Solar Design Software,” 2017. [Online]. Available: https://www.helioscope.com/. [Accessed: 12-Nov-2018].
[165] CalRecyle, “Residential Waste Stream by Material Type.” [Online]. Available: https://www2.calrecycle.ca.gov/WasteCharacterization/ResidentialStreams?lg=524&cy=30. [Accessed: 01-Oct-2018].
[166] CalRecycle, “Solid Waste Characterization Home Page: CalRecycle, California Department of Resources Recycling and Recovery.” [Online]. Available:

https://www2.calrecycle.ca.gov/wasteCharacterization/. [Accessed: 29-May-2017].
[167] J. Rapport, R. Zhang, B. M. Jenkins, and R. B. Williams, “Current Anaerobic Digestion Technologies Used for Treatment of Municipal Organic Solid Waste (Publication #IWMB-2008-011),” Sacramento, 2008.
[168] United States Department of Energy Office of Energy Efficiency & Renewable Energy, “Fact #621: May 3, 2010 Gross Vehicle Weight vs. Empty Vehicle Weight,” 2010. [Online]. Available: https://www.energy.gov/eere/vehicles/fact-621-may-3-2010-gross-vehicle-weight-vs-empty-vehicle-weight. [Accessed: 30-May-2018].
[169] “Carbon Intensity Lookup Table for Gasoline and Fuels that Substitute for Gasoline.”
[170] California Air Resources Board, “Monthly LCFS Credit Trading Activity Reports,” 2018. [Online]. Available: https://www.arb.ca.gov/fuels/lcfs/credit/lrtmonthlycreditreports.htm. [Accessed: 14-Dec-2018].
[171] California Air Resources Board, “The LCFS Credit Price Calculator – Alternative Fuel Toolkit,” 2017. [Online]. Available: http://altfueltoolkit.org/resource/the-lcfs-credit-price-calculator/. [Accessed: 20-Dec-2018].
[172] U.S. Environmental Protection Agency, A. Quality, and S. Division, “Cellulosic Waiver Credit Price Calculation for 2018 (EPA-420-B-17-036),” 2017.
[173] M. Mueller, K. Birkinshaw, M. Krebs, and B. B. Blevins, “Natural Gas in California: Environmental Impacts and Device Performance,” 2006.
[174] “Safety Data Sheet Natural Gas,” 2015.
[175] Engineering ToolBox, “Fans - Efficiency and Power Consumption,” 2003. [Online]. Available: https://www.engineeringtoolbox.com/fans-efficiency-power-consumption-d_197.html. [Accessed: 20-Nov-2018].
[176] U.S. Energy Information Administration, “California Gasoline and Diesel Retail Prices,” 2017. [Online]. Available: https://www.eia.gov/dnav/pet/pet_pri_gnd_dcus_sca_m.htm. [Accessed: 20-Dec-2018].
[177] G. Vishwanathan, J. P. Sculley, A. Fischer, and J.-C. Zhao, “Techno-economic analysis of high-efficiency natural-gas generators for residential combined heat and power,” *Appl. Energy*, vol. 226, pp. 1064–1075, Sep. 2018.